Protein reconstitution in giant vesicles

Dissertation

zur Erlangung des akademischen Grades
"doctor rerum naturalium" (Dr. rer. nat.)
in der Wissenschaftsdisziplin "Physikalische Biochemie"

eingereicht an der
Mathematisch-Naturwissenschaftlichen Fakultät
Institut für Biochemie und Biologie
der Universität Potsdam

von

Shreya Pramanik

Ort und Datum der Disputation: Potsdam, 16. Oktober 2023

Supervisors

1. Prof. Dr. Reinhard Lipowsky
Max Planck Institute of Colloids and Interfaces

2. Prof. Dr. Joachim Spatz
Max Planck Institute for Medical Research

Referees

1. Prof. Dr. Reinhard Lipowsky
2. Prof. Dr. Joachim Spatz
3. Prof. Dr. Ulrich Schwarz

Published online on the
Publication Server of the University of Potsdam:
https://doi.org/10.25932/publishup-61278
https://nbn-resolving.org/urn:nbn:de:kobv:517-opus4-612781

Zusammenfassung

Das Leben auf der Erde ist vielfältig und reicht von einzelligen Organismen bis hin zu mehrzelligen Lebewesen wie dem Menschen. Obwohl es Theorien darüber gibt, wie sich diese Organismen entwickelt haben könnten, verstehen wir nur wenig darüber, wie "Leben" aus Molekülen entstanden ist. Die synthetische Bottom-up-Biologie zielt darauf ab, minimale Zellen zu schaffen, indem sie verschiedene Module wie Kompartimentierung, Wachstum, Teilung und zelluläre Kommunikation kombiniert.

Alle lebenden Zellen haben eine Membran, die sie von dem sie umgebenden wässrigen Medium trennt und sie schützt. Darüber hinaus haben alle eukaryotischen Zellen Organellen, die von intrazellulären Membranen umschlossen sind. Jede Zellmembran besteht hauptsächlich aus einer Lipiddoppelschicht mit Membranproteinen. Lipide sind amphiphile Moleküle, die molekulare Doppelschichten aus zwei Lipid-Monoschichten oder Blättchen bilden. Die hydrophoben Ketten der Lipide sind einander zugewandt, während ihre hydrophilen Kopfgruppen die Grenzflächen zur wässrigen Umgebung bilden. Riesenvesikel sind Modellmembransysteme, die Kompartimente mit einer Größe von mehreren Mikrometern bilden und von einer einzigen Lipiddoppelschicht umgeben sind. Die Größe der Riesenvesikel ist mit der Größe von Zellen vergleichbar und macht sie zu guten Membranmodellen, die mit einem Lichtmikroskop untersucht werden können. Allerdings fehlen den Riesenvesikelmembranen nach der ersten Präparation Membranproteine, die in weiteren Präparationsschritten in diese Membranen eingebaut werden müssen. Je nach Protein kann es entweder über Ankerlipide an eines der Membranblättchen gebunden oder über seine Transmembrandomänen in die Lipiddoppelschicht eingebaut werden.

Diese Arbeit befasst sich mit der Herstellung von Riesenvesikeln und der Rekonstitution von Proteinen in diesen Vesikeln. Außerdem wird ein mikrofluidischer Chip entworfen, der in verschiedenen Experimenten verwendet werden kann. Die Ergebnisse dieser Arbeit werden anderen Forschern helfen, die Protokolle für die Herstellung von GUVs zu verstehen, Proteine in GUVs zu rekonstituieren und Experimente mit dem mikrofluidischen Chip durchzuführen. Auf diese Weise wird die vorliegende Arbeit für das langfristige Ziel von Nutzen sein, die verschiedenen Module der synthetischen Biologie zu kombinieren, um eine Minimalzelle zu schaffen.

Research summary

Life on Earth is diverse and ranges from unicellular organisms to multicellular creatures like humans. Although there are theories about how these organisms might have evolved, we understand little about how 'life' started from molecules. Bottom-up synthetic biology aims to create minimal cells by combining different modules, such as compartmentalization, growth, division, and cellular communication.

All living cells have a membrane that separates them from the surrounding aqueous medium and helps to protect them. In addition, all eukaryotic cells have organelles that are enclosed by intracellular membranes. Each cellular membrane is primarily made of a lipid bilayer with membrane proteins. Lipids are amphiphilic molecules that assemble into molecular bilayers consisting of two leaflets. The hydrophobic chains of the lipids in the two leaflets face each other, and their hydrophilic headgroups face the aqueous surroundings. Giant unilamellar vesicles (GUVs) are model membrane systems that form large compartments with a size of many micrometers and enclosed by a single lipid bilayer. The size of GUVs is comparable to the size of cells, making them good membrane models which can be studied using an optical microscope. However, after the initial preparation, GUV membranes lack membrane proteins which have to be reconstituted into these membranes by subsequent preparation steps. Depending on the protein, it can be either attached *via* anchor lipids to one of the membrane leaflets or inserted into the lipid bilayer *via* its transmembrane domains.

The first step is to prepare the GUVs and then expose them to an exterior solution with proteins. Various protocols have been developed for the initial preparation of GUVs. For the second step, the GUVs can be exposed to a bulk solution of protein or can be trapped in a microfluidic device and then supplied with the protein solution. To minimize the amount of solution and for more precise measurements, I have designed a microfluidic device that has a main channel, and several dead-end side channels that are perpendicular to the main channel. The GUVs are trapped in the dead-end channels. This design exchanges the solution around the GUVs *via* diffusion from the main channel, thus shielding the GUVs from the flow within the main channel. This device has a small volume of just 2.5 μL, can be used without a pump and can be combined with a confocal microscope, enabling uninterrupted imaging of the GUVs during the experiments. I used this device for most of the experiments on GUVs that are discussed in this thesis.

In the first project of the thesis, a lipid mixture doped with an anchor lipid was used that can bind to a histidine chain (referred to as His-tag(ged) or 6H) *via* the metal cation Ni^{2+}. This method is widely used for the biofunctionalization of GUVs by attaching proteins without a transmembrane domain. Fluorescently labeled His-tags which are bound to a membrane can be observed in a confocal microscope. Using the same lipid mixture, I prepared the GUVs with different protocols and investigated the membrane composition of the resulting GUVs by evaluating the amount of fluorescently labeled His-tagged molecules bound to their membranes. I used the microfluidic device described above to expose the

outer leaflet of the vesicle to a constant concentration of the His-tagged molecules. Two fluorescent molecules with a His-tag were studied and compared: green fluorescent protein (6H-GFP) and fluorescein isothiocyanate (6H-FITC). Although the quantum yield in solution is similar for both molecules, the brightness of the membrane-bound 6H-GFP is higher than the brightness of the membrane-bound 6H-FITC. The observed difference in the brightness reveals that the fluorescence of the 6H-FITC is quenched by the anchor lipid *via* the Ni^{2+} ion. Furthermore, my measurements also showed that the fluorescence intensity of the membrane-bound His-tagged molecules depends on microenvironmental factors such as pH. For both 6H-GFP and 6H-FITC, the interaction with the membrane is quantified by evaluating the equilibrium dissociation constant. The membrane fluorescence is measured as a function of the fluorophores' molar concentration. Theoretical analysis of these data leads to the equilibrium dissociation constants of (37.5 $\pm$ 7.5) nM for 6H-GFP and (18.5 $\pm$ 3.7) nM for 6H-FITC.

The anchor lipid mentioned previously used the metal cation Ni^{2+} to mediate the bond between the anchor lipid and the His-tag. The Ni^{2+} ion can be replaced by other transition metal ions. Studies have shown that Co^{3+} forms the strongest bonds with the His-tags attached to proteins. In these studies, strong oxidizing agents were used to oxidize the Co^{2+} mediated complex with the His-tagged protein to a Co^{3+} mediated complex. This procedure puts the proteins at risk of being oxidized as well. In this thesis, the vesicles were first prepared with anchor lipids without any metal cation. The Co^{3+} was added to these anchor lipids and finally the His-tagged protein was added to the GUVs to form the Co^{3+} mediated bond. This system was also established using the microfluidic device.

The different preparation procedures of GUVs usually lead to vesicles with a spherical morphology. On the other hand, many cell organelles have a more complex architecture with a non spherical topology. One fascinating example is provided by the endoplasmic reticulum (ER) which is made of a continuous membrane and extends throughout the cell in the form of tubes and sheets. The tubes are connected by three-way junctions and form a tubular network of irregular polygons. The formation and maintenance of these reticular networks requires membrane proteins that hydrolyize guanosine triphosphate (GTP). One of these membrane proteins is atlastin. In this thesis, I reconstituted the atlastin protein in GUV membranes using detergent-assisted reconstitution protocols to insert the proteins directly into lipid bilayers.

This thesis focuses on protein reconstitution by binding His-tagged proteins to anchor lipids and by detergent-assisted insertion of proteins with transmembrane domains. It also provides the design of a microfluidic device that can be used in various experiments, one example is the evaluation of the equilibrium dissociation constant for membrane-protein interactions. The results of this thesis will help other researchers to understand the protocols for preparing GUVs, to reconstitute proteins in GUVs, and to perform experiments using the microfluidic device. This knowledge should be beneficial for the long-term goal of combining the different modules of synthetic biology to make a minimal cell.

Disclaimer

Some of the results described in chapters 2, 3 and 4 have been published:
Title: Binding of His-tagged fluorophores to lipid bilayers of giant vesicles
Authors: **Shreya Pramanik**, Jan Steinkühler, Rumiana Dimova, Joachim Spatz and Reinhard Lipowsky
Soft Matter, 2022, 18, 6372–6383, DOI: 10.1039/d2sm00915c

The microfluidic device described in chapter 2 has been used for another research that is published:
Title: Biomimetic asymmetric bacterial membranes incorporating lipopolysaccharides
Authors: Mareike S. Stephan, Valentin Dunsing, **Shreya Pramanik**, Salvatore Chiantia, Stefanie Barbirz, Tom Robinson, and Rumiana Dimova
Biophysical Journal, 2022, Volume 122, Issue 11, 6 June 2023, Pages 2147-2161, DOI: 10.1016/j.bpj.2022.12.017

The results from chapter 6 have been accepted for publication:
Title: Elucidating the Morphology of the Endoplasmic Reticulum: Puzzles and Perspectives
Authors: Reinhard Lipowsky, **Shreya Pramanik**, Amelie S. Benk, Miroslaw Tarnawski, Joachim Spatz and Rumiana Dimova
ACS Nano (in press)

The protocols in chapter 3 will be published in The Giant Vesicle Book, 2^{nd} edition
Title: Preparation methods for giant unilamellar vesicles
Authors: **Shreya Pramanik**, Jan Steinkühler, Pasquale Stano, Peter Walde, Carlos M. Marques, Rumiana Dimova
Edited by Rumiana Dimova and Carlos M. Marques
CRC Press

I, Shreya Pramanik, have written all parts of this thesis, and performed all experiments and analyzed all the data. This thesis has not been submitted previously to any other university. The research was supported by the Max Planck School- Matter to Life.

Shreya Pramanik
Potsdam, 6^{th} June, 2023

List of abbreviations

Abbreviation	Meaning	Other information
POPC	1-palmitoyl-2-oleoyl-glycero-3-phosphocholine	
POPG	1-palmitoyl-2-oleoyl-sn-glycero-3-phospho-(1'-rac-glycerol) (sodium salt)	
Chol	Cholesterol (plant derived)	
DGS-NTA(Ni), Ni-NTA	1,2-dioleoyl-sn-glycero-3-[(N-(5-amino-1-carboxypentyl)iminodiacetic acid)succinyl] (nickel salt)	
DGS-NTA, Holo-NTA	1,2-dioleoyl-sn-glycero-3-[(N-(5-amino-1-carboxypentyl)iminodiacetic acid)succinyl] (ammonium salt)	
NBD-PG	1-oleoyl-2-6-[(7-nitro-2-1,3-benzoxadiazol-4-yl)amino]hexanoyl-sn-glycero-3-[phospho-rac-(1-glycerol)] (ammonium salt)	Ex/Em 461 nm/534 nm
DHPE-TR	Texas Red 1,2-Dihexadecanoyl-sn-Glycerin-3-Phosphoethanolamin, Triethylammoniumsalt	Ex/Em 583 nm/601 nm
His-tag(ged), 6H	Chain of six consecutive histidines joined by peptide bonds	
6H-FITC	His-tagged Fluoresceinisothiocyanate	Ex/Em 490 nm/525 nm
6H-GFP	His-tagged Green Fluorescent Protein	Ex/Em 475 nm/509 nm
DmATL	Drosophila melanogaster atlastin	
NaCl	Sodium chloride	
EDTA	Ethylenediaminetetraacetic acid	
HEPES	(4-(2-hydroxyethyl)-1-piperazineethanesulfonic acid)	
$MgCl_2$	Magnesium chloride	
GTP	Guanosine triphosphate	
GUV	Giant Unilamellar Vesicle	
LUV	Large Unilamellar Vesicle	

Contents

Chapter 1

Introduction

Matter to Life- Curiosity or playing God?

Cogito, ergo sum- I think, therefore I am- the famous quote by René Descartes (1596-1650), suggests that consciousness is a sign of existence. This raises the question if 'consciousness' is a necessary aspect of all living organisms, and if not, then what is the definition of life? If consciousness is removed, will all living creatures collapse owing to no decision-making power to survive any apocalypse? Over billions of years, a complex brain circuit has evolved to provide consciousness. However, simple unicellular organisms still exist on this planet, and sometimes even cause havoc to humans with disease outbreaks. The unicellular slime mold *Physarum polycephalum* can solve puzzles by rearranging its shape to find the shortest route between different food sources[1]. Does 'consciousness' require a complex brain circuit or is it a molecular term defined by genetic codes? Richard Dawkins in his book 'The Selfish Gene'[2] has an interesting take on this question. The genes do not expose themselves to the harsh external environment, by coiling up and having many layers of protective cellular material around it. Dawkins elaborates Charles Darwin's theory of natural selection from a 'gene's eye view' where the genes use the organisms as hosts for their survival and replication.

As we are already thinking in the molecular realm, another question

would be what drove the molecules to come together to form complex yet functional macromolecules like chromosomes and proteins. Were these molecules involved in conscious decision-making, or is life as we know, the result of stochastic molecular collisions? Erwin Schrödinger's 'What is Life?'[3] first published in 1944, defined life as a series of interactions between many atoms that are governed by the laws of physics. Since physical laws rest on atomic statistics, the presence of a large number of atoms is essential for proper functioning. In other words, if only a few atoms consisted of an organism, just one atom could affect the development or functioning of the whole organism. All atoms undergo random motion at all times, so just a few atoms would not be able to direct themselves in any orderly fashion. All these ideas beautifully explain the behavior and the reasons for life to be as it is. However, the question of how the 'living' could be distinguished from the 'non-living' still remains unanswered.

In the 1920s the idea of a primordial soup was first discussed by Oparin, who hypothesized a mixture of gases that could have been present on Earth. Chemical reactions in this mixture could result in the formation of complex organic molecules. In 1953, Stanley Miller and Harold Urey published their famous experiment, where they simulated the environmental conditions of the prebiotic earth[4]. They built an apparatus that circulated methane, ammonia, water, and hydrogen. As shown in Figure 1.1, evaporation and precipitation were simulated by heating water and a condenser. They passed an electric discharge through the gas mixture to mimic lightning and create free radicals. After about a week, they noticed the formation of hydrocarbons and amino acids. This was one of the pioneering experiments that initiated research in the direction to understand the origin of life. Since then, this experiment has been replicated by several groups[5–7].

The evolution from the basic organic molecules to the first living organism would have required the intermediate stage of bio-polymers. Some theories and experiments point towards the RNA (ribonucleic acid) or proto-RNA[8] possibly being the earliest macromolecules[9]. Other theories suggest protein-like polymers to have formed in the primordial soup[10]. The important features of these early polymers should be the ability to catalyze

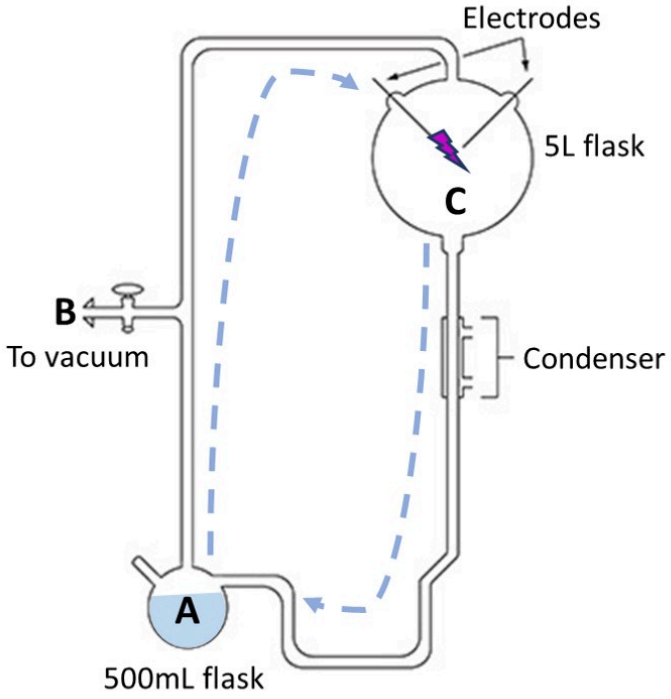

Figure 1.1: Schematic of the apparatus used in Miller-Urey experiment. Water is filled in flask A, and the rest of the air from the apparatus is removed by connecting it to a vacuum via the outlet. After filling in the other gases with appropriate partial pressures, the whole apparatus is sealed. The water in A is boiled, and the vapors mix with the rest of the gases. The gaseous mixture reaches flask C which is connected to electrodes that provide electric discharges. The condenser connected to C condenses the mixture and directs it back to A. The mixture circulates through the whole apparatus, as indicated by the dashed blue line.

their growth and self-replicate with minimum errors. In 1971, Manfred Eigen introduced a paradox that the errors in self-replication will result in loss of 'information', limiting the size of any prebiotic polymer[11]. He also hypothesized that the co-evolution of multiple macromolecules regulated the quality of each other's replication. This is very similar to how nucleic acids encode proteins and the proteins ensure proper replication of the nucleic acids during division. Hence there is a possibility that these molecules

evolved together rather that one after the other.

A modern-day cell is more complex with compartments and organelles, which obviously would have taken very long to form, and we do not yet understand how. Many studies approach this question from different directions. Some try to begin from scratch and slowly add one new component at a time, while others try removing components from a complete cell. Both, the bottom-up and the top-down approach, contribute to our understanding of life in simple terms. Will this knowledge challenge our philosophy of living? With scientific advancement, if we establish the technology to create life, would that make humans the most powerful being, often referred to as 'God'? There are more questions than answers. Scientists have made significant developments in answering the question of how life could have started. On the one hand, these insights are exciting but on the other hand, they often creates anxieties and worries among common people when the results are not communicated carefully. Along with scientific research, ethical considerations and science communication should be considered to ensure scientific progress. Research about the matter to life should help everyone satisfy their curiosity and not be afraid that scientists are trying to play God.

1.1 Synthetic biology and artificial cells

To study atomic structures, physicists and chemists start from the hydrogen atom which represents the simplest example of an atom. It is plausible to expect that whatever is true for the hydrogen atom should be true for the more complex atoms as well. Similarly, to understand the complex cellular functions, it is appealing to first study a minimal cell[12]. Even unicellular organisms have a complex genetic makeup, hence one would like to identify the essential genes for sustaining life. The mycoplasmas are unicellular organisms with a small genome known to sustain autonomous growth. In 1999, it was shown that the mycoplasmas had many genes that were nonessential for growth in a controlled environment like that in a laboratory[13]. In 2016, the same group designed and built the smallest genome

and transferred it into a cytoplasm. The resulting organism named JCVI-Syn3.0[14], has only 473 genes. This genome is smaller than that of any organism found in nature but JCVI-Syn3.0 can perform all basic functions including translation, transcription and self-replication. However, the minimal genome still involves many genes whose functions are yet unknown. Using this reductionist or top-down approach, the number of genes are successively removed to check the functionality of the resulting organism. Another way to make a minimal cell would be to work our way up from simple molecules which represent the bottom-up approach, by which we start from molecules to build up a minimal cell.

Synthetic biology is an interdisciplinary field of science that applies engineering principles to biology. One of the topics that comes under the umbrella of synthetic biology is to understand the minimal requirements for a self sustaining cell. In 1665, Robert Hooke observed a cork under a magnifying glass and saw honey-comb like structures and coined the term 'cell' to describe them. The natural cells are very complex with many biologically active molecules and organelles. Finding out the functions of each component becomes simpler if artificial cells with minimal components are studied. The artificial cells are systems that have one or more properties of a real cell. The synthetic cells must fulfill the basic requirements of life, i.e., provide a boundary to confine cellular components, undergo growth leading to division, be able to communicate with other cells and undergo apoptosis in case it encounters a defect beyond repair. Integrating all of these functions in one synthetic system is a very ambitious goal. However, various research groups are working on the different modules of synthetic cells, and have succeeded in accomplishing some of these modules. In the future, these modules can be combined to obtain a more realistic cell.

The first requirement to build a synthetic cell would be make a compartment that confines the cellular material inside. This could be achieved by membranes made of lipid bilayers, polymers[15] or protein coacervates[16,17]. Since the lipid bilayers mimic the cell membranes most closely, it is the most popular model system and also the model chosen for this study. Certain advances have been made using these model system, such as preparing multi-

compartment systems and establishing signaling between them[18], changing membrane properties by proteins[19–21], division of membrane compartments[22–24] and encapsulation of nucleic acids[25,26].

1.2 Structure of lipids and their assemblies

In this section, we will explore the chemical structure of lipids and how they can assemble into various supramolecular structures, the lipid bilayers being one of the many assemblies of lipids. The lipid molecules are amphiphilic, that is, they have a hydrophobic and a hydrophilic part known as lipid headgroups and lipid tails respectively. Lipids with phosphates as head groups are called the phospholipids. Depending on the chemical groups attached to the phosphate, the head groups are either charged or zwitterionic at physiological pH. Lipid tails correspond to long hydrocarbon chains and the physical properties of the lipid changes with the length of these chains and the degree of saturation.

The lipid molecules can assemble into various structures. This property is known as lipid polymorphism. The self-assembly into different phases depends on parameters such as the chemical structure of the lipid, water content, the solutes around it, pressure and temperature of the solution[27]. Some common lipid assemblies are- micelles, bilayers, hexagonal and cubic phases. See Figure 1.2 for these examples of self assembled structures made by lipids. The lipid disks and liposomes are of particular interest as they are similar to cell membranes. The hexagonal and the cubic assemblies can be used as drug or gene delivery agents[28].

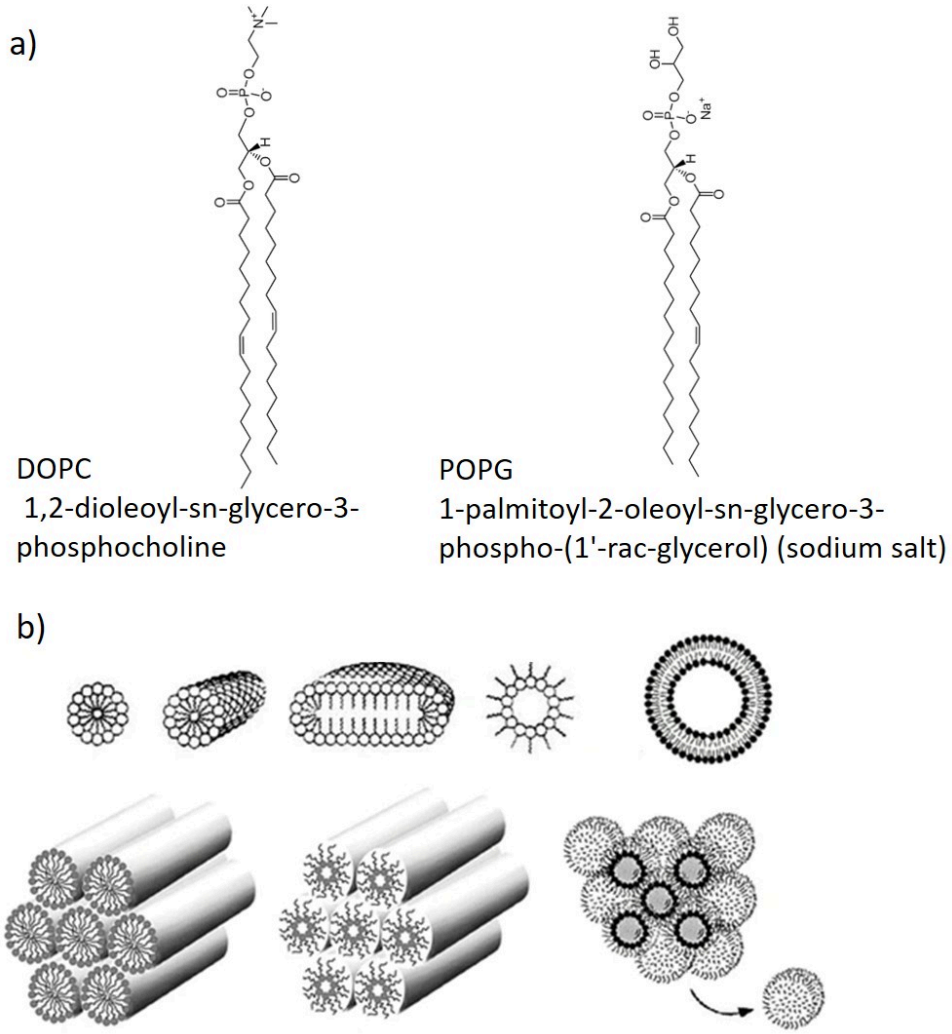

Figure 1.2: **a)** Examples of two phospholipids, DOPC with a zwitterionic head group and tail group with two unsaturated bonds, POPG with a negatively charged head group and tail group with one unsaturated bond. **b)** Different assemblies of lipids. Top row, left to right- spherical micelle, cylindrical micelle, lipid disk, inverted micelle and liposome. Bottom row, left to right- hexagonal phase, inverted hexagonal phase and inverted micellar cubic phase. The images in b) are adapted from Koynova et al.[27].

1.3 Types of model membrane systems

As mentioned in the previous section, lipids can arrange into various structures that have applications in different fields of science. Since the goal of this thesis is to make and study biomimetic membrane systems, this section would discuss only those lipid arrangements that can be used as model systems for cell membranes, see Figure 1.3.

Monolayer. Lipid monolayers are two-dimensional arrangements of lipids at a planar liquid-liquid interface. They represent half-a-membrane, i.e. only one leaflet, hence they are good models for a membrane surface but not adequate to study transport of molecules across the membrane. Lipid monolayers are formed at air-water interfaces with the lipid heads pointing towards the water. The aqueous phase provides a smooth and planer surface for the support of the lipid monolayer. Thermodynamic parameters such as surface pressure and temperature can be easily controlled. Monolayers have been used to investigate problems related to the insertion of particles into one leaflet of a lipid membrane[29].

Supported lipid bilayer (SLB). SLBs are formed on solid supports, but not covalently attached to the support. As SLBs are bilayers, they consist of both leaflets and thus provide better model systems compared to monolayers. SLBs are useful for surface-sensitive measurement techniques like surface plasmon resonance or the atomic force microscopy[30]. Silica surfaces are popular choices to be used as solid substrates for SLBs which can also be formed on spherical supports. Spherical SLBs can used as systems to study the compounds that disrupt membranes by forming pores. The presence of the solid silica sphere under the membrane facilitates such studies. It still remains intact and contains traces of membrane active molecules that disrupts the membrane[31].

Free standing planar bilayer. The free standing bilayers do not require any solid support for the lipid membrane. They are formed between solid

grids, supported by a ring of oil and have aqueous solutions on both sides. These can be made of grids with many individual membrane systems, which increases the sample size for each experiment[32]. Black lipid membranes (BLMs) are also a type of free standing membranes. This BLM is useful for precise measurements of tensions required to open mechanosensitive ion channels in the membrane[33].

Unilamellar Vesicle. Uilamellar vesicles are formed by a single lipid bilayers that closes upon themselves. The vesicle membrane divides the aqueous medium into two compartments, the outer compartment that surrounds the vesicles and the inner compartment which is inside the vesicle. Depending on the size of the vesicles one distinguishes between of small, large and giant unilamellar vesicles, abbreviated as SUVs, LUVs and GUVs, respectively. GUVs have a size of several micrometers, which is comparable to the size of living cells. Due of their large size, GUVs can be directly studied by optical microscopy. In this thesis, the GUVs are used as the model membrane system. The protocols for making GUVs and attaching proteins to their membranes are detailed in the following sections and chapters. The inner aqueous solution of a GUV can contain other smaller vesicles such as LUVs. Such a vesicle-inside-vesicle system would mimic the organelles in a cell.

Giant Plasma Membrane Vesicle (GPMV). The bilayers made of synthetic lipids lack the exact lipidome or proteome of a real cell, therefore the GPMVs provide a model system that mimics the plasma membrane more closely. The GPMVs are derived from cells and do not involve components of the cellular cytoskeleton. This makes it a good model to study the mechanical properties of the plama membrane[34].

Computer simulations. Conventional light microscopic techniques generally represent global phenomena at long time scales, and fail to capture details in the nanometer and nanosecond domain. This is where the computer simulations come in and expand our knowledge in the nanoregime.

Model membrane systems can be simulated as planar bilayers or even as nanovesicles. Depending on the spatio-termporal resolution to be achieved, the membrane can be simulated at an atomistic level or a coarse-grained level[35]. All-atom systems are very detailed and hence come with a high computational cost. In coarse-grained simulations, some atoms of a molecule are grouped together to form a bead, which reduces the time for computation. The nanovesicles made of coarse-grained lipids and solvents, exhibit properties similar to those of GUVs obtained in the wet lab[36].

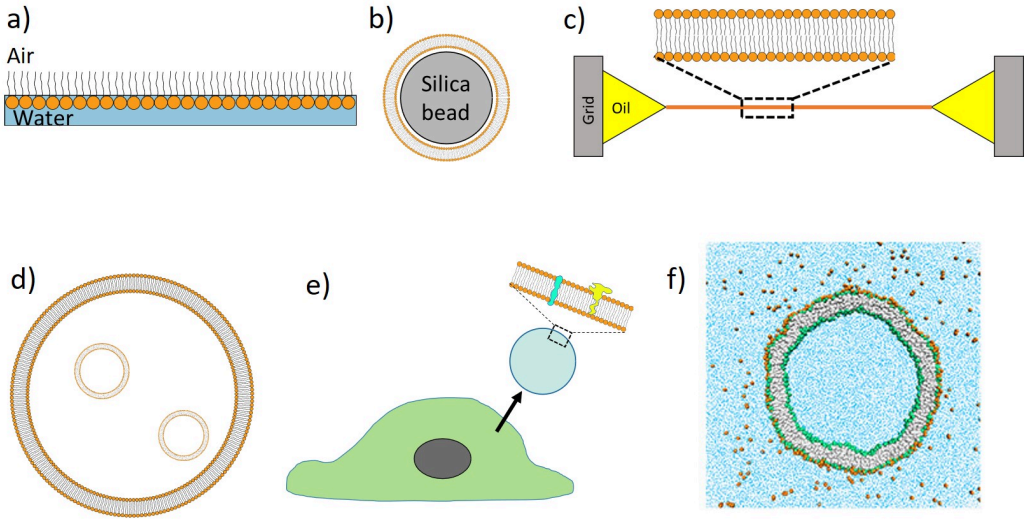

Figure 1.3: Model membrane systems: a) Monolayer at the air-water interface, b) Spherical supported lipid bilayer on a silica bead, c) Free standing planar lipid bilayer prepared on a grid, d) Vesicles inside a giant unilamellar vesicle, e) Giant plasma membrane vesicle with native lipids and proteins from the plasma membrane of the cell, f) Computer simulation of a coarse-grained nanovesicle (image adapted from Ghosh et al.[36]).

1.4 Biofunctionalization of giant vesicles

The giant vesicles introduced in the previous section have membranes, which are composed only of lipids. Since GUVs are models for the plasma membrane, it becomes important to add biological macromolecules such as proteins to the membranes. Two broad categories of membrane pro-

teins can be distinguished. First, integral membrane proteins have one or several transbilayer domains, which span the hydrophobic core of the bilayer membranes. Second, peripheral membrane proteins, which take part in cell signaling and membrane trafficking, can attach to one leaflet of the bilayer membranes by binding to a specific lipid or to a small cluster of several lipids. Likewise, to achieve biofunctionalization of GUVs, integral membrane proteins are inserted into the membranes using detergents[37] or proteoliposomes[38,39] whereas peripheral membrane proteins are attached *via* chemical linkage (Figure 1.4).

Some examples of such chemical linkages between lipid and proteins are- binding of cystine residues to maleimide-functionalized lipids, or binding lysine to succinyl-functionalized headgroups of lipids. Furthermore biotinylated proteins can be attached to biotinylated lipid head groups *via* a streptavidin linkage and proteins with a histidine chain can be attached to lipids head groups functionalized with nickel-nitrilotriacetic acid (Ni-NTA)[40]. The functionalization of lipid head groups with Ni-NTA is a popular choice because it is based on a weaker coordinate bond instead of a covalent bond. This interaction between the protein and the lipid mediated by Ni-NTA is reversible.

Poly-histidine tags are generally attached to one of the terminals of the proteins for their purification[41]. Hence, this specific interaction can be harnessed to attach proteins to lipid bilayers. These Ni-NTA functionalized lipids were synthesized and characterized by Schmitt et al in 1994[42]. Currently, the 1,2-dioleoyl-sn-glycero-3-[(N-(5-amino-1-carboxypentyl) iminodiacetic acid)succinyl] (nickel salt) lipid, abbreviated as DGS-NTA(Ni), is available commercially for direct use to make model membranes. The NTA(Ni) in the lipid head group forms an octahedral coordinate complex with poly-histidine chains. Four vertices of the octahedron are occupied by the NTA group, leaving two vertices for the binding of two electron donating groups such as imidazole. Histidine has imidazole as its side chain. One of the nitrogen from the imidazole donates electrons to form the coordinate bond, see Figure 1.5. The optimal length of the histidine chain to bind to NTA(Ni) lipids consists of six residues, corresponding to the maximum of

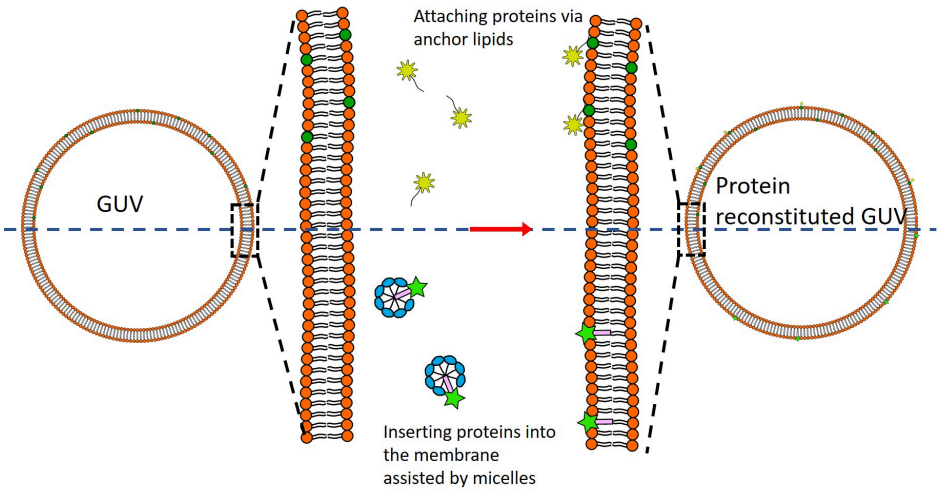

Figure 1.4: Biofunctionalization of GUV membranes can be achieved by reconstituting proteins in the membrane. The proteins can be attached to one leaflet of lipid bilayer via anchor lipids or inserted into the bilayer assisted by detergent micelles.

the equilibrium association constant as a function of chain length[43]. The chain of six histidines represents one example for a His-tag and will be abbreviated 6H for the rest of the thesis.

In this thesis, the His-tag is attached to fluorescent molecules, namely to green fluorescent protein (6H-GFP) and fluorescein isothiocyanate (6H-FITC). The molecular weight of the two fluorophores is quite different: GFP has a molecular weight of 27 kDa whereas FITC has a much smaller molecular weight of only 389 Da. Therefore, the two fluorophores are also different in their sizes. The fluorescent molecules help in tracking the His-tag and in quantifying the number of His-tag molecules binding to the DGS-NTA(Ni) lipids in the GUV membranes.

The binding between His-tagged proteins and DGS-NTA(Ni) lipids has been frequently used in previous studies. Examples include protein crowding on vesicles[44], lipid-coated substrates for drug delivery systems[45], artificial cell adhesion[46], and high spontaneous curvature generated by the dilute concentration of surface proteins[22]. In general, the Ni^{2+} ion can be replaced by other transition metal cations in the NTA group. Previous

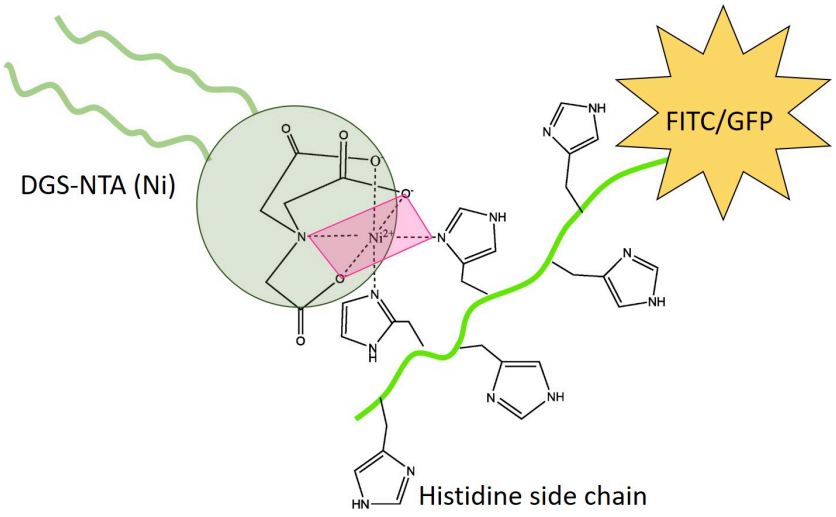

Figure 1.5: A chain of six histidine (6H) binds to the Ni-NTA functionalized lipid, DGS-NTA(Ni). To monitor the binding of this His-tag, it is attached to fluorescent molecules like GFP and FITC. The imidazole side chains of two histidines interact with the Ni-NTA to form an octahedral complex. Four vertices of this octahedron (pink) are occupied by three oxygens and one nitrogen from the lipid head group, and the other two vertices by two nitrogens from the imidazole side chains.[43]

studies have shown that the Co^{3+} ion mediates a stronger and less labile coordinate bond between the NTA and the His-tag, than that compared to the corresponding bond mediated by the Ni^{2+} ion[47–49]. In these studies, the Co^{3+} was formed by using a strong oxidising agents, which puts the biological macromolecules in the risk of getting oxidised. In this thesis, the Co^{3+} mediated bond was prepared without using any oxidizing agents.

As mentioned previously, the natural cell membranes also contain integral proteins that have one or several transmembrane domains which are hydrophobic. Such proteins with transmembrane domains are generally purified from native cell membranes with the help of detergent. Above a critical concentration the detergents form spherical aggregates, called micelles. These micelles disintegrate the native membrane and extract the membrane protein. Without the detergents, the proteins will aggregate to protect their hydrophobic regions and precipitate out of the aqueous solu-

tion[50]. To reconstitute these membrane proteins in synthetic lipid bilayers, the interaction between the lipids need to be disturbed. Since the proteins are already solubilized by detergent, it is convenient to add the protein-detergent mixture to the preformed vesicles. Once the protein is inserted in the membrane of the vesicle, the excess detergent can be removed via dialysis or adsorption on polystyrene beads[51]. This technique has been successfully used to reconstitute various proteins into vesicle membranes[37]. In this thesis, I have reconstituted the integral membrane protein atlastin, into GUV membrane. Atlastin, which plays an important role for the formation of the endoplasmic reticulum, has been expressed in bacterial cells and purified in the detergent Triton X-100.

1.5 Optical microscopy of giant vesicles

The size of GUVs is in the range of micrometers. One advantage of using GUVs as model membranes is that they can be observed using an optical microscope. Depending on the hardware available with the microscope, various imaging techniques can be used to obtain different information. My experiments were performed using commercial confocal microscopes (Leica microsystems TCS SP8 or SP5, Wetzler, Germany). These microscopes are also equipped to image with transmitted light. Bright field imaging is one example of transmitted light microscopy methods, where the light directly illuminates the specimen and is observed using a combination of lenses. The aqueous solution inside and outside the GUVs is transparent, hence brightfield imaging fails to provide a good contrast to see the GUVs. Phase contrast microscopy, another form of transmitted light microscopy, generates high contrast in the images of a transparent sample. The contrast is generated by the difference in the optical path of the lights rays when they pass through different refractive indices in the sample. GUVs are generally made with sucrose solution inside and then suspended in an equiosmolar glucose solution. This sugar asymmetry on the two sides of the GUV membrane serves two purposes. The enclosed sucrose solution is denser compared to the glucose solution on the outside which suppresses

the movement of the GUVs by settling them at the bottom of the slide. Sucrose and glucose solutions also have different refractive indices, which helps in phase contrast imaging.

1.5.1 Confocal microscope

Transmitted light microscopy improves the contrast of the image but still fails to image the details of a specimen. The presence of fluorescent dyes in the specimen enables fluorescence microscopy. When such a fluorescently labeled specimen is illuminated with light of wavelengths corresponding to the excitation wavelength of the fluorescent dye, via a microscope objective, all the dye molecules in the light path are excited. This includes the fluorescent molecules above and below the intended focal plane. When the fluorescence emission is collected, the resulting image is blurry due to the out-of-focus fluorescence signal.

A confocal microscope filters out the out-of focus light with a pinhole. This improves the image quality and provides an opportunity to perform three dimensional scans of the specimen. While the entire field of view is illuminated, and the fluorescent molecules in it are excited, the emission signal from only those molecules are collected that are in the focal plane, see Figure 1.6 for a simple schematic of a confocal microscope.

The principle of a confocal microscope is that the illumination and the detection optics are focused on the same spot in the specimen. For each plane the specimen is imaged by moving the focal point across the sample. The focal plane is adjusted to obtain a three-dimensional image. Some of the important optical components of the confocal microscope are, a laser, dichroic mirror, objective, pinhole and a detector. The laser provides the illumination light corresponding to the excitation wavelength of the fluorophores in the specimen. The dichroic mirror reflects the light towards the microscope objective. The excitation light overfills the back aperture of the objective and is focused on a plane in the sample. Practically, all the light is not tightly focused, rather there is a region of illumination around the focus. The fluorophores in this region of illumination are excited and emit fluorescence signal at a higher wavelength. The same objective col-

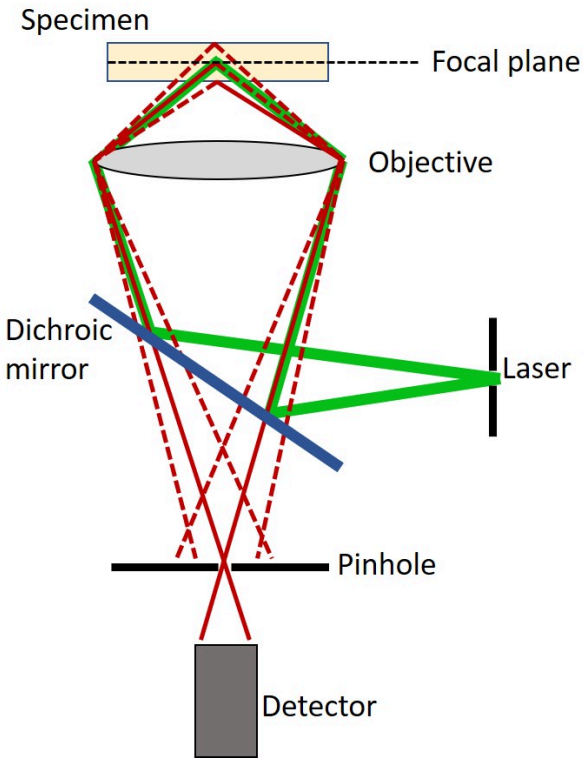

Figure 1.6: Schematic of a confocal microscope. The excitation light (green) is reflected by the dichroic mirror to focus at the specimen. The fluorescent molecules in the specimen are excited by the incident. The fluorescence emissions from all the molecules are collected by the same objective. The fluorescence wavelength is transmitted through the dichroic mirror. A carefully placed pinhole rejects the out-of-focus signal (dashed red lines) and allows only the signal from the focus (solid red lines) to reach the detector.

lects the fluorescence signal. Since the wavelength of emission signal is different from the excitation wavelength, the dichroic mirror transmits the light through it. The pinhole after the dichroic mirror rejects the light from out-of-focus and passes only the light from the focus to the detector.

To obtain confocal images of GUVs, its membrane is doped with fluorescently labeled lipids, or the proteins to be reconstituted are fluorescently labeled. In this thesis, both of these methods were used for different experiments.

1.6 Overview of the thesis

This thesis is about reconstitution of proteins in GUVs using anchor lipids and by detergent assisted insertion of the protein into the lipid bilayer. The thesis is divided into six chapters. Chapter 1, which is about to end here, is an introduction to the field of synthetic biology, the system of my study and the techniques used. Chapter 2 describes the microfluidic device that I have designed and how it can be used for different experiments. This device has been used for most of the experiments in this thesis. In chapter 3, I demonstrate that the choice of protocol to prepare GUVs affects the membrane composition. Chapter 4 shows how the microenvironmental factors such as lipid composition, pH and presence of metal ions can affect the binding of proteins and the fluorescence of the fluorophore. Chapter 5 describes a modification of the anchor lipid used in chapters 3 and 4, and shows that this modification forms a stronger bond between the protein and the lipid. Finally, chapter 6 is about detergent assisted reconstitution of atlastin proteins into the GUV membrane.

Chapter 2

Microfluidic device

Introduction

Microfluidics represents a recently developed technology to manipulate small amounts of fluids using channels of dimensions in micrometers. The small microchannels are advantageous as they reduce reagent usage and provide the option of controlling the volumes and reagent mixing times. The field of microfluidics gained popularity in the 1990s and has become more and more important for multidisciplinary applications[52]. Microfluidics can integrate sample preparation, reactions, experimental characterization, and data collecting in the same device. Inside the microchannels, fluids behave differently compared to their behavior on the macroscopic scale. In the micro-regime, the effects related to the viscosity of the fluid dominates over the effects related to inertia. One dimensionless quantity to describe the physics in this regime is the Reynolds number. It is the ratio of inertial force to viscous force. The field of microfluidics has many applications, such as organ-on-a-chip, immobilising and studying *C. elegans*[53], manipulation of droplets[54], synthetic biology research[55], and many more.

One of the major developments and applications of microfluidic technology is the organ-on-a-chip[56] (OOAC). These combine a range of chemical and biological concepts to simulate an organ-like environment. Human physiology is complex and it is important to study dysfunctions and patho-

genesis for further prevention and treatment of diseases. Since the throughput of drug developments is very low in the *in vivo* experiments, scientists use two-dimensional (2D) cell cultures to simulate organs. This has its drawbacks as it is not an accurate model for the three-dimensional tissues and organs and often requires further experiments in model animals[56]. However, the physiology of these animal models and the human body is different, hence the drug-organ interactions are not reproducible. OOAC enables scientists to regulate key parameters such as concentration[57], shear force[58], drug interactions[59], cell patterning[60] and tissue boundaries[61]. Using microchannels, target cells are delivered to pre-designated locations and maintained over time with the supply of nutrients and waste disposal. These cell cultures are monitored by either coupling a sensor with the output component or by imaging using a light microscope[62]. One way of preparing an OOAC is via stem cell cultivation. Stem cells have the potential to mature and differentiate into more than one kind of specialized cells. These could be extracted from the human body without causing much harm[63]. Some of the major OOAC are liver[64], lungs[65], kidney[66], heart[67] and intestine[68].

Like the OOAC, drug screening can also be performed on small model organisms using microfluidic traps. *C. elegans* are primary model organisms to study aging[69]. Microfluidics provides a platform for automation of experiments to immobilize the worms, image and acquire data. This also enables users to monitor the a large number of worms over weeks. Formation and manipulation of uniform micron-sized droplets can also be achieved by using microfluidic devices.These droplets can be used to encapsulate cells for high-throughput single cell analysis. The cells can undergo lysis and multiple enzymatic reactions for further study. The droplets can also act as the confinement chambers for polymerase chain reaction (PCR) for nucleic acid amplification[70] and undergo thermal chain reactions. The droplets can also be used to make lipid vesicles and further the research in the making of artificial cells[71].

The microfluidic chips can produce large number of monodisperse giant vesicles in a short time[72]. Some of these methods are based on assembly

of bilayers on droplets stabilized by surfactant[54], microfluidic jetting[73] and double emulsion[72]. Small liposomes and some ions are introduced in the droplets stabilized by surfactants using a microfluidic chip. The ions promote the breaking and resealing of the small vesicles into giant vesicles. With this method, functional proteins and ions can be sequentially introduced in the vesicles by picoinjection. In the end, free standing giant vesicles can be separated from the droplets. One of the disadvantage of this technique can be some surfactant could potentially remain the in the lipid membrane. In the microfluidic jetting technique, a microjet blows the inner solution on a planar bilayer and deforms it. Similar to blowing bubbles, the inner solution fills the bilayers and detaches it. In the double emulsion technique, a water-oil-water emulsion system is made using T-junction microchannels. The oil layer has premixed lipids that rearrange to form the bilayers of the vesicle.

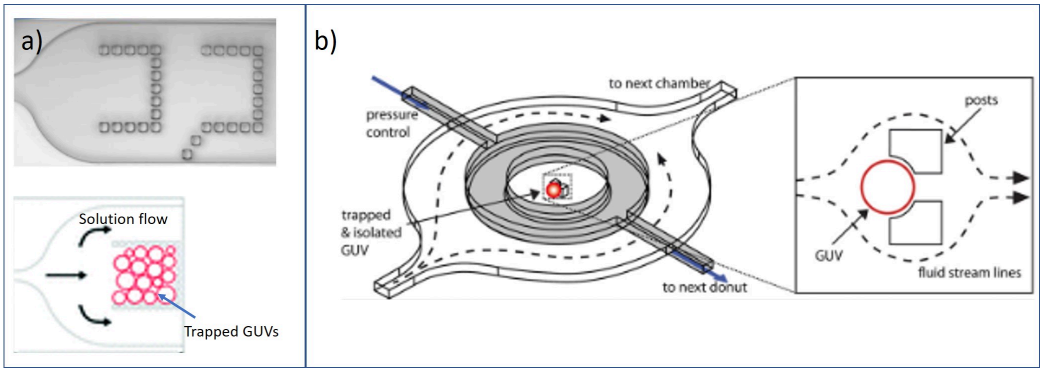

Figure 2.1: Designs of microfluidic trapping devices. a) Bucket like traps, image adapted from Yandrapalli and Robinson[74] and Zhao et al.[75]. Donut like traps, image adapted from Robinson et al.[76].

The microfluidic devices can also used to trap and experiment on the vesicles. Some traps are used to deform the vesicles by sequentially trapping and pushing the vesicle through constricted walls to study the effect on the protein in the vesicle lumen[21]. Vesicles can be selected based on their size for further experiments using a microfluidic device[77]. Some vesicle trapping devices include bucket like traps made of poles separated by small

distances to ensure proper the flow of aqueous solution around the GUV[74], double layered donut like traps to isolate and control pressure around GUVs to study transport through membrane pores[76], see Figure 2.1. In all these devices, the vesicles are trapped in the direction of flow of the solution. This creates an asymmetry between the inner and outer leaflet of the bilayer because the flow of the aqueous solution is only in contact with the outer leaflet during the solution exchange. If the vesicles are trapped in the dead-end side channel, perpendicular to the direction of the flow, they can be shielded from the flow of solution and the solution exchange around the GUV occurs only via diffusion[22]. Such a design diminishes perturbations caused by the flow on the vesicle membrane which facilitates the measurements of sensitive parameters such as the spontaneous curvature of GUV membranes. The device used in my work is an improvement of the device mentioned in[22]. The new version of the device has two parallel main channels and more dead-end side channels. The size and volume of the device is also reduced to 2.5 μL which leads to smaller production costs as multiple devices can be fitted on one cover-slip. The small size of the channels makes it possible to use the microfluidic device without any pumps. The required flow of the solution can be achieved by using just the height difference between of water columns in small reservoirs attached to inlet and outlet of the device (see Figure 2.5).

2.1 Device fabrication

The material of the microfluidic device should be carefully chosen on the basis of the final application of the device. Some of the common materials used are silicon, glass, ceramics and certain polymers. Each of the material has advantages and disadvantages associated with its use. The silicon devices have semiconducting properties but are not transparent which makes them difficult to use for *in situ* imaging. The ceramic devices are resistant to most chemicals but are also very brittle in nature, that is a disadvantage for their production, handling and cleaning. Glass shares its chemical inertness and brittleness with the ceramic material. Due to the transparency,

glass is easy to integrate into devices for optical imaging. Polymers provide a more versatile platform for sculpturing the devices and can be chosen to be biocompatible. Such biocompatible polymers are gaining popularity for the manufacturing of microfluidic device. Some of the popular polymers are polydimethylsiloxane (PDMS), polymethylmethacrylate (PMMA), fluoropolymers, cyclo-olefin polymers and copolymers (COPs/COCs), and Thiol-ene polymers (TEs). PDMS is an elastomer used for molding the devices. It is transparent, permeable to gases, compatible with biomimetic systems and has very low autofluorescence. These properties make it ideal to use in biological experiments like cell culturing, cell screening, detection of proteins, DNA and diagnosis of diseases. However, organic chemicals such as hexane, chloroform and toluene adsorb on the surface of PDMS hence it can not be used for systems that involve these organic chemicals. The other previously mentioned polymers have slightly different solvent compatibility. All these materials can be combined to make a hybrid microfluidic device with desired properties.

As previously described, there is a plethora of material to make a device. Since all these material have different physical and chemical properties, the fabrication processes for the devices made of these material are also different. Fortunately, over the last 50 years many techniques for microfluidic device fabrication have been established. The devices can be made by either removing or deposition of material. Chemical, mechanical and laser based techniques are used for this purpose. Manufacture of silicon and glass based devices can be achieved by etching using a corrosive chemical such as hydrofluoric acid. This method is problematic due to environmental concerns. An electrochemical discharge is also used for chemical or thermal etching of non-conductive material. Mechanical processes such micromachining, micromilling and urtrasonic machining are used for silicon, glass and polymer based devices. One of the main drawbacks of the mechanical processes is the reduced precision. Injection molding and hot embossing are used for thermoplastic based devices. Molten plastic is injected or poured into heated casts of devices and allowed to cool down and take the shape of the cast. Soft lithography is popular for elastomeric de-

vices such as PDMS. In this method, initially a hard stamp cast is created and then a liquid polymer solution is poured over it. Once the elastomer has polymerised by heat curing, it is removed form the hard stamp and used. The main advantage of soft lithography is the number of replicas that can made from the same cast. Since the elastomer is a soft material, the resulting device is prone to deformation. Laser based techniques include engraving microstructures by thermal degradation and photolithography. In photolithography, photopolymers are crosslinked using focused lasers or UV lamps. A combination of these techniques can also be used for making devices.

For the fabrication of the microfluidic device used in my work, I used soft photolithography. The hard stamp or the wafer was prepared using an epoxy based negative photoresist, SU-8. The negative photoresist crosslinks on exposure to UV light while the rest of the polymer remains fluid and can be removed by rinsing. The device is designed using a computer- aided design software (AutoCAD). The UV exposure was performed through a film mask from Micro Photolithography Services. The design is printed transparently on a dark plastic film mask. The SU-8 photoresist is spin coated on a quartz substrate. The speed and time of spin coating is programmed according to the Microchem manual for a particular height of the channels. The photomask film is placed over the SU-8 coated substrate and exposed to UV light. This procedure crosslinks the region on the substrate that is under the transparent part of the design. This is followed by steps of soft and hard baking on hot plates as specified in the manual. The excess SU-8 is rinsed using iso-propyl alcohol. To prevent unwanted adhesion of PDMS on the wafer, it was silanised by placing it overnight inside a desiccator with 50 μL of 1H,1H,2H,2H-perfluorodecyltrichlorosilane.

Once the wafer is ready, PDMS and the crosslinker are mixed in the ratio of 9:1. The mixture is degassed by placing it in a vacuum dessicator for 30 mins. Then the mixture is poured over the wafer that was produced in the previous step. The whole setup is again placed in the dessicator to remove the bubbles that got introduced while pouring the PDMS. After this the whole setup is placed in an oven preheated to 90°C for 3 hours. Once

the PDMS has cooled down, the wafer is carefully removed from the PDMS cast. The devices are cut out and shaped using a sharp and heavy knife. Holes of 1.5 μm are made using biopsy punches for the inlet and the outlet of the device. At this point, the PDMS has the negative of the design on the wafer. The microchannels are formed but they are still open from one side. This open side of the device is covered by thin glass coverslides. Clean glass slides and the PDMS casts are treated using plasma for a minute. They are then stuck together and placed on a hot plate heated to 60°C for further strengthening of the bonds and ensuring that no leakage can occur from the channels.

2.2 The microfluidic trapping device

2.2.1 Design

There are several microfluidic devices available for trapping GUVs and performing experiments. One of the major advantages of the proposed device is the shielding of the GUVs from the flow of the solution in the main channel. There are reports of GUVs dividing due to the shear forces of the solution exerted on them. In the device described here, the GUVs are positioned at a distance and perpendicular to the direction of the main flow. The solution exchange in the side channels occurs only by diffusion, as shown in Figure 2.3. The side channels are 250 μm long and 100 μm wide. The height of the device is approximately 80 μm. There are 56 of such side channels. The volume of approximately 2.5 μL and the complete solution exchange from the side channels takes place in about 2 minutes. The total dimension of the device is 18 mm in length and 3 mm in width. This makes it possible to accommodate around five of the devices on one cover slip, thereby reducing the cost and time for making each device, see Figure 2.2.

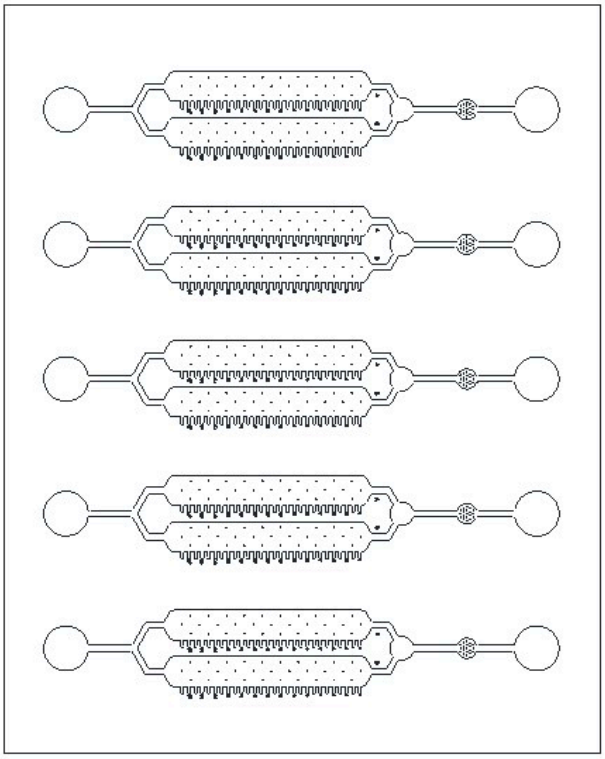

Figure 2.2: The microfluidic chip has five devices. All the devices can operate independent of each other. Such a design reduces the cost and time for device fabrication and makes it easier to perform experiments on parallel devices at the same time.

2.2.2 Operation of the microfluidic device

Since the microfluidic device described here is used for imaging GUVs, it is passivized by coating with bovine serum albumin (BSA). Cut-out pipette tips are used as reservoirs for the solution, (see Figure 2.5). A volume of 50 μL of 2 mg/mL BSA solution is introduced in one of the reservoirs and the device is placed in a swinging bucket centrifuge. The device is centrifuged for 10 min at 900 g to ensure proper coating by BSA and to push out the air bubbles. This is followed by removing the excess BSA from the two reservoirs. The BSA inside the device is removed by successively rinsing four times with the solution that is used as the exterior solution for the GUVs. The rinsing step is important to remove excess BSA so that it

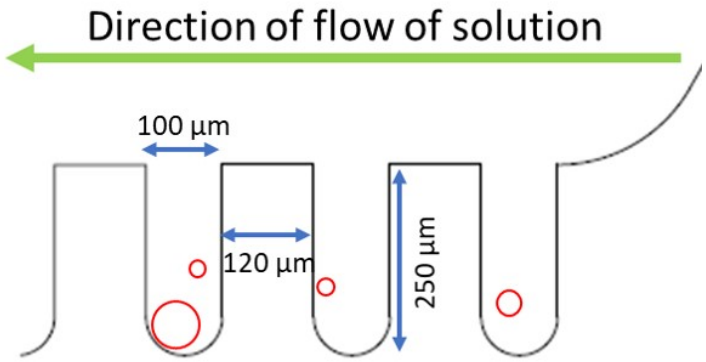

Figure 2.3: Decoupling the GUVs from the hydrodynamic flow in the microfluidic device. The GUVs are trapped in the dead-end channels while the solution flows through the main channel. The solution within the side channels is exchanged by diffusion. The device can be mounted on an inverted microscope for simultaneous imaging.

does not interfere with the experiments that follow. The final solution to be left in the device must be equiosmolar with the solution that is inside the GUVs and of lower density. The low density will assist the GUVs to be trapped in the dead-end side channels.

After rinsing out the BSA, the microfluidic device is ready to be use for experiments. There are two ways to perform the experiments, either the liquid columns in the two pipette tips can be used to drive the flow of solution, or a syringe pump can be connected to the outlet to draw the solution from the reservoir at the inlet. See the illustrations in Figure 2.5 for the two modes of operation of the microfluidic device. Using a syringe pump for the operation allows for precise control over the flow rate of the solution in the microfludic device. Whereas, the operation of device without the pump offers little control. The next steps mentioned in this section are for the operation with the pump. Most of the experiments performed in this thesis were also performed using the pump. This microfludic device reduces the total volume of samples required for the experiment.

The GUVs are introduced in the inlet reservoir. The inside solution of the GUVs is osmotically balanced with the outside solution, but it is of a

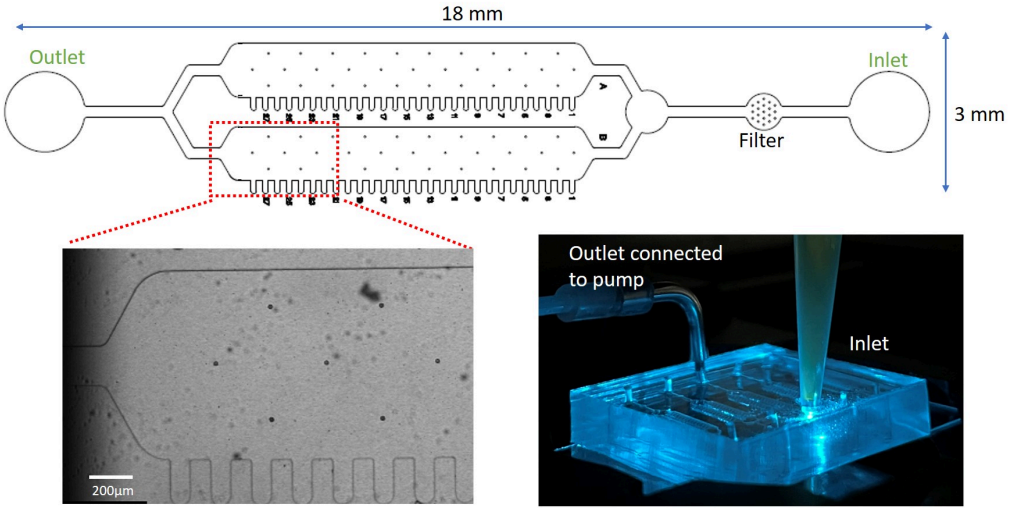

Figure 2.4: Design of microfluidic chip: The device has two main channels parallel to each other. The filter (next to the inlet) traps any dirt particles from entering the main channel. As shown in the (bottom,right) panel, a pipette tip is used as the reservoir for the solution at the inlet. A syringe pump connected to the outlet draws the solution from the reservoir to the outlet via the main channels. The side channels trap the GUVs; and (Bottom, left) Bright field image showing and magnifying the portion of the chip within the broken red frame. The solution within the side channels is exchanged by diffusion from the main channel. The complete solution exchange including the side channels takes about 3.5 mins.

higher density. As density difference ensures that the GUVs to settle at the bottom of the reservoir. Once the pump starts drawing the solution, the GUVs are drawn into the main channel (typical speed for loading vesicles 20-50 μL/hr). The pumps is stopped and the device is oriented vertically for 15-20 minutes. For the vertical orientation, the chip can be temporarily fixed to the wall with adhesive tape. The GUVs slowly fall into the side channels. If the overall yield of the GUV is low, this process of loading the GUVs in the side channel could be repeated multiple times. The device can be placed on an inverted microscope for further experiments. These experiments are mainly based on the exchange of the outer solution or introduction of other molecules like proteins (typical speeds for solution ex-

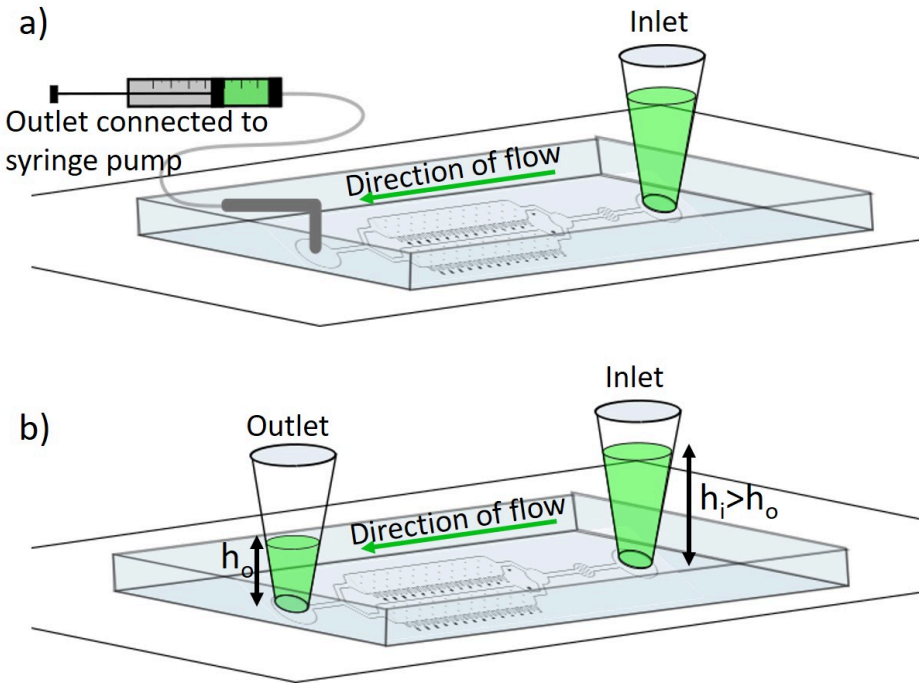

Figure 2.5: Illustration to use the microfluidic device for the experiments. The microfluidic device can be operated in two ways. In both setups, a pipette tip is used as a water reservoirs, the outlet could be connected to **a)** a syringe, that is connected to a pump to control the flow of the solution in the device, or **b)** to another reservoirs. In this case the direction and flow of the solution can be adjusted by the height of the water columns.

change 50-200 μL/hr). The GUVs can be directly imaged while exchanging the solution. As a consequence, it is possible to screen GUVs and perform experiments on single vesicles, especially when monitoring the change in shape of the GUV.

As mentioned above and shown in Figure 2.5, the device in can be used with out a pump. The difference in the water height in the two reservoirs is sufficient to drive the flow of solution. If the study does not depend significantly on the speed of solution exchange, then using the device without the syringe provides a simpler experimental setup. The microfluidic chip consists of five parallel devices that are independent of each other (2.2). Multiple independent experiments can be performed and in the parallel

devices at the same time with ease.

2.3 Examples of experiments

The ease of using the newly developed microfluidic device described in this thesis makes it adaptable for various experiments, some of which are described in this section. As previously mentioned in this chapter, the exchange of solution can be achieved either by a pump or simply by the difference in the water column height. Since the device is made on a thin glass coverslide, it can be placed on an inverted microscope. As a consequence, this device makes it possible to image the same vesicles throughout the experiment. In all these experiments, the vesicles were trapped in the side channels and the outer solution was exchanged. The trapped vesicles were imaged using a laser scanning confocal microscope.

2.3.1 Deducing the dissociation constant

The newly developed microfluidic chip has been used for deducing the dissociation constant for the binding of a fluorescent protein to a GUV membrane. The dissociation constant provides a quantitative measure for the affinity of the protein to the membrane. There are various experimental setups to measure dissociation constant such as flow cytometry[78], surface plasmon resonance[43] and fluorescence correlation spectroscopy[79 80]. In my experimental setup, the GUVs are trapped in the microfluidic device. The outer solution of the GUV is exchanged with increasing concentrations of the fluorescently tagged protein. The fluorescence intensity on the GUV membrane is quantified using the image processing software, FIJI (an open source platform for image processing). The measure intensity on the membrane is then plotted versus the concentration of the fluorescent protein. The resulting curve is fitted to a model for binding. Then the dissociation constant of the membrane- protein interaction is deduced from fitting the data. More about such interactions is described in the further chapters (chapters 4, 5).

As shown in the Figure 2.6, the dissociation constant for the interaction between 6H-GFP and vesicles composed of POPC:cholesterol and doped with

3% DGS-NTA(Ni) lipids is $(37.5 \pm 7.5)nM$.

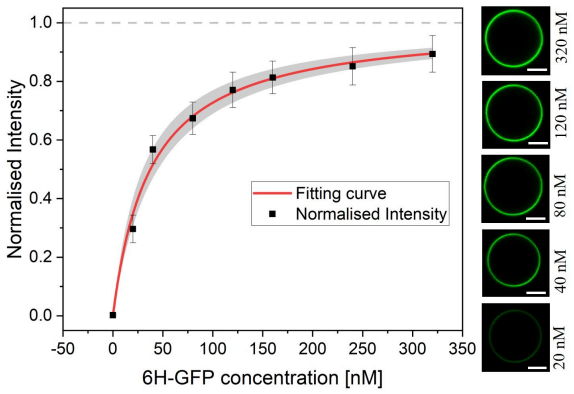

Figure 2.6: Normalised membrane fluorescence intensity *versus* molar concentration of 6H-GFP. The reperesentative images of the GUVs are shown on the right. Scale bar: 10 μm. The vesicles composition is POPC:Chol and doped with 3% of DGS-NTA(Ni) lipid. The GUVs trapped in the microfluidic device are exposed to increasing concentrations of 6H-GFP. The fitting curve in red leads to a dissociation constant $K_d = (37.5 \pm 7.5)nM$. The grey shaded area represents the confidence interval for K_d

2.3.2 Effect of sugar asymmetry on vesicle morphology

The vesicle morphology can be modified by exposing the two leaflets of the vesicle bilayer to different types of sugar compositions.[81]. Solutions across the vesicle are osmotically balanced by using the same number of osmolytes across the membrane. In this experiment, the vesicles composed of POPC:cholesterol (8:2) were prepared in 100 mM sucrose solution. These vesicles were trapped in the microfluidic device. The osmolarity of the outer solution was increased stepwise by increasing the concentration of sucrose in the reservoir of the device to 140 mM. Ths osmolarity increase caused the vesicle to deflate, increase its excess area, and change the shape from a sphere to a prolate. The asymmetry across the membrane is created by exchanging the sucrose on the outside for 140 mM glucose solution. This asymmetry generates a spontaneous curvature. The combination of volume changes and spontaneous curvature generation gives rise to various mor-

phological changes of the vesicle.

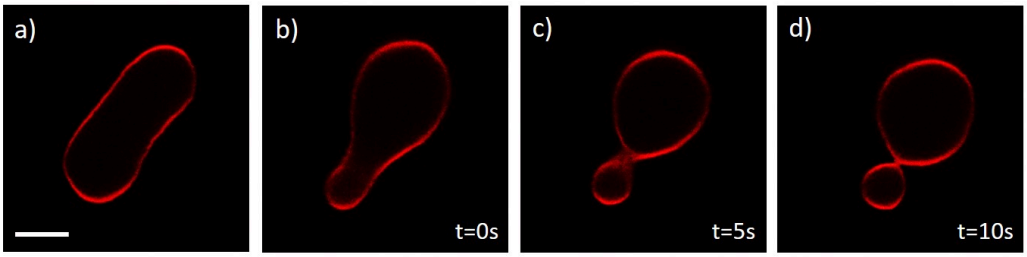

Figure 2.7: Vesicle shape transformation from prolate shape to a dumbbell shape with a closed membrane neck. Vesicle composed of POPC:chol (8:2) enclosing 100 mM of sucrose solution. a) The concentration of sucrose is increased stepwise to 140 mM. During this osmotic deflation procedure, the volume of the GUV is reduced and the vesicle then attains a prolate shape. b) The sucrose outside the vesicle is exchanged for glucose increasing the spontaneous curvature and transforming the vesicle into a pear-like shape. The time stamp t=0 s corresponds to 15 min after the initial exchange of sucrose by glucose. c) Closure of the membrane neck is induced due to the asymmetry across the membrane. d) Dumbbell shape of the vesicle with closed neck. Scale bar: 10 μm

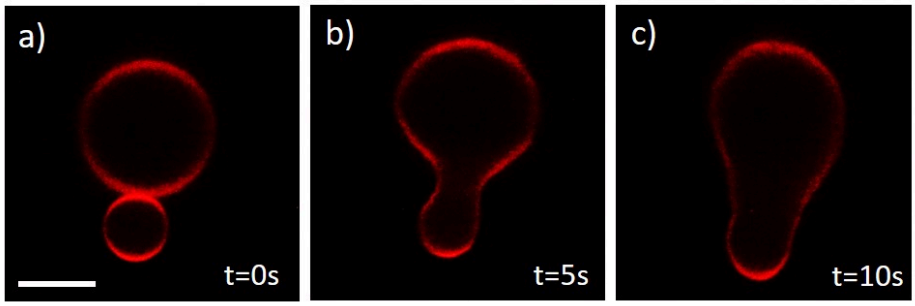

Figure 2.8: Vesicle shape transformation from closed neck dumbbell to pear-like shape. Vesicle composed of POPC:chol (8:2) enclosing 100 mM of sucrose solution. a) The glucose outside the vesicle is exchanged for sucrose, decreasing the asymmetry. The time stamp t=0 s corresponds to 7min after the beginning of the exchange of sucrose from glucose. b) The neck opening is induced due to the regaining the symmetry of sugar across the membrane. c) Pear-like shape of the vesicle. Scale bar: 10 μm

As shown in Figure 2.7, the vesicle shape changes from a prolate to a

dumbbell with a closed neck. Using the microfluidic device for such experiments is advantageous as one could check for the opposite effect on the same vesicle. As shown in Figure 2.8, the vesicle goes back from the closed neck dumbbell shape to the pear like shape, by reversing the asymmetry caused by the two sugars. The latter experiment demonstrates that the formation of a closed neck represents a reversible shape transformation.

2.3.3 Effect of pH on vesicle morphology

As previously described, lipids have a hydrophilic head group and a hydrophobic tail. In a vesicle, the head groups of the two leaflets are exposed to aqueous solutions. Once a vesicle is formed, only the aqueous solution on the outside of the vesicle can be directly controlled. The lipid head groups could be zwitterionic or charged. For this experiment, I have used a lipid mixture of POPC and POPG. POPC has a zwitterionic head group whereas POPG is negatively charged with a pKa of 3.5[82]. When the pH is lowered below 3.5 the head group get protonated and the head group area decreases.

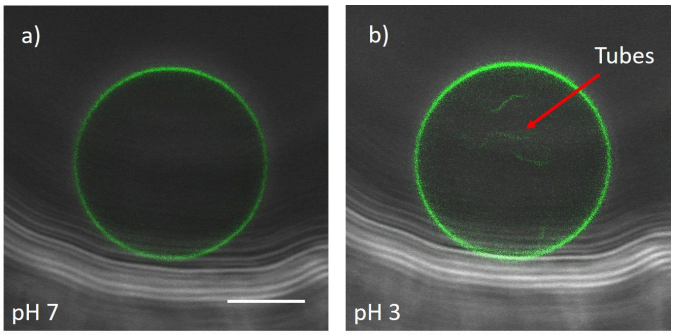

Figure 2.9: Overlay of phase contrast and fluorescence image a vesicle at different pH. The vesicle composition is POPC:POPG 8:2, 1% NBD-PG for the fluorescence. The inside solution of the vesicle is 200 mM sucrose at ph 7. The vesicle was trapped in the side channel of the device. The outer solution of the vesicle was exchanged with a mixture of 180 mM glucose and 20 mM sucrose. The pH of this outer solution was changed from pH 7 (left) to pH 3 (right). The osmolarity of the inside and outside solutions of the vesicle was balanced and kept constant throughout the experiment. Tubes start to appear when the pH 7 is reduced to pH 3. Scale bar: 10 μm

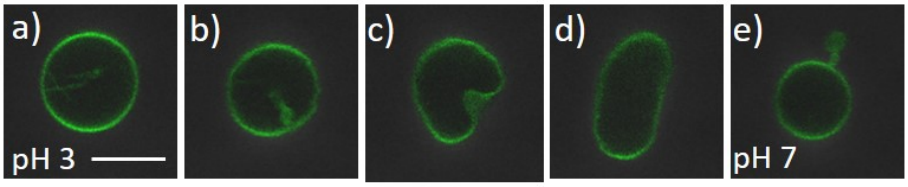

Figure 2.10: Overlay of phase contrast and fluorescence image of a vesicle at recorded during changing the pH from pH 3 to pH 7 (a to e). The vesicle composition is POPC: POPG 8:2, 1% NBD-PG for the fluorescence. The vesicle was trapped in the side channel pH 7 and the solution was exchanged to pH 3 to obtain the GUV with inward tubes (a and b). The outer solution was again exchanged with a solution at pH 7 and outward tubes appeared (e). The change in the vesicle morphology was recorded while changing the pH of the outer solution. Scale bar- 10 μm

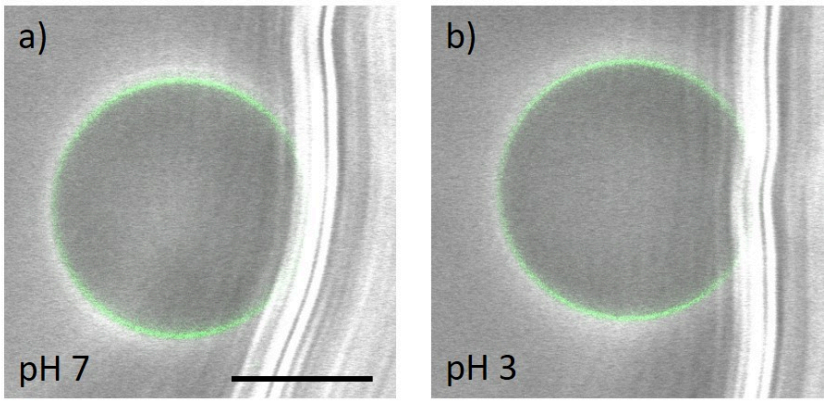

Figure 2.11: Overlay of phase contrast and fluorescence image a vesicle at different pH. The vesicle composition is POPC and 1% NBD-PG for the fluorescence. The inside solution of the vesicle is 200mM sucrose at pH 7. The vesicle was trapped in the side channel of the device. The outer solution of the vesicle was exchanged with a mixture of 180mM glucose and 20mM sucrose. The pH of this outer solution was changed from pH 7 (left) to pH 3 (right). The osmolarity of the inside and outside solutions of the vesicle was balanced and kept constant throughout the experiment. No tubes observed when the pH 7 is reduced to pH 3. Scale bar: 10μm

Vesicles composed of a lipid mixture of POPC: POPG in the ratio of 8:2 and 1 mol% NBD-PG (a fluorescently labeled lipid) were prepared in 200 mM sucrose at pH 7. The vesicles were trapped in the microfluidic de-

vice and the solution on the outside was changed to a mixture of 180 mM glucose and 20 mM sucrose at pH 7. The pH of the outer solution was reduced to pH 3. As shown in Figure 2.9, inward pointing tubes were observed. These tubes could be reversed as well by changing the pH of the outer solution back to pH 7, as shown in Figure 2.10. Control experiments with POPC and 1 mol% NBD-PG were also performed. No tubes were observed on exchanging the pH of the outer solution to pH 3, see Figure 2.11.

2.3.4 Vesicle shape oscillation with Min proteins

In an *E. Coli* cell, a system of Min proteins helps to determine the center of the cell. This results in two equal daughter cells after cell division. The Min system consists of three different proteins, MinC, MinD and MinE. The MinD is an adenosine triphosphatesase (ATPase) that attaches to the membranes and directs Min C towards the membrane. MinE competes with MinC for binding to the MinD and stimulates hydrolysis of ATP by MinD. This cycle continues in the cell cytoplasm and the chemical gradient is created in the cell. The pole-to-pole oscillation of the Min proteins marks the center of the cell. Other proteins such as FtsZ then attach to the center and induce the necessary constriction force for cell division[83].

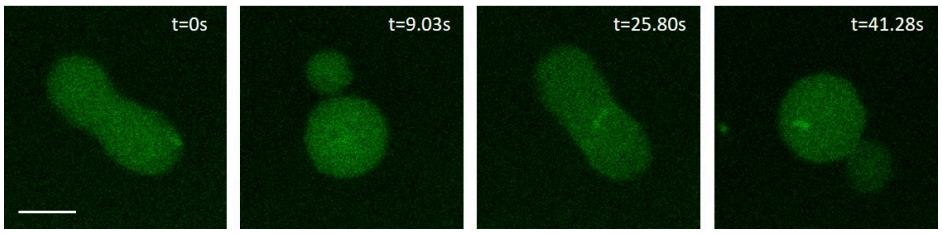

Figure 2.12: Fluorescent image of a vesicle encapsulating the preoteins MinC, MinD, MinE and ATP. The vesicle composition is POPC: DOPG (4:1). The image with time scale t=0 is recorded after the deflation of the vesicle by increasing the concentration of glucose outside. Scale bar: 10 μm Image courtesy: Lars Henning Hansen

The reconstitution of the Min proteins system has advanced the understanding about such pole-to-pole oscillation. The *in vitro* encapsulation of the Min proteins in vesicles also induces shape changes in the vesicle[19].

The oscillation of the in proteins in a deflated vesicle cause a cycle of closing and opening of membrane necks. As shown in Figure 2.12, a vesicle encapsulating the min protein undergoes shape oscillation from a prolate shape to a closed neck dumbbell. The MinD protein in labelled with GFP to track the protein oscillation. This experiment was also performed in the microfuidic device with the idea to introduce another protein machinery to cleave the closed neck in during the formation of the dumbbell.

2.4 Conclusion

The microfluidic device presented here has advantages over the other devices that are shown in Figure 2.1. The vesicles are trapped perpendicular to the flow direction of the solution which implies that they are shielded from the shearing forces of the aqueous solution. The vesicles are trapped by orienting the device vertically. Once the vesicles are trapped in the side channels, the device is placed on the microscope. The side channels are marked with numbers so tracking each vesicle becomes simple. The net volume of the device is approximately 2.5 μL.

When a syringe pump is attached to the outlet to draw out the solution from the reservoir at the inlet, the complete exchange of the solution takes place in 2 - 3 minutes. However, the device can be used even without the syringe pump by maintaining the height of the water columns. The volume of the water in the inlet reservoir should be higher than that in the outlet, causing the water to flow. In this setup, the speed of the water flow can not be quantified, nevertheless, the complete exchange of the solution around the vesicle is achieved. This improvement makes it possible to use the device for different experiments where the effect of a particular molecule on the vesicle morphology needs to be studied.

Chapter 3

Dependence of membrane composition on preparation protocol

Introduction

Most life forms have compartments that enclose the essential molecules and prevent them from spreading and mixing with the surrounding environment. Since the primordial soup is assumed to be made of formamide and water molecules[84], the first living molecules must have been in an aqueous medium. This condition imposed two constraints on the compartments: they have to confine the interior aqueous solution but at the same time, they should allow for the exchange of certain molecules between the interior and exterior solution. Amphiphilic molecules such as lipids can self-assemble to form a semipermeable membrane. The lipids have a hydrophilic head group and a hydrophobic tail. They form a bilayer sheet such that the tails are inside and facing away from the aqueous surrounding while the head groups are in contact with the surrounding solution. When these bilayer sheets close upon themselves, they form closed membrane compartments called vesicles. In natural cells, the outermost membrane made of lipid bilayer is called the plasma membrane. Depending on

the type of cell, the plasma membrane can have protective sugar groups or proteins to make it functional. The organelles inside the cells are also enclosed by lipid membranes of different compositions. The differently sized lipid compartments, ranging from nanometers to micrometers, are crucial for the maintenance and functioning of the cell.

Giant unilamellar vesicles (GUVs) are model membrane systems that form closed compartments consisting of single lipid bilayers. Each lipid bilayer divides the aqueous media into the inner and outer compartments. The size of the GUVs is in the order of micrometers. An optical microscope can be used to image and study these micrometer-sized GUVs. Since these GUVs are made of synthetic lipids, there are multiple options for selecting the lipids and preparing the vesicle with different compositions. The lipids can be chosen with charged head groups or neutral headgroups to mimic different membrane systems found in nature. The GUVs can be made with symmetric bilayers (both leaflets with the same compositions) or with asymmetric bilayers (the two leaflets have different compositions). The aqueous solution can also contain various ions or sugars of choice.

Several protocols have been developed to prepare the GUVs including swelling on a substrate, sequentially assembling each leaftlet of the bilayer or droplet stabilized GUVs. The protocols for swelling of lipid bilayers, involve three main steps: spreading the lipids on a clean substrate, addition of hydrating aqueous solution and harvesting the vesicles[85,86]. For the sequential assembly of the bilayers, one lipid leaflet is formed as a monolayer on a water-oil interface. The other leaflet is added on top of it in the form of emulsion droplets. Using a centrifuge, the emulsion droplets are pushed across the monolayer formed in the previous step. This way free floating GUVs are obtained. This protocol is very useful for making asymmetric GUVs[87]. The droplet stabilized GUVs trap large unilamellar vesicles (LUVs) made of negatively charged lipids with positively charged metals ions in a water droplet that is stabilized by detergents which are also negatively charged. The electrostatic interactions between the detergent, metal ions and the LUVs, cause the LUVs to rupture and reseal to form GUVs, close to the surface of the droplet. The GUVs can be peeled out of the droplet

using destabilizing agents that break the detergent layer[54,88]. For a sketch regarding the formation of GUVs using various protocols, see Figure 3.1. All the protocols have advantages and disadvantages associated with them. For preparing GUVs with electroformation[89], aqueous solutions with high salt concentrations cannot be used. For hydrogel assisted swelling of the GUVs, the hydrogels get incorporated into the bilayer membranes, changing the physical properties of the membranes[90]. The emulsion transfer protocol depends primarily on the partition of the lipids between oil and water. Hence this protocol requires a long optimization process when a new lipid is used. Free floating GUVs can be extracted from the droplet stabilized GUVs but small amounts of surfactant in the membrane can alter the membrane properties. A careful study of the advantages and disadvantaged associated with each protocol is necessary before choosing a particular protocol for the experiments.

The spontaneous swelling technique was introduced by Reeves and Dowben in 1969, when they observed cell-sized GUVs grown form pure phospholipids deposited on glass surface by controlling the hydration[91]. Their protocol started with uniform spreading of lipids dissolved in organic solvents on a flat-bottom flask. The organic solvent was removed by drying under nitrogen, ensuring that the lipid solution isn't agitated by the nitrogen. Aqueous solutions containing sugars or ions are added on top of the lipid film and left undisturbed for the lipid bilayers to transform into vesicles. This work concluded that the formation of GUVs occurs only when the hydration step is carried out in a defined and controlled way. The combination of factors such as osmotic pressure, electrostatic interaction between the lipid films and hydrophobic interactions drive the formation of free floating GUVs[92]. It takes very long to obtain vesicles with this technique. Sometimes the process of swelling can take as long as 24-48 hours. Oxidation of the lipids is a major concern when using this protocol and waiting for so long.

In this thesis, I have used PVA assisted swelling and electroformation on different conductive surfaces(Indium Tin Oxide, ITO glasses and Pt wire). Both techniques represent improvements of the spontaneous swelling pro-

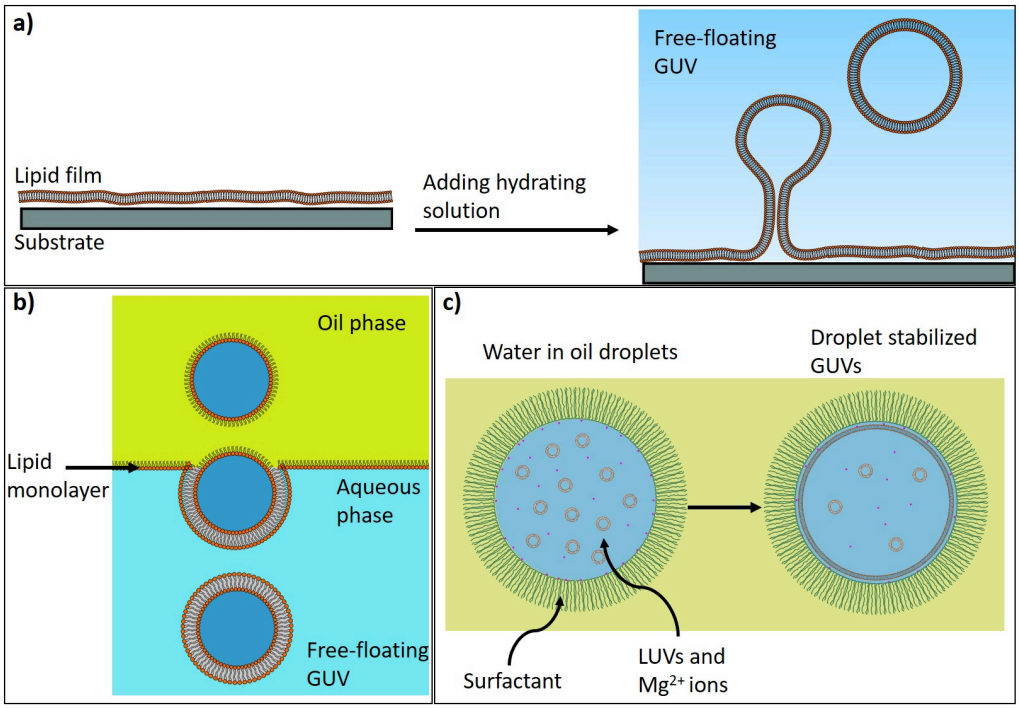

Figure 3.1: Different preparation methods for making vesicles: **a) Swelling on substrate**: The lipid film is dried on a substrate and a hydrating solution is added on the top. The aqueous solution swells the lipid film to form free-floating GUVs. For the protocol with spontaneous swelling ,the substrate could be a non-reactive surface like Teflon, glass or silica beads. For PVA assisted swelling, the substrate is dry PVA. For the electroformation protocols, the substrate is a conductive material such as Platinum wires or ITO coated glass. **b) Emulsion transfer method**: A water-in-oil emulsion is formed with the lipids forming the inner leaflet of the vesicle. The outer (second) leaflet is assembled as a monolayer on an oil- water interface. The emulsion is pushed through the lipid monolayer to form free floating GUVs. **c) Droplet stabilised GUVs**: Negatively charged surfactants are used to stabilize water-in-oil droplets. The aqueous solution inside contains negatively charged LUVs and positively charged magnesium ions. Due to electrostatic interactions LUVs rupture and reseal to form droplet stabilized GUVs.

tocol[93]. Including a hydrogel or applying alternating current (AC), fastens the process of swelling and reduces the time of vesicle formation to just a few hours. This chapter describes the general advantages, challenges and

optimized protocols for PVA assisted swelling and elecrtofomation on ITO glasses or Pt wire. Latter sections discuss my own research as well as results and conclusions regarding the different protocols.

3.1 Hydrogel-assisted swelling

In this protocol, the substrate for the deposition of the lipid film is a polymer-based hydrogel. When the aqueous solution is added the hydrogel substrate swells and enhances the influx of the aqueous solution in the lipid film. This method has been successfully used to encapsulate biologically relevant molecules and also for protein reconstitution in the membrane[39,94]. Different gels such as agarose, PVA[90] or PAA[95] (polyacrylamide) have been used to make GUVs without any visible defects. I have used PVA gel assisted swelling for my study because the agarose gel-swelling leads to the encapsulation of a lot of polymer in the lipid bilayers and also affects the mechanical properties of the vesicles[96 90]. The agarose gel also exhibits auto-fluorescence which interferes with fluorescence imaging.

The next subsection describes the generic protocol for making vesicles using the PVA-assisted swelling. This description includes the detailed steps of the protocol and provides tips about how to improve the quality and yield of the vesicles.

3.1.1 Protocol

The protocol for PVA assisted swelling involves four major steps: preparing the hydrogel and substrate, uniform spreading of the lipid film, adding the hydrating solution, and harvesting the vesicles. What follows is the generic protocol for making vesicles using the PVA-assisted swelling. For other hydrogels, the basic protocol would remain the same but smaller aspects such as the volume and concentration of the hydrogel, the time and the temperature for the drying of the hydrogel, the amount of lipids used, etc. could change.

1. Preparing the PVA hydrogel and the substrate

    1.1. Calculate and weigh the amount of PVA (molecular mass >150kDa)

required to make a 5% (w/w) solution in water. 1mL of 5% (w/w) PVA solution is sufficient for around 10 rounds of vesicle preparations.

1.2. Add water to the PVA and heat it to 90°C using a thermomixer for continuous shaking and mixing.

1.3. Deposit 20-40 μL of the PVA solution on the center and smear it using a pipette tip, covering an approximate 2cm $\times$ 2cm patch of the coverslide.

1.4. Dry the PVA by placing the coated coverslide on hot plate at 60°C for 30 mins.

2. Spreading the lipid mixture

2.1. Spread 4 μL of 4mM lipid mixture on the prepared PVA bed. The organic solvent can be removed by placing it under a vacuum for 2 hours.

3. Adding the hydrating solution

3.1. Make a closed chamber around the lipid-coated PVA part using a Teflon spacer and folding back clips.

3.2. Fill the closed chamber with the aqueous solution of choice and leave it undisturbed for 30 mins at room temperature. The temperature can be increased to ensure that lipids are in their fluid state.

4. Harvesting the vesicles

4.1. Gently tap the chamber to facilitate the detachment of the vesicles form the PVA bed.

4.2. Aspirate the vesicles using a pipette, ensuring not to disturb the PVA bed. This procedure reduces the PVA debris in the final solution containing the vesicles.

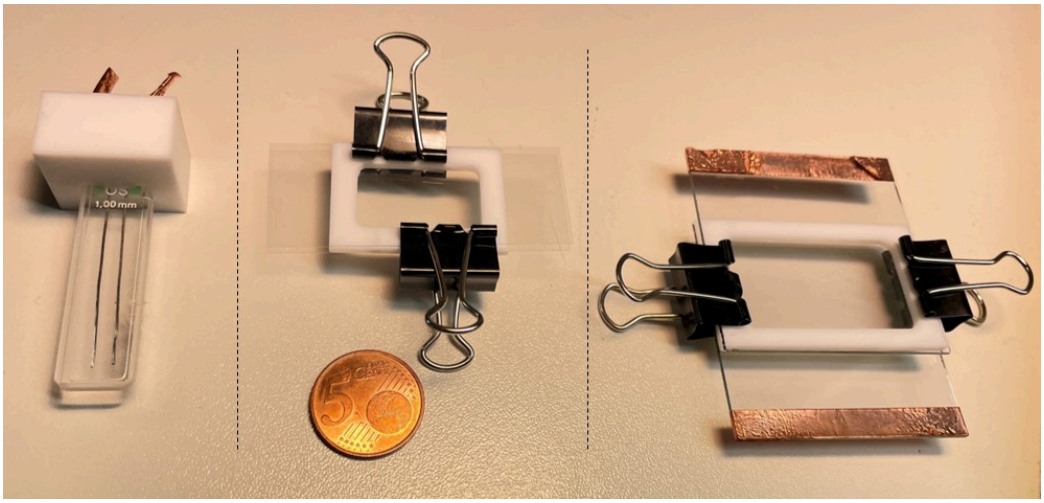

Figure 3.2: Experimental setup for preparation of GUVs using (left to right) electroformation on Pt wires, PVA assisted swelling and electroformation on ITO glasses. The chamber around the Pt wires is made using a quartz cuvette. The chambers for the PVA assisted gel swelling and ITO glass electroformation are arranged using a teflon spacer and folding-back clips. The 5 Euro cent is provided to estimate the sizes of the setups.

3.2 Electroformation

Eletroformation or electroswelling was developed by Angelova and Dimitrov in 1986[97]. Similar to the gel assisted swelling, this was an improvement over the spontaneous swelling. In this case, the hydration of the lipid film is enhanced by applying an external alternating current (AC). The lipid film is deposited on a conductive surface like platinum (Pt) wires[97 40], ITO coated glasses[98 99], stainless steel wires[100] copper electrodes[101], and carbon fiber microelectrodes[102]. Although electroformation was introduced, using the Pt wire[97], the ITO glasses have gained popularity because of the increased yield of vesicles[103]. The ITO glasses are transparent, making it possible to image the vesicle formation[104]. Under normal conditions, vesicles can be obtained with zwitterionic lipids using electroformation on ITO glass in pure water or aqueous solution with low salt concentration. However the composition of the lipids, the ionic strength of the aqueous

solution, the quality and the yield of the GUV is affected[98,105]. Steinkühler et. al[98] showed that the presence of charged lipids leads to a transbilayer asymmetry of the lipid membrane, that is indicated by the formation of tubes on deflation of the GUV. The presence of ions in physiological buffer conditions shield the electric field, hence the protocol changes a little. In the work by Pott et. al[105], it is shown that the frequency of the AC should be increased to 500 Hz to obtain vesicles in the presence of salt at physiological concentrations. Sometimes the quality of the ITO glasses deteriorates over time but it can be reversed by annealing at a high temperature[106]. Other developments for electroforming on ITO glasses involve interdigiting ITO electrodes[107], asymmetric ITO glasses[108] and growing vesicles on non-conductive polymers places on ITO substrates[99,104]. The conductive surfaces with the lipid film are separated from each other using a non-conductive spacer. The two surface are connected to a signal generator that is used to generate a sine wave AC. In the following section, the basic protocol for electroformation of vesicles is provided. The protocol can be altered depending on the geometry of the substrate, on the lipids or on the ionic strength of aqueous solution. For my project, I used the ITO coated glasses and the Pt wires.

3.2.1 Protocol

Apart from cleaning of electrodes and chambers, this protocol involves four major steps: spreading a uniform lipid film, adding the hydrating buffer, applying an alternating current, and harvesting the vesicles. This section includes detailed steps, suggestions to get good quality and yield of the vesicles. Depending on the chosen electrodes, lipid mixtures, and ionic constituents of the hydrating buffer, the temperature, voltage, and frequency of the AC, and the time of electroformation need to be optimized. The following sections is also divided into five steps. Wherever there is a difference in the protocols for the two substrates (*ITO glass* and *Pt wires*), it is explicitly mentioned.

1. Preparing electrodes and chambers

    1.1. Clean the *Pt wires*, the chambers, or the *ITO glasses* with chloroform, ethanol, and water The quality of ITO glasses deteriorates over time and use. They can be annealed by placing them on a hot plate at 150°C for 20 mins.

2. Spreading the lipid mixture

    2.1. *ITO glass*- Using a glass syringe, spread 4 μL of 4mM lipid mixture on each of the clean ITO glass surfaces which have a dimensions of about 2cm $\times$ 4cm.

    2.2. *Pt wire*- For 3cm of Pt wire, spread 8 μL of 0.4mM lipid mix by making small equidistant droplets along the length of the wire; and wait for it to dry and repeat the process until the whole volume has been deposited on the wire.

    2.3. Place resulting lipid film under vacuum for an to hour remove trace amount of chloroform.

3. Adding the hydrating solution

    3.1. *ITO glass*- Assemble a chamber using a Teflon spacer and folding back clips.

    3.2. *Pt wire*- A cuvette can be used to make a chamber with two Pt wires.

    3.3. Fill the chamber with the hydrating solution.

4. Applying alternating current

    4.1. Connect the ITO glasses or the Pt wire to an AC field generator and generate a sine wave with frequency and voltage as specified below.

    4.2. *ITO glass*-10 Hz and 2 Volt (peak-to-peak voltage) for 2 hours.

    4.3. *Pt wire*-10 Hz and 3 Volt (peak-to-peak voltage) for 2 hours.

5. Harvesting the vesicles

   5.1. Detach the vesicles from the electrodes by reducing the frequency to 5 Hz for 5 – 10 mins.

   5.2. Aspirate the entire vesicle solution using a pipette.

Figure 3.2 shows the setups used to prepare GUVs using the three protocols, electroformation on Pt wires, PVA assisted gel swelling and electroformationon ITO glasses.

3.3 Experimental methods

Membrane proteins play an important role for transmembrane ion transport , cell signaling, adhesion, etc. Therefore, to mimic cellular membranes more closely, it is necessary to biofunctionalize the synthetic membranes by membrane proteins. These proteins can be integrated in the membrane by either inserting the hydrophobic transmembrane domain of the protein in the membrane or by binding the proteins to the membranes using coordinate bonds. As introduced in the first chapter, the DGS-NTA(Ni) lipid is used to achieve attachment of proteins with a histidine rich region or a chain of histidines attached to the terminal. Like other lipids, the DGS-NTA(Ni) lipid has a hydrophobic tail and a hydrophilic headgroup. The headgroup also includes the NTA complex that forms a co-ordinate complex with the Ni^{2+} ion. This complex provides six co-ordinate bonds, out of which four are occupied by the NTA group, leaving two unoccupied sites. These two sites can be occupied by any electron donating group. In normal aqueous solutions, these sites are occupied by the water molecules. A chemical group such as the imidazole group from the side chain of His-tag can occupy the binding site of the NTA-Ni^{2+} complex. This property is harnessed to bind proteins to membranes.

In this study I used a lipid mix of phospholipid (POPC) and cholesterol in the molar ratio of 8:2, doped with 3 mol% DGS-NTA(Ni) lipid. In the literature, it is commonly assumed that the membranes of the resulting GUVs have the same composition as the lipid mixture that was used in the begin-

ning of the preparation. To investigate this assumption, I made the vesicles using three protocols, PVA assisted swelling as well as electroformation on ITO-coated glass and Pt wire. All vesicles were prepared in such a way that the inner solution contained 50 mM sucrose in 2 mM HEPES buffer at pH 7.4. The vesicles were subsequently suspended in a solution of NaCl such that the final composition of the outer solution was 22.5 mM NaCl and 5 mM sucrose in 2 mM HEPES at pH 7.4. The addition of NaCl served two purposes, (i) the presence of the ions was important for the interaction between the His-tagged molecules and the NTA(Ni), and (ii) the outer solution was lower in density compared to the inner solution. This density difference helped to settle and immobilize the GUVs for imaging. The GUVs were exposed to fluorescently labeled His-tags. Analyzing the membrane fluorescence after the binding of these fluorescently labeled His-tags would quantify the amount of anchor lipids present in the vesicle membrane. The His-tag consists of a chain of six histidines. The two His-tagged fluorescent molecules studied are 6H-GFP and 6H-FITC. These molecules differ in their size and were investigated in order to find out whether the binding of 6H to NTA(Ni) is affected by this size.

I have performed the experiments in two independent setups: in a bulk solution and on the microfluidic device. Both sets of experiments lead to similar results. For the bulk experiments, the GUVs were suspended in a solution containing the His-tagged molecules. The vesicles were imaged afterwards using a confocal microscope. One of the drawback for the bulk experiments is that the vesicle yield was different hence it was not possible to perform a quantitative study to determine the binding of the His-tagged molecules to the membrane. To avoid this difficulty, the microfluidic device was used to trap the GUVs in the side channels and to exchange the outer solution with the His-tagged molecules. The GUVs were loaded in the device according to section 2.2.2. Briefly, the GUVs were mixed with an equi-osmolar NaCl solution (25 mM), and this was filled in the reservoir at the inlet. The outlet of the microfluidic device was connected to a syringe pump and the solution was drawn from the reservoir. After the GUVs has started to flow in the main channel, the pump was stopped and the vesicles

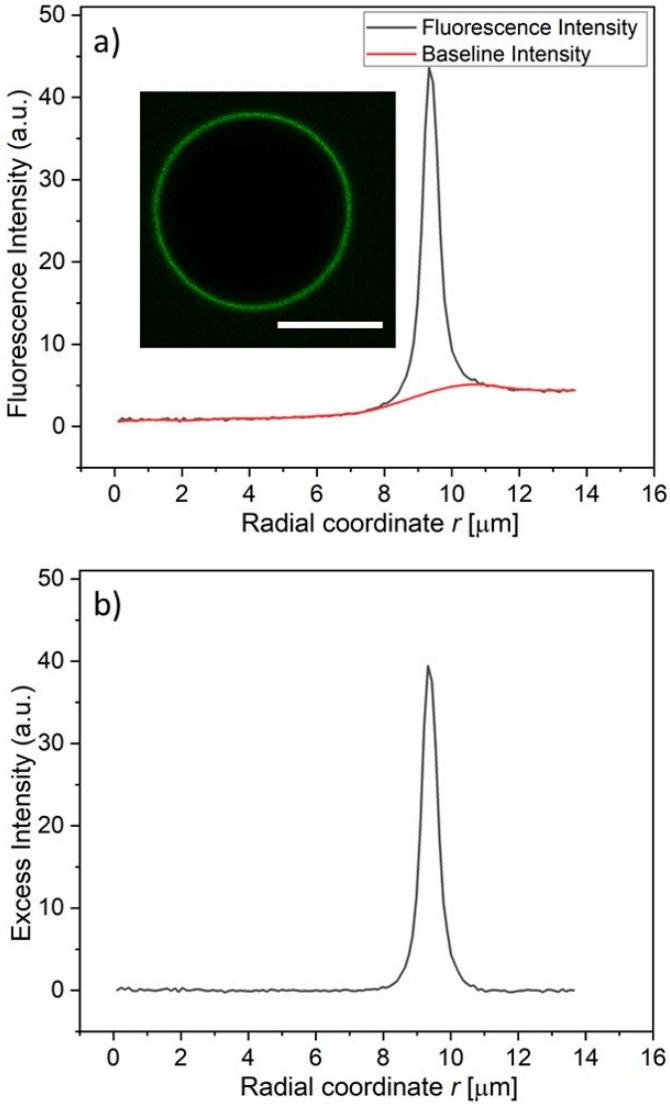

Figure 3.3: Measurement of membrane fluorescence from His-tagged fluorophores bound to a GUV membrane: (a) fuorescence intensity (black) and baseline intensity (red) as a function of the radial coordinate r, which measures the distance from the vesicle center. The fluorescence intensity was determined via the image processing software ImageJ, the baseline intensity via OriginLab; and (b) excess intensity obtained by subtracting the baseline intensity from the fluorescence intensity in (a). The membrane fluorescence is obtained by integrating the excess intensity over the radial coordinate r. The intensities were obtained for the vesicle displayed in the inset of (a), corresponding to 3 mol% DGS-NTA(Ni), 120 nM 6H-FITC, and pH 7.45. Scale bar: 10 mm

could be observed settling in the main channel. The device was oriented vertically for 15 to 20 mins, and the GUVs moved to and settled in the side channels. After the previous step was completed, the device was placed on the microscope for further experiments. Trapping the GUVs in the microfluidic side channels ensured that they were always exposed to an excess of His-tagged molecules. To quantify the binding, I measured the intensity line profile across the GUV membrane using the softwares FIJI and Origin.

For a spherical GUV, the membrane fluorescence can be determined quantitatively by measuring the fluorescence intensity profile as a function of the radial coordinate r, which represents the distance from the center of the vesicle. One example for such a profile is shown in the Figure 3.3 together with the baseline intensity that interpolates smoothly between the background intensities of the interior and exterior solutions. The excess intensity of the fluorescence is equal to the difference between the total fluorescence and the baseline intensity. The membrane fluorescence is obtained by integrating this excess intensity over the radial coordinate r.

3.4 Results and discussion

3.4.1 Dependence of fluorescence intensities on protocol

As mentioned in the previous section, we exposed the GUVs to a specific concentration of the His-tagged molecules and quantified their brightness at the membrane. The observed brightness of the GUV membranes depends both on the His-tagged fluorophore and on the preparation method. For both fluorophores, the GUVs are observed to have the largest brightness when prepared by Pt wire electroformation.

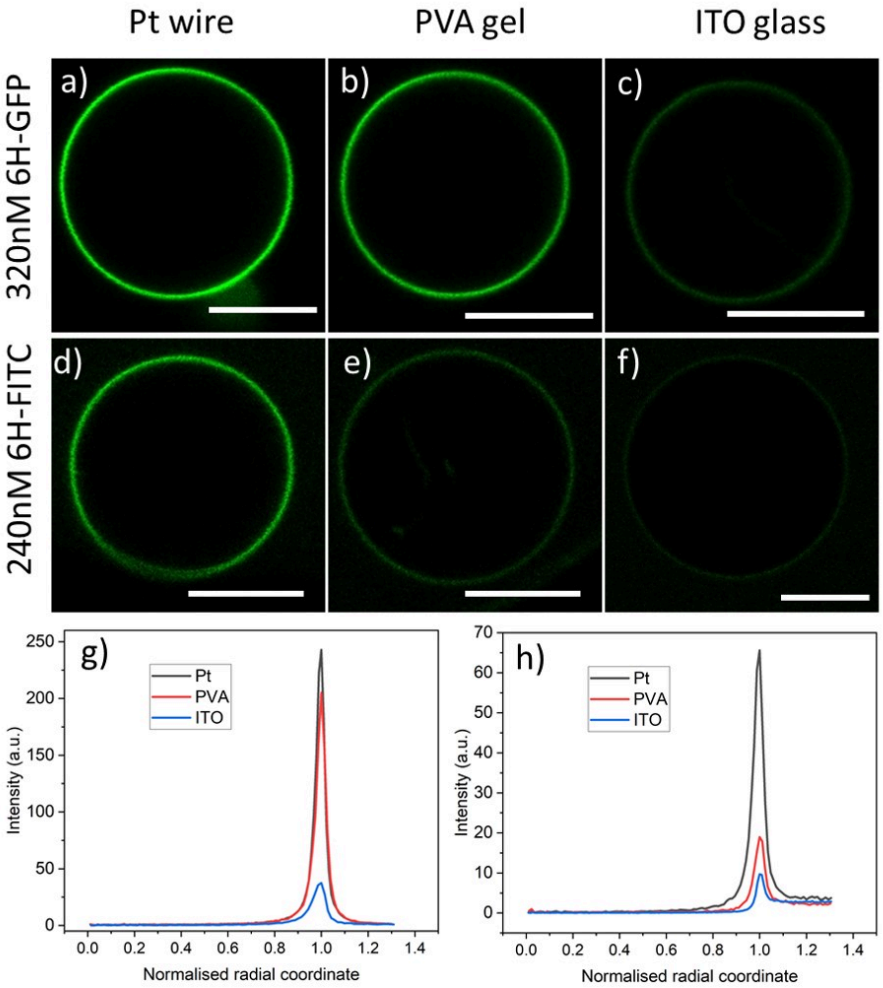

Figure 3.4: Brightness of GUV membranes doped with DGS-NTA(Ni) for three preparation methods corresponding to the three columns: (a–c) GUV membranes exposed to an exterior solution with 320 nM of 6H-GFP. The Pt wire method leads to a strongly fluorescent membrane whereas this fluorescence is strongly reduced for the ITO glass method; and (d–f) GUV membranes exposed to an exterior solution with 240 nM of 6H-FITC. The membrane fluorescence is visible for both the Pt wire and the PVA gel methods but strongly reduced for the ITO glass method. The lipid composition used for the GUVs is POPC:Chol (8:2) and 3 mol% DGS- NTA(Ni). In all cases, the GUV encloses a 50 mM sucrose solution and is exposed to an exterior solution of 22.5 mM NaCl and 5 mM sucrose at pH 7.45 with either 6H-GFP or 6H-FITC. All scale bars: 10 μm; and (g and h) line profiles of fluorescence excess intensity versus normalized radial coordinate; for more details, see Fig. 4. The excess intensity profiles in (g and h) correspond to the images in (a–c) and (d–f), respectively.

3.4.2 Surface coverage by His-tagged molecules

To calculate the surface density of the His-tagged molecules, we considered the vesicles electroformed on Pt wires to contain all the NTA(Ni) lipids being used in the preparation of the membranes.In the next chapter, it is shown that the surface density of the membrane-bound molecules becomes saturated for a solution concentration of 320 nM for 6H-GFP and 240 nM for 6H-FITC. The In other words each of the NTA(Ni) group is occupied by just one His-tagged molecule. In this saturation regime,the surface coverage, $\Gamma_{\mathrm{bH}}^{\mathrm{eq}}$, of the membrane-bound fluorophores is equal to the surface density ρ_{anc} of the NTA(Ni) lipids, which implies

$$\Gamma_{\mathrm{bH}}^{\mathrm{eq}} = \rho_{\mathrm{anc}} \frac{I_{\mathrm{flu}}}{I_{\mathrm{sat}}} \tag{3.1}$$

The surface coverage, $\Gamma_{\mathrm{bH}}^{\mathrm{eq}}$, of the His-tagged molecules can be estimated from the surface density ρ_{anc} of the NTA(Ni) lipids, and from the ratio of the observed fluorescence I_{flu} and the maximum intensity I_{sat} of the vesicles decorated with the His-tagged molecules. The different surface coverages by the His-tagged molecules, resulting from the difference in the protocols have been plotted in Figure 3.5. The absolute values of the surface coverages as obtained for the solution concentrations of two His-tagged molecules, 320 nM concentration of 6H-GFP and 240 nM concentration of 6H-FITC are given in Appendix D.

3.4.3 Interaction between ITO glass and DGS-NTA(Ni)

As shown in Figure 3.4, the GUVs made using the electroformation method with ITO glass exhibit the lowest fluorescence signal of the membrane. Additionally, once trapped in the microfluidic device and exposed to the his-tagged molecules, a very few GUVs showed a significant fluorescence intensity, see Figure 3.6. This inhomogenous membrane fluorescence inspired the search for an explanation of what happens at the surface of ITO glass.

The low fluorescence intensity as shown in Figure3.4 for GUVs made

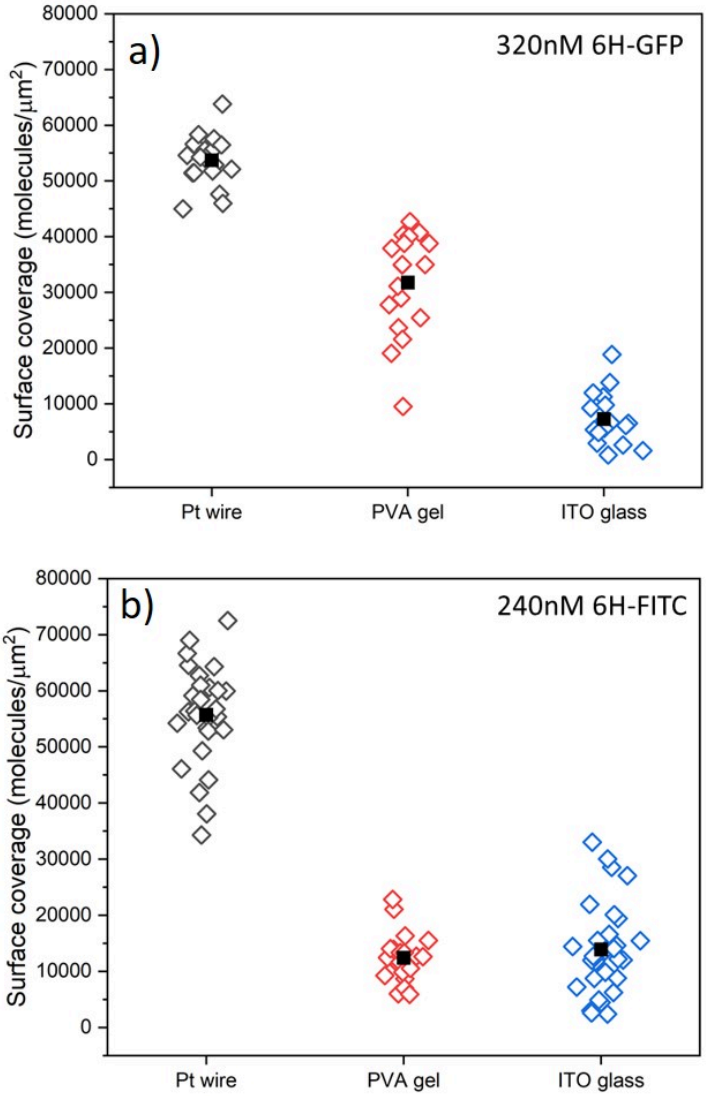

Figure 3.5: Surface coverage of GUV membranes by His-tagged molecules for different GUV preparation protocols. All GUVs were prepared with POPC:Chol in the molar ratio (8:2), doped with 3 mol% of NTA(Ni) lipids. The inside solution is 50 mM sucrose in 2 mM HRPES buffer at pH 7.5. The GUVs were exposed to a solution mixture of 22.5 mM NaCl, 5 mM sucrose in 2 mM HEPES at pH 7.5. In addition, the outer solution was supplemented with- **a)** 320 nM 6H-GFP. The three sets of data were obtained for 19, 18, and 18 vesicles using the protocol based on Pt wire, PVA gel, and ITO glass, respectively; and **b)** 240 nM 6H-FITC. The three sets of data were obtained for 17, 11, and 12 vesicles using the protocol based on Pt wire, PVA gel, and ITO glass, respectively.

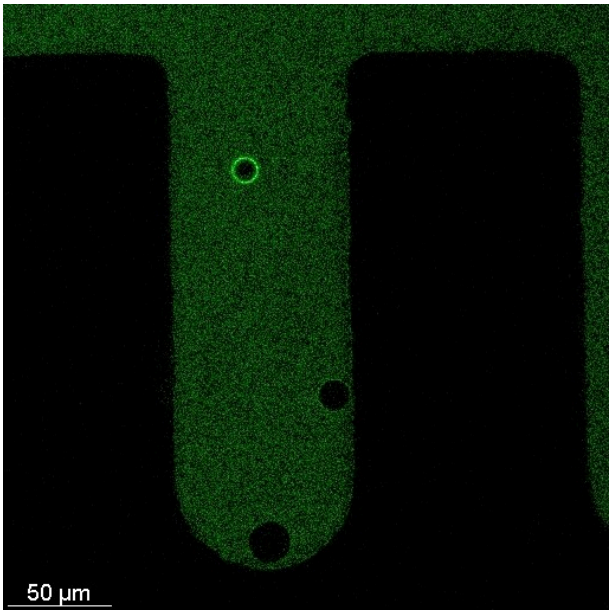

Figure 3.6: GUVs with membrane composition POPC:Chol (8:2) and 3 mol% DGS- NTA(Ni), electroformed on ITO coated glasses. The GUVs enclose 50 mM sucrose and 2 mM HEPES at pH 7.45 solution and are exposed to an exterior solution of 22.5 mM NaCl and 5 mM sucrose at pH 7.45 with 240 nM 6H-FITC, using the microfluidic device. One GUV shows a strong green membrane signal compared to the other two GUVs, implying an inhomogenous distribution of the DGS-NTA(Ni) lipid. Scale bar: 50 μm.

with ITO glass electroformation, indicates either the absence of the Ni^{2+} ion that mediates the association of the His-tag with the NTA lipid, or the absence of the whole DGS-NTA(Ni) lipid. According to the first hypothesis, the Ni^{2+} would have been lost during the electroformation leaving the NTA moieties empty in the lipids. These could be easily re-filled with nickel sulphate ($NiSO_4$) salts or with other transition metal cations. This methods of replenishing the NTA with Ni^{2+} is used to replenish the Ni-NTA columns for protein purification[109]. I tested it by preparing GUVs with DGS-NTA(Ni) lipid using the ITO glass electroformation. The resulting GUVs were trapped in the microfluidic device and supplemented with an aqueous solution of Co^{3+} cations (more about Co^{3+} in chapter 5). After the treatment with Co^{3+}, the GUVs were exposed to 6H-GFP (See AppendixB). No GFP signal was observed at the membrane, indicating that

the membranes do not have any anchor lipids.

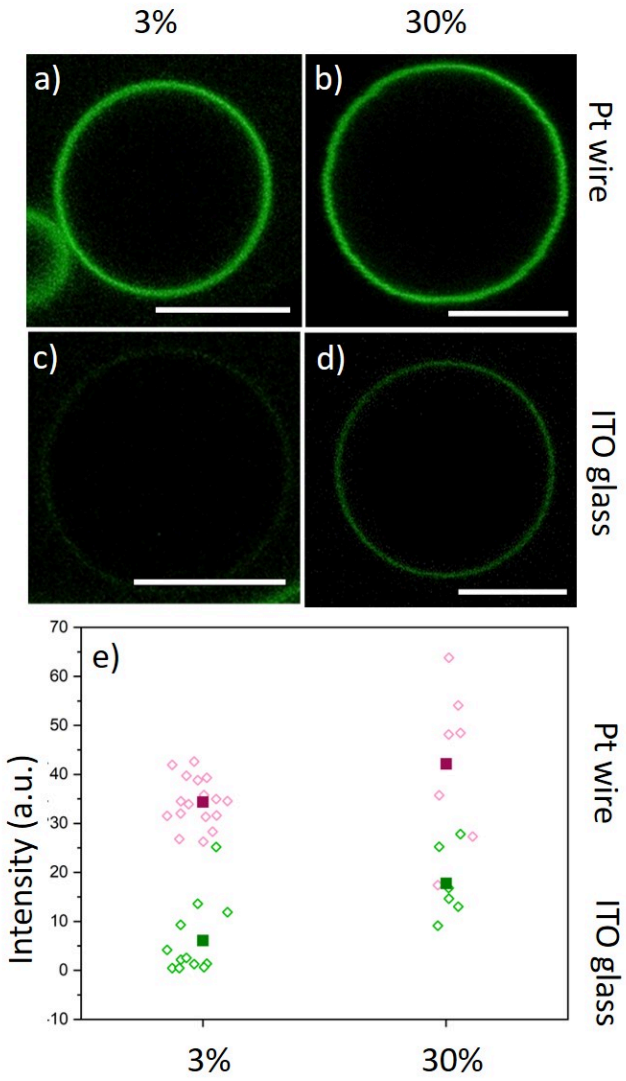

Figure 3.7: Binding of 6H-FITC to GUV membranes with 3 mol% and 30 mol% DGS-NTA(Ni) anchor lipid. The GUVs are composed of POPC: Chol (8:2) and either 3 mol% (a,c) or 30 mol% (b,d) DGS-NTA(Ni) lipids, and formed by electroformation on Pt wire (a,b) or on ITO glasses (c,d). All GUVs enclose 50 mM sucrose in 2 mM HEPES buffer at pH 7.45 and are exposed to 120 nM 6H-FITC in 22.5 mM NaCl and 5 mM sucrose at pH 7.45; (e) Membrane fluorescence for the four preparation conditions in (a-d). The filled squares represent the mean values of the respective data. All scale bars are 10 μm.

The second hypothesis, that the whole DGS-NTA(Ni) lipid is absent from the GUV, would imply that this lipid interacts with the ITO surface and sticks to it. The surface properties of the ITO glass are likely to affect the properties of the produced vesicles[106]. The ITO film consists of indium(III) ions, which can bind to NTA[110,111]. Presumably, the NTA lipid prefers to stay close to the ITO surface and forms a weak bond with indium, when the lipid stock dissolved in chloroform is deposited on the ITO surface. Following this hypothesis, I increased the mole fraction of the DGS-NTA(Ni) lipid from 3 mol% to 30 mol%. After harvesting the GUVs, they are exposed to 120 nM 6H-FITC in the exterior solution. As shown in Figure 3.7, the GUVs prepared by electroformation on ITO glass exhibit a smaller membrane fluorescence than GUVs prepared by electroformation on platinum wire, indicating that only a fraction of the DGS-NTA(Ni) lipid deposited on the ITO glass becomes incorporated into the vesicles. However, for both electroformation methods, the fluorescence increases with increasing mole fraction of the NTA lipids. This confirms the hypothesis that the DGS-NTA(Ni) sticks to the ITO glass. On increasing the mole fraction of this lipid, the ITO surface gets saturated with some fraction of the DGS-NTA(Ni) lipid that is in the mixture. The rest of the lipids takes part in the formation of the vesicle, thus exhibiting fluorescence at the membrane (Figure 3.7d). The data for the Figure 3.7 is provided in Appendix A.

3.5 Conclusions

In this chapter the different protocols for making GUVs (PVA assisted swelling, as well as electroformation on ITO glass and Pt wire) were explained in detail with their respective advantages and disadvantages. I have optimized these protocols to obtain a good yield of GUVs. The first question assessed in this chapter was if the vesicles formed using different protocols yielded the same membrane composition in the resulting GUVs. To investigate this issue, GUVs were made with different protocols starting from the same lipid mixture. The lipid mixture was doped with the DGS-NTA(Ni) lipid. The resulting GUVs were exposed to His-tagged molecules

with a fluorescent probe. We observed that the Pt wire electroformed GUVs showed the largest intensity at the membrane, indicating the presence of the DGS-NTA(Ni) lipid. On the other hand, the ITO glass electroformed vesicles showed very low intensity of the His-tagged fluorophore at the membrane. We hypothesized that the DGS-NTA(Ni) lipid sticks to the ITO glass and does not take part in the formation of the GUV. We confirmed this hypothesis by making GUVs with a high fraction of the DGS-NTA(Ni) lipid and exposing those to His-tagged fluorophores. In conclusion, when a lipid mixture contains the DGS-NTA(Ni) lipid, electroformation on ITO glass leads to vesicles with compositions that were different from the initial one. The experiments in this chapter involved two His-tagged fluorophores with different sizes; the difference in their interaction with the membranes is explored in the next chapter.

Chapter 4

Local environment of membranes affects GUV brightness

Introduction

The addition of proteins or nucleic acids to synthetic bio-mimetic membrane system brings us one step closer to real biological systems. The lipid membranes form micrometer sized closed compartments termed GUVs. Their size makes them comparable to the size of cells. There are several protocols that can be used to make GUVs, some of which have been discussed in detail in the previous chapter 3. Depending on the composition of the membrane and the solutions used to prepare them, many properties are affected[112–115]. The GUVs are more than three orders of magnitudes bigger in size compared to lipids which are in the range of nanometers. The micro-environment around the lipids, or to be more precise the nano-environment, can change the property of the whole membrane system. Furthermore, the lipid composition also affects the interaction of proteins with membranes[20,116].

In a biological sample, the various organelles and the plasma membrane have very specific yet different lipid compositions. Although proteins and lipids comprise almost equal fractions of the membrane, but the property of the bilayer can be attributed just to the lipids. Hence it makes sense to

use lipid bilayers as the simplest model systems of plasma membrane. The properties of a lipid bilayer depend on its molecular composition. Some lipid compositions give rise to phase separation[117]. The separation of lipids into two lipid phases is believed to be primarily driven by the shape and structure of the hydrophobic tails of the lipids. It can be enhanced by the presence of charged head groups[118] or by impurities in the surrounding aqueous solutions[119]. The line tension of the domain boundary between two domains of a GUV arising from the phase separation can be harnessed to divide the vesicle[23,120].

Buffers are important for biological and biomimetic system as they maintain their pH. Minor pH changes could arise from the mixing of carbon dioxide from the atmosphere. A study by Peiró-Salvador et al suggests that buffers adversely affect the membrane[121], by making the membrane soft and affecting its elastic properties. Another study by Bouvrais et al[112] also show that buffers affect the bending rigidity of the GUVs. These studies make a point that the choice of buffers is very important for studies related to vesicles. This choice should be made at the beginning and should not be changed the whole experiment.

Sugars serve multiple purposes in cells like making the glycocalix that consists of sugar groups attached to the membrane protein, maintaining osmotic pressure, storing energy, cell signaling and as transport molecules[122]. Thus, one would like to include some sugars in biomimetic systems such as GUVs. Including sugars in the GUV formation also helps to settle the vesicles down on the cover slide. The presence of two different sugars in the interior and exterior solution provides a density difference across the membrane. Sucrose being a disaccharide (fructose and glucose monomers) is denser than the monosaccharide glucose. Generally, the vesicles are made using the denser sugar solution (sucrose) and later suspended in an equi-osmolar low-density sugar solution (glucose). This makes the interior solution to be pure sucrose and the exterior solution to be a mixture of sucrose and glucose. When the osmolarity is matched, the GUVs remain spherical and settle down because of the density difference. This procedure not only helps to immobilize the vesicles for better confocal imaging,

but also provides a contrast in the optical path of transmitted light. This difference in optical path is necessary for phase contrast and differential interference contrast imaging. The presence of sugars can affect the lipid membrane by changing nanoscopic properties such as membrane thickness or even macroscopic properties involving changes in the vesicle morphology[36,81,123,124]. According to Anderson et al,[123], at low concentrations, sugars adsorb onto the membrane or intercalate between the lipids thus reducing the membrane thickness. At higher concentrations, sugars are mainly excluded form the membrane surface. This work also suggests that the monomeric sugars (like glucose) have a different effect on the membrane compared to disaccharides (like sucrose). As mentioned before, the GUVs are exposed to different sugars in the interior and exterior solution for experimental convenience. The asymmetry between the leaflets of the bilayers caused by the sugar asymmetry can cause morphological changes. As shown by Bhatia et al[81], the sugar asymmetry can give rise to multi-spherical shapes of GUVs that are connected by closed membrane necks. To avoid the sugar-membrane interactions, many studies often use OptiPrep (trademark of Serumwerk Bernburg AG) which is a 60% (w/v) solution of iodixanol in water[125–127]. OptiPrep is a replacement for sugar solution and it provides high density for lower osmolarity.

The biological systems regulate ionic concentrations for homeostasis and signaling between cells. This regulation is used, in particular, by the nervous system where sodium and potassium ions are crucial for communication between neurons. Therefore, it is important to study ion-membrane interactions. It has been shown that the presence of salt influences membrane properties such as spontaneous curvature and bending rigidity[113,128]. The metal cations of simple salts penetrate the lipid head groups and form coordinate bonds, while counter ions stay at the membrane surface[129].

All the studies mentioned above show that the mesoscopic membrane properties of the GUVs are affected by the local molecular environments of the membrane. Continuing the study regarding the membrane protein binding via the DGS-NTA(Ni) and His-tag, we will explore the effect of different fluorophores and pH. The His-tag binds to the DGS-NTA(Ni) by a

coordinate bond. We will estimate the equilibrium dissociation constant for this system. We also report fluoroscence quenching by the Ni^{2+} ion. In the previous chapter we explored how the protocol for the preparation of GUVs could affect the binding of the His-tagged molecule to the membrane. One of the conclusions was that electroformation on Pt wires, ensures a good quality and yield of vesicles. For this chapter, we continue making the GUVs via electroformation on Pt wires and expose them to His-tagged molecules using the microfluidic device discussed in chapter 2.

4.1 Experimental methods

We consider GUV membrane with a with lipid composition POPC:Chol in the molar ratio of 8:2, doped with 3 mol% DGS-NTA(Ni) (unless stated otherwise) and formed by electroformation on Pt wires as described in section 3.2. Briefly, 6 μL of a 0.5 mM solution of the lipid mix was spread on two platinum wires via a syringe. The wires were kept under vacuum for an hour to remove traces of chloroform. The wires were then dipped in a quartz cuvette, which was filled with 50 mM of sucrose in 2 mM HEPES buffer (pH 7.4). An AC electric field with peak-to-peak voltage of 3 V and frequency of 10 Hz was applied for 2 hours at 35 °C to speed up the vesicle swelling process. Subsequently, the frequency of the AC field was reduced to 3 Hz and the low-frequency field was applied for 5 min, to detach the vesicles from the wires. After cooling to room temperature, the vesicles were harvested using a micropipette with a broad tip.

The GUVs were trapped in the microfluidic device using the same protocol as mentioned in section 3.3. Briefly, the GUVs were filled in the reservoir with equiosmolar NaCl solution, and drawn into the main channel using a syringe pump connected to the outlet. Once the GUVs were settled in the main channel, the device was oriented vertically for the GUVs to settle in the side channels. The device was placed over a confocal microscope and the solution outside the GUVs was exchanged by changing the solution in the reservoir and drawing it out via the outlet of the device.

In this chapter, we calculate the surface density of the NTA(Ni) lipid on

the GUV. Based on this surface density, we will be able to check whether or not the His-tagged molecules are crowding on the membrane surface. We also investigate the effect of cholesterol on the binding of His-tagged molecules. Furthermore, we study the effect of pH on the binding and calculate the equilibrium dissociation constant for both His-tagged molecules and at different pH values. In the end, we report fluorescence quenching by the nickel cation present in the NTA(Ni) lipid.

4.1.1 Surface density of DGS-NTA(Ni) lipid

The average lipid head group area for a membrane composed of POPC:Chol in the molar ratio of 8:2 is 0.5 nm^2.[130,131] As mentioned above, the membrane is doped with 3 mol% of DGS-NTA(Ni) lipid. For such a lipid mixture, the NTA(Ni) lipids will be separated spatially by 4.08 nm. This separation determines the surface density ρ_{anc} of the NTA(Ni) lipids via

$$\rho_{\text{anc}} = \frac{1}{(4.08\,\text{nm})^2} = \frac{6.0 \times 10^4}{\mu\text{m}^2} \tag{4.1}$$

When each NTA(Ni) lipid is occupied by one His-tagged molecule, corresponding to the saturation regime, the surface density ρ_{anc} of the anchor lipids is equal to the surface density or coverage of the His-tagged fluorophores.

To estimate whether or not this saturation regime leads to crowding of the membrane-bound fluorophores, we compare the average separation of the NTA anchor lipids with the lateral size of the membrane-bound fluorophores. The lateral size of membrane-bound 6H-GFP should be comparable to the diameter of its β-barrel structure. This diameter is about 3 nm which is smaller than the separation of NTA(Ni) lipids (4.08 nm) [22,132]. Therefore, the crowding effects between membrane-bound 6H-GFP molecules can be ignored even when all the NTA(Ni) lipids are occupied by 6H-GFP. The 6H-FITC peptide, on the other hand, has a linear extension of about 3.2 nm which provides an upper bound on the lateral size of membrane-bound 6H-FITC. This upper bound on the lateral size is again smaller than the average separation of the NTA(Ni) lipids. Hence, the

crowding effects between membrane-bound 6H-FITC molecules can also be ignored when all NTA(Ni) binding sites are saturated with 6H-FITC.

This conclusion about the surface density NTA(Ni) lipid and the non-crowding of His-tagged molecules will be used for the calculation of the equilibrium dissociation constant in section 4.2.3.

4.2 Results and discussion

4.2.1 Lipid composition

GUVs with two different lipid compositions, (i) POPC:Chol (8:2) and 3 mol% NTA(Ni) lipid, (ii) POPC and 3 mol% NTA(Ni) lipid are prepared by electroformation on Pt wires. The vesicles are exposed to 120 nM 6H-FITC. Although both vesicle populations have membrane compositions with 3 mol% NTA lipids, they differ in their mole fractions of cholesterol. For vesicles with 20 mol% cholesterol, the fluorescence intensity is about twice as large as for vesicles without cholesterol, see Figure 4.1. The data for Figure 4.1 is provided in Appendix E.

This change in the intensity can arise from two different mechanisms. First, the cholesterol may reduce the effect of the fluorescence quenching by the NTA(Ni) lipids; second, it may increase the surface coverage of 6H-FITC. For a certain variant of His-tagged GFP, its binding affinity to lipid bilayers was found to increase with the mole fraction of cholesterol[133]. Based on this result, we decided to include 20 mol% cholesterol in all subsequent preparations of GUVs.

4.2.2 Changing membrane fluorescence by pH

The images and data shown in section 3.4.1 in the Figures 3.4 and 3.5 were obtained at pH 7.4. The pH was maintained by 2 mM HEPES buffer. Inspection of Figure 4.2, reveals that the fluorescence at the membrane depends on the pH of the solution. For a systematic study, the vesicles were electroformed on Pt wire. The swelling solution consisted of 50 mM sucrose and 2 mM HEPES buffer at pH 7.4. The vesicles were then exposed to an exterior solution containing 20 nM 6H-GFP or 120 nM 6H-FITC as

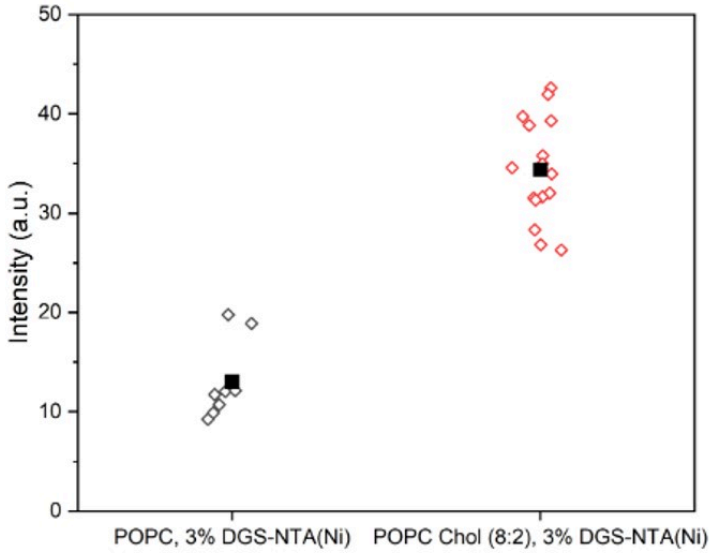

Figure 4.1: Influence of cholesterol on the fluorescence intensity of GUV membranes:The GUVs are prepared by platinum wire electroformation and exposed to 120 nM 6H-FITC for two different lipid compositions. In the presence of 20 mol% cholesterol, the intensity is about twice as large as in the absence of cholesterol. This change in intensity can arise by two different mechanisms. First, cholesterol may reduce the fluorescence quenching by the NTA lipids; second it may increase the surface coverage by 6H-FITC.

well as 22.5 mM NaCl, 5 mM sucrose and 2 mM HEPES buffer. The pH of these solutions was increased and decreased by adding sodium hydroxide (NaOH) and hydrochloric acid (HCl), respectively.

For each pH value, the membrane fluorescence was determined via the method described in Figure 3.3. The resulting fluorescence intensities of the GUV membranes are plotted in Figure 4.3 (a) and (b) for 6H-GFP and 6H-FITC, respectively as a functionof pH. For 6H-GFP, the membrane fluorescence first increases and then saturates for pH values above pH 8.5. For 6H-FITC, the intensity exhibits a pronounced maximum at about pH 8.5. The data for Figure 4.3 is in Appendix F.

In general, the fluorescence of a dye molecule can vary with the pH value even in the absence of lipids. In order to determine the latter pH de-

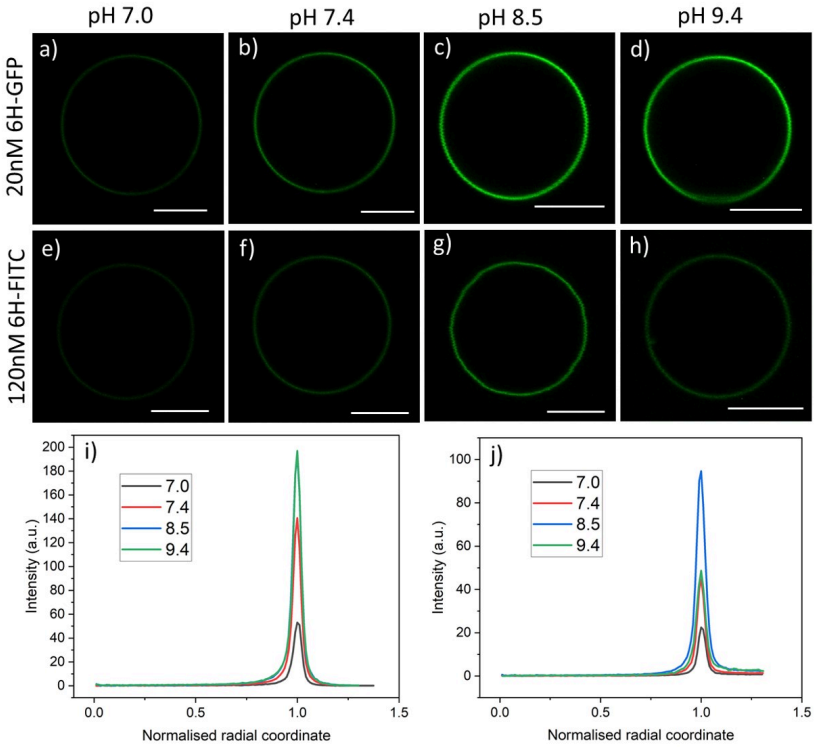

Figure 4.2: Brightness of membrane fluorescence for 3 mol% NTA lipids and two types of His-tagged molecules, 6H-GFP and 6H-FITC, as observed for different pH-values of the exterior solution: GUVs exposed to 20 nM solution of 6H-GFP in (a–d) and to 120 nM of 6H-FITC in (e–h). All GUVs are prepared using the platinum wire method. All scale bars: 10 mm; and (i and j) corresponding fluorescence intensity profiles as obtained by the method described in Fig. 4. The intensity profiles in (i) and (j) correspond to the images in (a–d) and (e–h), respectively. In (i), the curve for pH 8.5 (blue) is masked by the one for pH 9.4 (green).

pendence, we also measured the background intensities for 6H-GFP and 6H-FITC in the exterior solution far away from the vesicle membranes, see the corresponding data in Figure 4.3. Inspection of both panels shows that the background intensity in the exterior solution is negligible over the whole range of pH values studied here. Therefore, the pH dependence of the membrane fluorescence in Figure 4.3 is caused by the pH dependence of the membrane-bound fluorophores rather than by the intrinsic pH dependence of these dye molecules in solution.

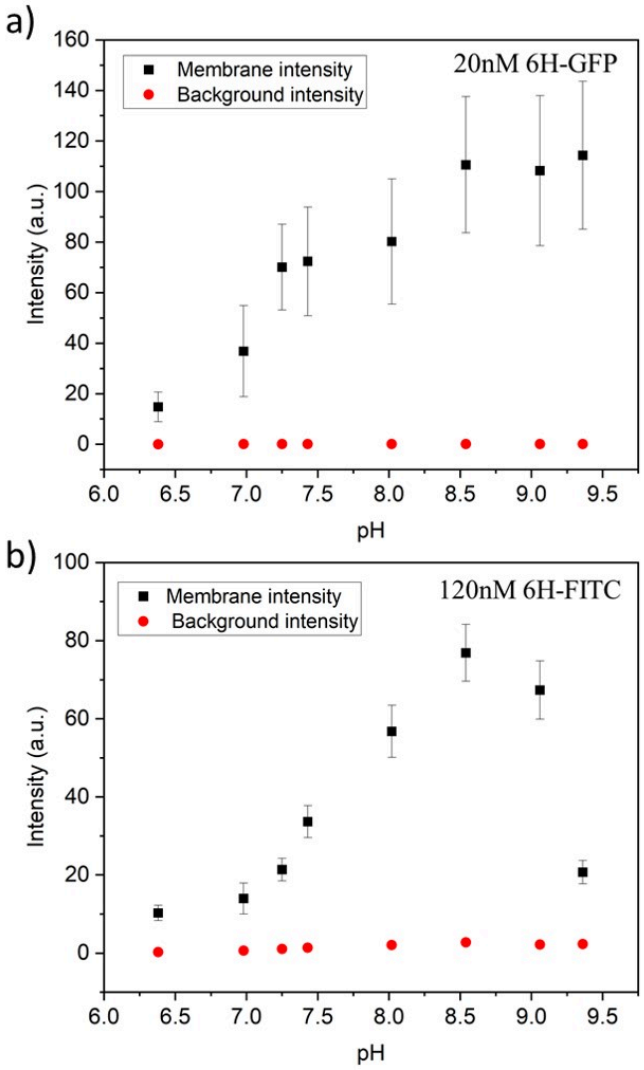

Figure 4.3: Membrane intensities (black squares) and background intensities (red circles) versus pH of exterior solution for GUV membranes with 3 mol% NTA lipids. All GUVs were electroformed on Pt wire. **(a)** For GUVs exposed to 20 nM 6H-GFP, the membrane intensity increases with increasing pH for $6.38 \leq pH \leq 8.5$ and then saturates. **(b)** For GUVs exposed to 120 nM 6H-FITC, the membrane intensity exhibits a pronounced maximum close to pH 8.5. For both 6H-GFP and 6H-FITC, the background intensities (red circles) are negligible over the whole range of pH values, which demonstrates that the pH dependence of the membrane fluorescence arises from the pH dependence of the His-NTA binding affinity.

4.2.3 Equilibrium dissociation constant

The DGS-NTA(Ni) lipids provide the binding sites for the His-tagged molecules. We consider a simple binding model, of which each DGS-NTA(Ni) lipid can bind at most one His-tagged molecule and and for which each His-tagged molecule binds to only one DGS-NTA(Ni) lipid. The outer leaflet of the GUV membrane contains a total number of N_{anc} anchor lipids which can bind N_{bH} His-tagged molecules with $N_{\mathrm{bH}} \leq N_{\mathrm{anc}}$. For each anchor lipid, the binding (or association) rate is taken to be proportional to the molar concentration X of the His-tagged molecule. The resulting association rate is then given by $\kappa_{\mathrm{on}} X$ where κ_{on} is the association rate constant. The unbinding (or dissociation) is an activated process with the dissociation rate ω_{off}. The number N_{bH} of bound His-tagged molecules changes with time t according to the evolution equation

$$dN_{\mathrm{bH}}/dt = \kappa_{\mathrm{on}} X \left(N_{\mathrm{anc}} - N_{\mathrm{bH}}\right) - \omega_{\mathrm{off}} N_{\mathrm{bH}}. \tag{4.2}$$

At equilibrium, the binding flux is equal to the unbinding flux which implies $dN_{\mathrm{bH}}/dt = 0$. Solving the latter equation for N_{bH} equilibrium value $N_{bH} = N_{bH}^{eq}$ of the bound His-tagged molecules is given by

$$N_{\mathrm{bH}}^{\mathrm{eq}} = N_{\mathrm{anc}} \frac{X}{K_d + X}, \tag{4.3}$$

which depends on the equilibrium dissociation constant K_d as-

$$K_d \equiv \omega_{\mathrm{off}}/\kappa_{\mathrm{on}}. \tag{4.4}$$

When eqn(4.3) is divided by the surface area A of the membrane, the equilibrium surface density or coverage $\Gamma_{\mathrm{bH}}^{\mathrm{eq}}$ of the His-tagged molecules is obtained. The coverage $\Gamma_{\mathrm{bH}}^{\mathrm{eq}}$ depends on the surface density ρ_{anc} of the DGS-NTA(Ni) lipids and on the molar concentration X of the His-tagged

molecule according to

$$\Gamma_{\mathrm{bH}}^{\mathrm{eq}} = \frac{N_{\mathrm{bH}}^{\mathrm{eq}}}{A} = \frac{N_{\mathrm{anc}}}{A}\frac{X}{K_d + X} = \rho_{\mathrm{anc}}\frac{X}{K_d + X} \tag{4.5}$$

For 3 mol% NTA lipids, the surface density ρ_{anc} is equal to 6.0×10^4 molecules per μm^2 as in eqn (4.1).

To calculate the dissociation constant K_d from the confocal images, we measure the membrane fluorescence of the GUVs with the His-tagged molecules, as described in section 4.2.3 Figure 3.3. We assume that the fluorescence intensity of the membrane-bound fluorophores is directly proportional to their number, or their surface density. The fluorescence of these fluorophores can be quenched by the NTA(Ni) lipids. To describe such a quenching, we introduce a reduction factor ϕ with $0 < \phi \leq 1$ for the fluorescence of a fluorophore bound to the NTA(Ni) lipid[134]. We then obtain the relationship

$$I_{\mathrm{flu}} = I_{\mathrm{sat}}\frac{X}{K_d + X} \quad \text{with } I_{\mathrm{sat}} = \phi\,\rho_{\mathrm{anc}} \tag{4.6}$$

between the fluorescence intensity I_{flu} and the molar concentration X. As a consequence, the fluorescence intensity I_{flu} increases monotonically with the molar concentration X and attains its saturation value $I_{\mathrm{flu}} \approx I_{\mathrm{sat}} = \phi\rho_{\mathrm{anc}}$ for large X.

For 6H-GFP and 6H-FITC, the measured fluorescence intensities attain the saturation values $I_{\mathrm{GFP}} = 320.4$ a.u. and $I_{\mathrm{FITC}} = 40.9$ a.u. as obtained from the HyD detector on the Leica SP8 confocal microscope. Taking into account that the data in Figures 4.4 were obtained for GUV membranes with the same mole fraction of 3 mol% NTA lipids and thus with the same surface density ρ_{anc}, we obtain the ratio

$$\frac{I_{\mathrm{FITC}}}{I_{\mathrm{GFP}}} = \frac{\phi_{\mathrm{FITC}}}{\phi_{\mathrm{GFP}}} = \frac{40.9}{320.4} = 0.13 \tag{4.7}$$

of the two fluorescence reduction factors ϕ_{FITC} and ϕ_{GFP}. It then follows from $\phi_{\mathrm{GFP}} = 1$ for 6H-GFP, that the fluorescence of membrane-bound 6H-

FITC molecules is reduced by the factor $\phi_{\text{FITC}} = 0.13$.

A shown in Figure 4.3b, the membrane bound 6H-FITC shows the maximum fluorescence intensity at pH 8.3. This could be attributed to three factors, 1) the change in the fluorescence intensity of the FITC molecule, 2) change in the binding between the NTA(Ni) and the His-tagged, and 3) change in the fluorescence quenching by nickel cations. The background intensity in Figure 4.3b, shows that the fluorescence intensity of FITC does not change much. To study the effect on the binding, we calculate the K_d of this system for pH 8.3 which is found to be 48.2$\pm$9.6 nM, see Figure 4.5. This is more than the K_d at pH 7.4, indicating that the interaction between the NTA(Ni) and the His-tag is weaker. It is possible that this could also affect the fluorescence quenching by the nickel cation. The corresponding data for the Figures 4.4 and 4.5 are provided in Appendix G

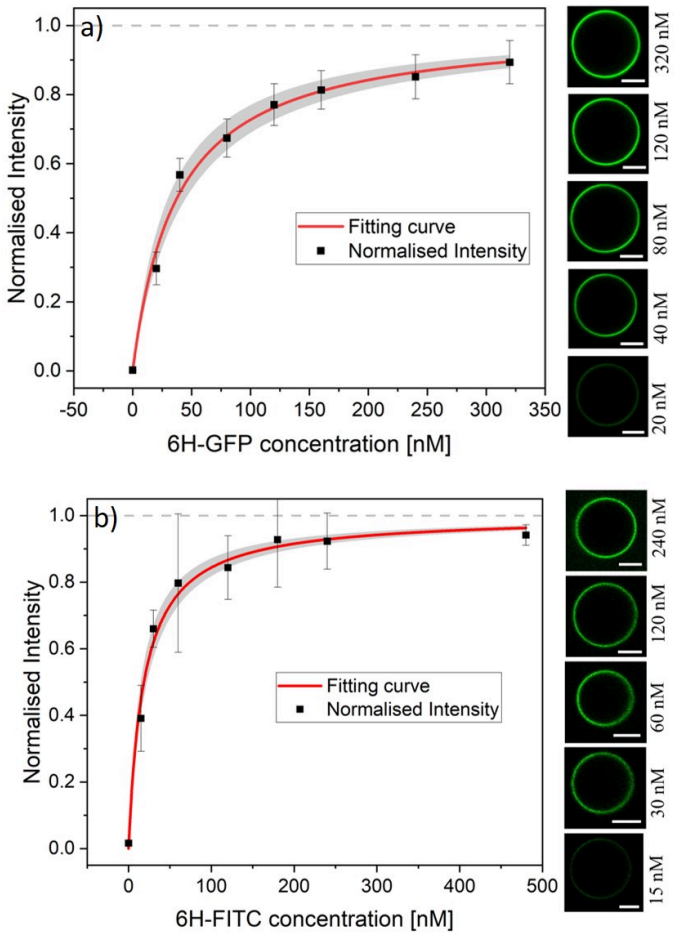

Figure 4.4: Normalized membrane fluorescence *versus* molar concentration of the His-tagged molecules. The GUVs composed of POPC: Chol in the molar ratio (8:2) and doped with 3 mol% NTA(Ni) lipid, were electroformed on Pt wires. The inside solution of the GUVs was 50 mM sucrose in 2 mM HEPES buffer at pH 7.5. The vesicles were exposed to a mixture of 22.5 mM NaCl, 5 mM sucrose in 2 mM HEPES buffer at pH 7.5. The outer solution is supplemented with increasing concentrations of the His-tagged molecules. The dissociation constant K_d is obtained by a fit to equation 4.6 (red). The confidence interval for K_d corresponds to the shaded strip (light grey) around the red fitting curve. The images on the right display the brightness of the GUV membranes as directly observed in the microscope for the different molar concentrations. All scale bars: 10 μm **a)** For vesicles exposed to 6H-GFP over the range $0 \leq X \leq 320nM$. The the red fitting curve leads to the dissociation constant $K_d = 37.5 \pm 7.5nM$; and **b)** For vesicles exposed to 6H-FITC over the range $0 \leq X \leq 240nM$. The the red fitting curve implies the dissociation constant $K_d = 18.5 \pm 3.7nM$.

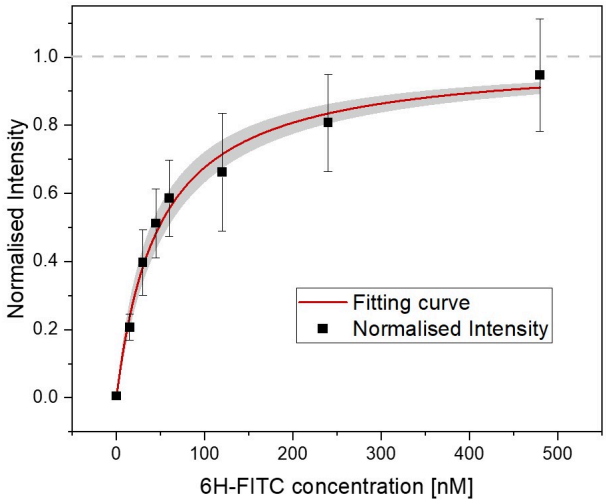

Figure 4.5: Normalised membrane fluorescence *versus* molar concentration of 6H-FITC at pH 8.3. The GUVs, composed of POPC: Chol in the molar ratio (8:2) and doped with 3 mol% NTA(Ni) lipid, were electroformed on Pt wires. The inside solution of the GUVs was 50 mM sucrose in 2 mM HEPES buffer at pH 7.5. The vesicles were exposed to a mixture of 22.5 mM NaCl, 5 mM sucrose in 2 mM HEPES buffer at pH 8.5. The outer solution is supplemented with increasing concentrations of the 6H-FITC molecules up to 480 nM. The dissociation constant K_d is $48.2 \pm 9.6 nM$ as follows form the fit to equation 4.6 (red curve). The confidence interval for K_d corresponds to the shaded strip (light grey) around the red fitting curve.

4.2.4 Fluorescence quenching by Ni^{2+} cation

To determine the different quantum yields of the two fluorophores, the detector gain was adjusted to give the same intensity for the same molar concentrations of 6H-FITC and 6H-GFP in the absence of lipids. Briefly, 100 nM solutions of 6H-FITC and 6H-GFP were imaged using the HyD detector on the Leica SP8 confocal microscope. Both molecules were excited using a 488 nm Argon laser and emission was collected between 495 and 550 nm. The detector gain was adjusted to obtain the same brightness for both solutions. From this adjustment, we concluded that 6H-FITC is about 1.2 times brighter than 6H-GFP. With this information, some of the results seemed

very contradictory. For example, Figure 3.4 g and h in section 3.4.1, show that the intensity of the membrane bound 6H-GFP is very high compared to that of 6H-FITC. Likewise, the saturation intensity $I_{\mathrm{GFP}} = 320.4$ a.u. and $I_{\mathrm{FITC}} = 40.9$ a.u. are very different for the two fluorophores. This different behavior indicates that the fluorescence of 6H-FITC is quenched when this molecule is bound to the membrane or, more precisely, to an NTA(Ni) lipid.

To elucidate the quenching effect of the NTA lipids, for each fluorophore, we added an increasing concentration of NTA(Ni) lipids to a 120 nM solution of the fluorophore. The resulting fluorescence intensities are displayed in Figure 4.6 As shown in Figure 4.6a, the fluorescence of 6H-GFP is hardly affected by large concentrations of NTA lipids, whereas the fluorescence of 6H-FITC is strongly reduced by small concentration of these lipids, see Figure 4.6b.

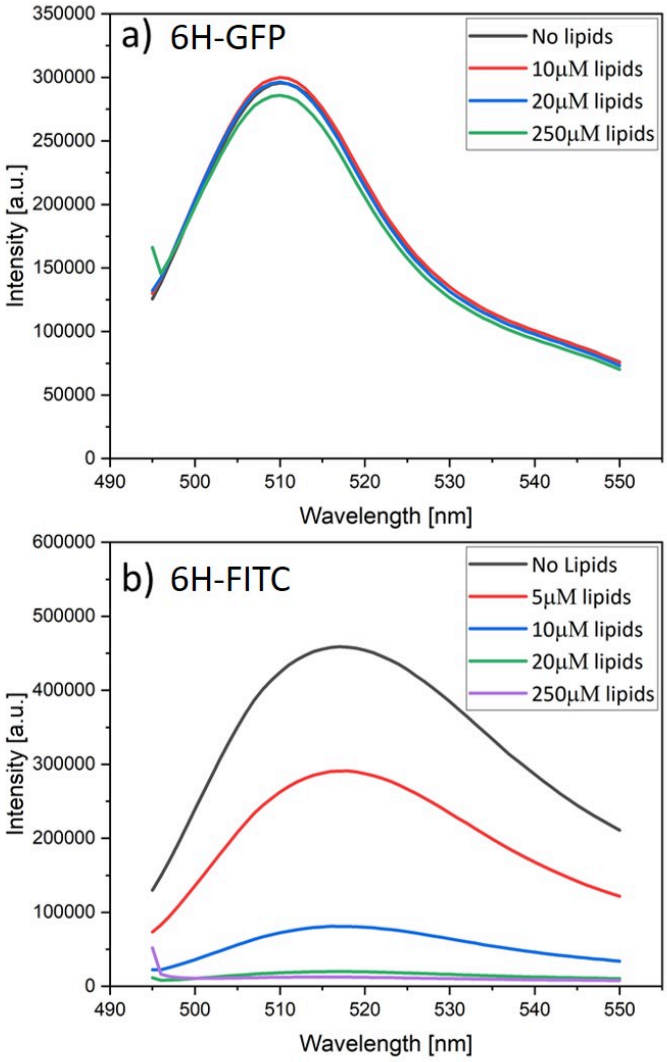

Figure 4.6: Fluorescence intensity versus wavelength as measured for a 120 nM solution of (a) 6H-GFP and (b) 6H-FITC. Both solutions are exposed to an increasing concentration of lipids in the form of liposomes containing 30 mol% NTA lipids, see color codes in the insets. The fluorescence intensity of 6H-GFP in (a) is hardly affected by the lipids whereas the fluorescence intensity of 6H-FITC in (b) is strongly reduced. In (a), the 'no lipids' curve (black) is masked by the blue curve for 20 mM.

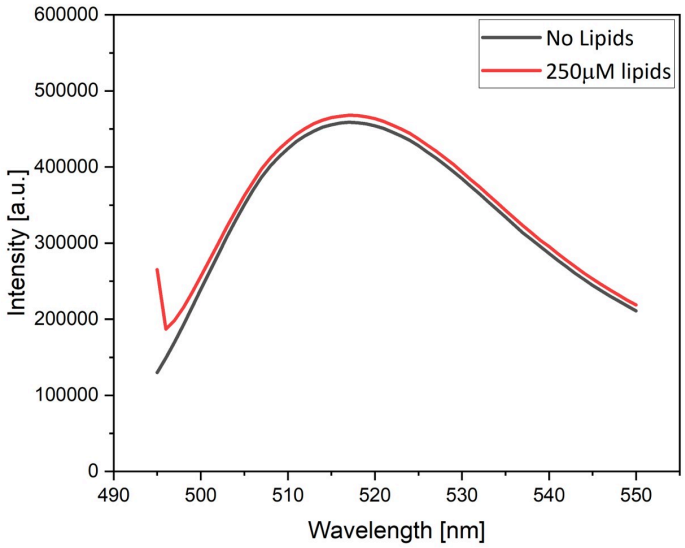

Figure 4.7: Control experiments to demonstrate that the fluorescence of 6H-FITC is not quenched by liposomes which contain a mixture of POPC and cholesterol with a molar ratio of 8:2 but no NTA(Ni) lipids.

The data in Figure 4.6a and b were obtained by adding liposomes with the lipid composition POPC : Chol : NTA(Ni) in the molar ratio 6:1:3. Similar quenching effects were observed when the fluorophores were exposed to nickel sulphate (see Appendix C). On the other hand, no fluorescence quenching of 6H-FITC was observed when the liposomes contained only POPC and cholesterol but no NTA lipids, as demonstrated in Figure4.7.

Therefore, the fluorescence quenching of 6H-FITC is caused by NTA(Ni) lipids which bind the fluorophore *via* their Ni^{2+} ion. Fluorescence quenching by Ni^{2+} ions has been previously reported for a variety of fluorophores [135–137]. For membrane-bound 6H-GFP, such a quenching effect does not occur because the chromophore of 6H-GFP is located in the middle of the protein's β-barrel [138] and well-separated from the Ni^{2+} ion of the NTA(Ni) lipid. In contrast, the fluorescein group of membrane-bound 6H-FITC is much closer to this Ni^{2+} ion, which explains the strong quenching effect in Figure 4.6.

4.3 Conclusion

A chain of histidine molecules binds to NTA(Ni) via two coordinate bonds. The NTA(Ni) group can be attached via four coordinate bonds to the head group of a lipid. Commercially one such lipid is available in the form of DGS-NTA(Ni) lipid. In this chapter, we doped vesicle membrane with 3 mol% of the DGS-NTA(Ni) lipid prepared using the protocol of electroformation on Pt wires. The vesicles were trapped in the microfluidic device and exposed to His-tag molecules attached to the two fluorophores 6H-GFP and 6H-FITC. We explored the effect of local molecular environment on the binding of the His-tag molecules to the vesicle membranes. First we checked the effect of cholesterol in the membrane and concluded that its presence leads to a brighter fluorescence of the bound His-tag molecule. Next we studied how the fluorescence intensity of the membrane bound His-tagged fluorophores was affected by changes in pH. The effect on the membrane bound 6H-GFP is relatively small but the effect on 6H-FITC is very pronounced. This could be due to increased binding of the 6H-FITC or a reduction in the fluorescence quenching by the NTA(Ni) lipid. Next we determined the equilibrium dissociation constant K_d for the interaction between NTA(Ni) and 6H-GFP or 6H-FITC. Based on the data in Figure 4.4, we obtained $K_d = 37.5 \pm 7.5$ nM for 6H-GFP and $K_d = 18.5 \pm 3.7$ nM for 6H-FITC. Finally, we discovered that the NTA(Ni) lipid quenches the fluorescence of 6H-FITC.

Chapter 5

Co(III) forms stable complexes between NTA lipids and His-tags

Introduction

Synthetic biology has the long term goal to make cell-like systems, which implies that integrating proteins into the membrane system becomes an important step. Membrane proteins play a crucial role in cell signaling and cell adhesion. Biofunctionalization of cell-sized GUVs can be achieved either by encapsulating the bioactive molecules or by inserting the proteins into the membranes. Understanding these effects of membrane surface functionalization methods is important to design systematic experiments. Nanoscale changes in the membrane's surrounding can affect the overall membrane mechanics, hence a detailed study of protein immobilization on the membrane surface is necessary to understand other biophysical parameters.

In the last two chapters, I have described the application of the commercially available DGS-NTA(Ni) lipid, that interacts with the histidine chains to bind proteins to membranes. The DGS-NTA lipids containing metal ions is inspired by the chemistry of protein purification. The Ni^{2+} ion mediates the binding of the NTA to the protein. Instead of the Ni^{2+}, other transition metals ions such as Co^{2+}, Zn^{2+}, Fe^{2+}, Cu^{2+}, etc. can be used for the con-

jugation between the NTA and the histidine chain[41,48]. In the context of protein purification, the NTA moiety coordinated with the nickel cation is immobilized in a matrix made of agarose beads. This NTA(Ni) containing matrix is filled in a column and a mixture of proteins with other impurities is passed through it. Electron donating atoms such as oxygen, sulphur or nitrogen in the protein, bind the proteins to the matrix. Since the side chains of amino acids usually consist of these atoms, the proteins get immobilized on the matrix. Out of all the amino acids, histidine binds most specifically to the matrix. The proteins with short histidine chains or histidine rich regions specifically bind with the NTA-Ni complex.

The side chain of the histidine has an electron donating group (with two nitrogen atoms) that forms a coordinate bond with the NTA-Ni complex. When the aromatic side chains of tryptophan, phenylalanine and tyrosine are in the vicinity of histidine, they also seem to contribute by donating electrons to the NTA-metal complex[139]. The adsorption of protein on the matrix is performed at pH values for which the imidazole group in the histidine side chain is in a deprotonated state. NTA coordinated with Ni^{2+} has become popular for the purification of proteins because the interaction between the NTA-Ni complex and the protein can take place at mild conditions, such as in the presence of various salts and at a neutral pH. However, the Ni^{2+} mediated interaction between the NTA and the His-tag has a low affinity and is very sensitive to the presence of other chelators (such as EDTA or imidazole) and to acidic solution. Another limitation for the Ni^{2+} mediated system is that it is kinetically labile and thus undergoes rapid ligand exchange.

When DGS-NTA(Ni) is incorporated into a lipid bilayer the system works similar to the protein purification matrix. Instead of purifying the protein, the lipid bilayer works as a platform for the protein to be immobilized. As mentioned above, the Ni^{2+} mediated complex between the NTA and the histdine chain is reversible. Such a complex is useful when the reversible interaction between the membrane and protein is crucial[22], but does not allow a stronger immobilization of proteins. A strong protein immobilization is important for studies related to cell-cell adhesion[49,140]. To increase the

strength of the NTA-protein bond one may increase the chain length of the histidine, or adding multiple NTA groups to one lipid head group[134,135]. Preparation of such a multi NTA group requires complex chemistry and preparing a lipid with multiple NTA groups would further increase the complexity. Another way to increase the affinity between the NTA lipids and the His-tags is to try different metal ions that mediate this interaction.

Wegner et al.[47] showed that trivalent cobalt ion (Co^{3+}) makes a stable and inert mediator for the NTA and the histidine tag. The Co^{3+} undergoes very slow ligand exchanges and is stable against chelators and reducing agents. The Co^{3+} forms an octahedral complex with NTA occupying four site and two sites are occupied by the histidine chain. The divalent Ni^{2+} or Co^{2+} have a ligand exchange rate of 3×10^6 per second, whereas the Co^{3+} has a ligand exchange rate of 10^{-6} per second.[141] In the former study by Wegner et al., the NTA-Co^{3+}-His-tag was obtained indirectly by first forming a NTA-Co^{2+}-His-tag complex and then oxidising the Co^{2+} by incubating it with hydrogen peroxide (H_2O_2) (Figure 5.1 Strategy 1). However, using such strong oxidising reagent to prepare the NTA-Co^{3+}-His tag complex puts the protein and the lipids at risk of being oxidised and becoming non-functional. This difficulty calls for a different approach to prepare the complex mediated by Co^{3+}. Our collaborators, recently invented a different chemical route to make this complex, without any oxidising reagents[142]. This route starts with Co^{3+} complexed with three carbonate ions. When this complex comes close to the NTA, two carbonates are released and the NTA replaces those coordination sites on the Co^{3+}. The last carbonate is released as carbon dioxide and the His-tag replaces the coordination site (Figure 5.1 Strategy 2). The carbonate of Co^{3+} can be stored for a long time as a powder.

In this chapter, I made the NTA(Co^{3+}) complex on the vesicle membrane. The efficiency of this system is tested by adding a fluorescent labeled His-tagged molecule (6H-GFP) and checking its stability against chelating agents. All experiments and tests were performed using the microfluidic device that was introduced in chapter 2.

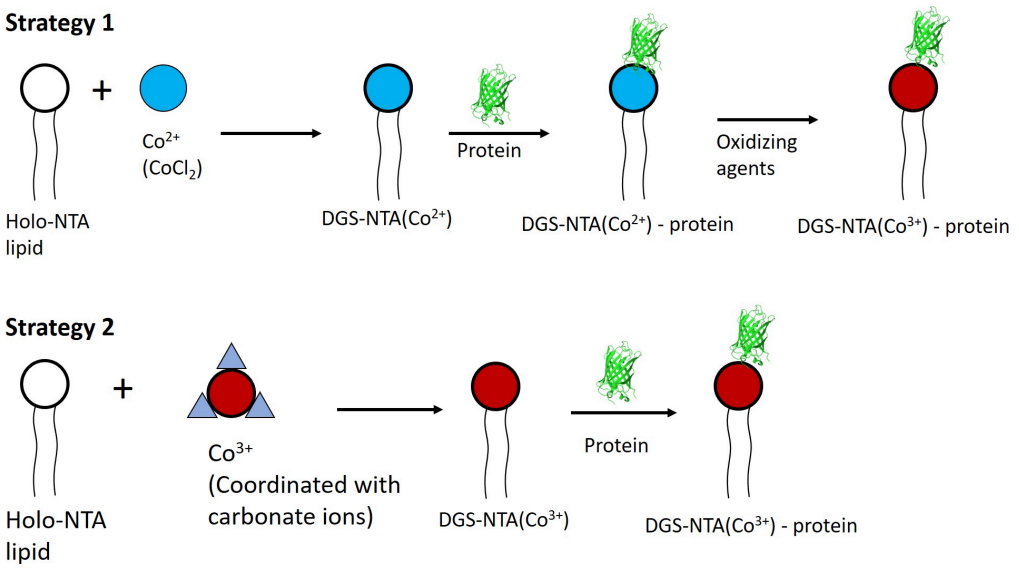

Figure 5.1: Different strategies to prepare Co^{3+} mediated NTA and His-tag interaction. **Strategy 1** Holo NTA lipids in the vesicle membrane are exposed to Co^{2+} in the form of the salt cobalt chloride, forming the intermediate complex NTA(Co^{2+}). His-tag protein is added to form the NTA(Co^{2+})-His-tag complex. The protocol is completed by the addition of oxidising agents, finally yielding the required NTA(Co^{3+})-His-tag complex. **Strategy 2** The Holo-NTA lipids are exposed to Co^{3+} with carbonate ligands (blue triangles) forming the NTA(Co^{3+}) part of the complex. This is followed by adding the His-tagged protein to form the required NTA(Co^{3+})-His-tag complex.

5.1 Experimental method

For simplicity, for the rest of this chapter, the term Ni-NTA will be used as an abbreviation for DGS-NTA(Ni) lipid and Holo-NTA will be used to refer to the DGS-NTA lipid without any metal ion. Before attempting to make the NTA(Co^{3+}) complex, we need to have the Holo-NTA lipid. For the addition of the Co^{3+} ions, the GUV membrane must contain the NTA group with no metal ions. Since I had studied the Ni-NTA lipid in great detail, I started with GUVs made with Ni-NTA. The Ni^{2+} was removed using EDTA. Unfortunately, this procedure affected the GUV membrane and interfered

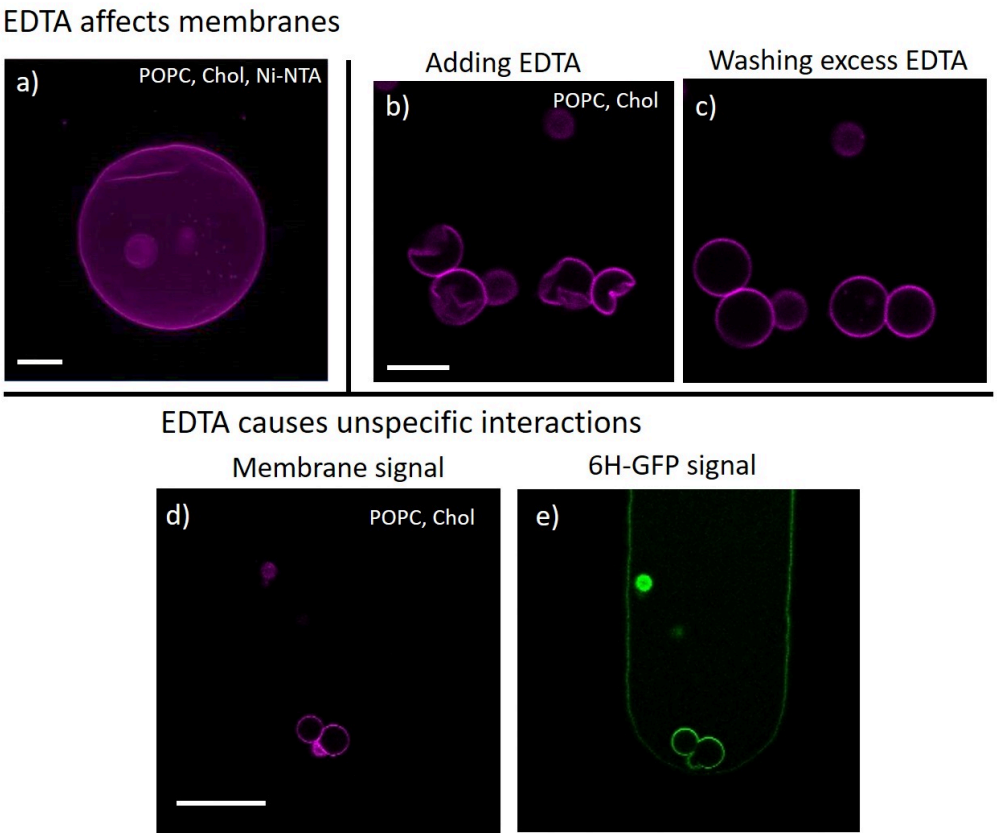

Figure 5.2: Challenges of removing Ni^{2+} from Ni-NTA using EDTA. **a)** Maximum z-projection of a series of confocal images of a vesicle consisting of POPC:Chol in molar ratio of 7:3 and doped with 1% Ni-NTA and 0.05% DHPE-TR (red fluorescent lipid). The vesicles were trapped in the microfluidic device and EDTA was added to the outer solution to remove the Ni^{2+} ion. The vesicle formed solid phases, visible as sharp kinks in the membrane. **b and c)** Confocal images of vesicles trapped in the microfluidic device. Vesicles composed of POPC:Chol (7:3) doped with 0.05% DHPE-TR. When exposed to EDTA, the vesicles attained deformed shapes as in (b) which relaxed back to normal shapes once EDTA was washed out as in (c). **d)** Confocal image of the vesicle. The membrane is doped with 0.05% DHPE-TR. **e)** Confocal image showing unspecific interaction between 6H-GFP and the vesicle membrane (with no Ni-NTA), after addition of EDTA. Scale bars: (a-c) 10 μm, (d-e) 50 μm

with the reaction that we aimed for. As shown in Figure 5.2, the addition of EDTA to GUVs containing the Ni-NTA lipid caused deformations of the GUVs. To find out if this deformation arose from the loss of the Ni^{2+} ion, the control with no NTA lipids was also treated with EDTA. Figure 5.2b shows that the addition of EDTA to a GUV causes membrane deformations even without the Ni-NTA lipid. The removal of EDTA brings back the smoothly curved shapes of the GUVs as in Figure5.2c. However, when these EDTA-treated GUVs were exposed to 6H-GFP, a GFP signal was observed at the membrane. It is important to note that, these GUVs did not contain any NTA lipids, indicating that the GFP signal from the membrane is an artifact caused by EDTA.

For the further experiments, GUVs were prepared using a lipid mixture of POPC and cholesterol in the molar ratio 7:3, doped with either 1mol% Ni-NTA lipid or 1mol% Holo-NTA lipid. For imaging the GUVs in confocal mode, the lipid mixture also contained 0.05 mol% of DHPE-TR dye. The GUVs were made using PVA gel assisted swelling. The GUVs were grown in 10mM HEPES buffer at pH 7.4 with 500mM sucrose. Even though electroformation on Pt wires leads to a better quality and to a higher number of GUVs, the conditions required for the addition of Co^{3+} to NTA were not suitable for electroformation. The Holo-NTA could bind to the metal impurities in the Pt wire and interfere with the addition of Co^{3+}

The chemical process shown in Figure 5.1 Strategy 2 is used obtain the desired NTA(Co^{3+}). The GUVs were trapped in the side channel of the microfluidic device and the solution outside the vesicle was exchanged with 250 mM NaCl in 10 mM HEPES buffer at pH 7.4 to prevent unspecific interactions. Next the Co^{3+} was added in the form of carbonates which was dissolved in sodium bi-carbonate solution. The carbonate solution was washed away with 250 mM NaCl in 10 mM HEPES buffer at pH 7.4. To test the formation of the NTA-Co^{3+} complex, 500 nM of 6H-GFP was added to the outer solution. The stability of the Co^{3+} mediated NTA and 6H-GFP complex was tested by washing away the excess 6H-GFP, calculating the dissociation constant by exchanging the outer solution with increasing concentration of 6H-GFP and adding chelating agents such as imidazole.

5.2 Results and discussions

5.2.1 Establishing the DGS-NTA(Co^{3+}) on the vesicles

As described in the previous section, the GUVs were trapped in the microfluidic device. For this study, first the GUVs doped with 1 mol% Holo-NTA were exposed to 500 nM 6H-GFP. Since this system did not contain any metal ion, no binding could be observed as expected. The trapped GUVs were exposed to the solution containing Co^{3+} coordinated with carbonates. After 20 mins incubation in this solution, the excess Co^{3+} was washed away and 500 nM 6H-GFP was added. As a result the binding of the 6H-GFP to the vesicles membrane was observed as an increased green fluorescence at the membrane.

As shown in Figure 5.3b, when the GUV with the Holo-NTA lipid were exposed to 6H-GFP, they showed no significant membrane fluorescence. This observation excluded any unspecific binding between the GUV membrane and the His-tagged molecule. Following the treatment with Co^{3+}, when the same GUV was again exposed to 6H-GFP, a strong signal of GFP could be observed at the membrane. The binding of the 6H-GFP is used as a read-out for the NTA(Co^{3+}) formation.

5.2.2 Stability against imidazole

The stability of the coordinate bond between the NTA(Co^{3+}) and the 6H-GFP can be tested by exchanging the exterior solution with excess buffer or by subjecting it to chelating agents such as imidazole. For this type of experiment, the GUVs were trapped in the microfluidic device. The GUVs were first treated with Co^{3+} ions and then exposed to 500 nM 6H-GFP. During the experiment the osmolarity across the GUV membrane was balanced by changing the concentration of sucrose and NaCl. After 6H-GFP was bound to the GUV membrane, excess buffer was exchanged to see the stability against washing. Then the buffer was supplemented with 25 mM imidazole. The imidazole competes with the His-tag to bind to the metal cation by donating its electrons. For the control experiment, GUVs were

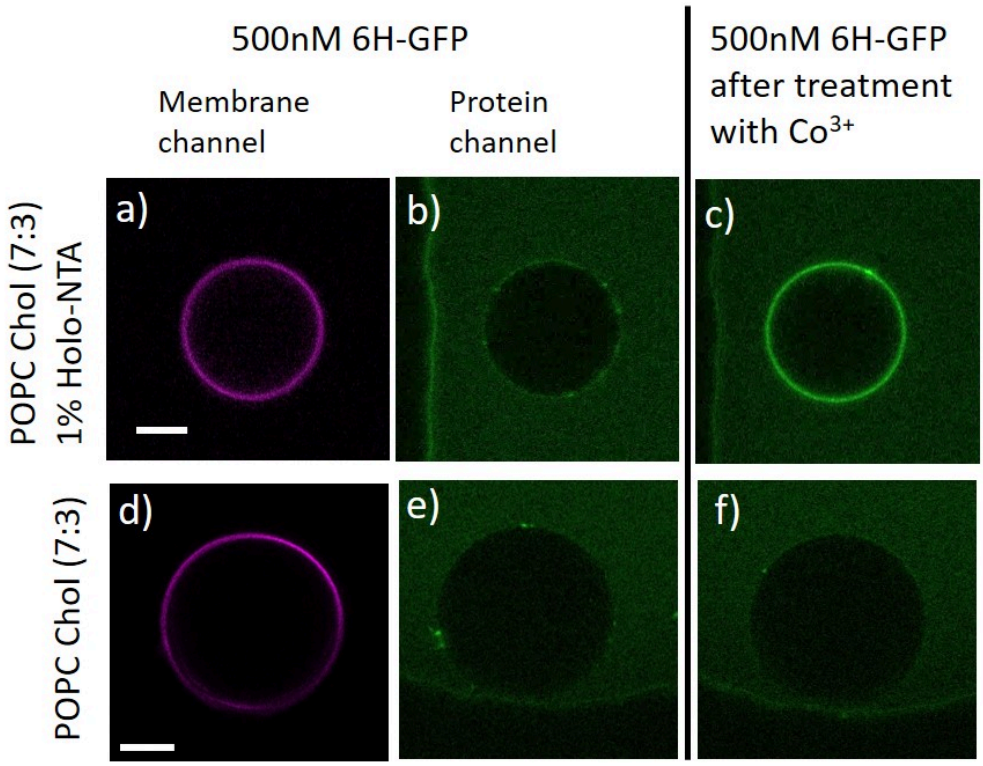

Figure 5.3: Formation of DGS-NTA(Co^{3+}) lipids on GUV membrane. The GUVs were composed of POPC and cholesterol in the molar ratio 7:3 only, as in (d-f) or doped with 1 mol% Holo-NTA, as in (a-c) using PVA assisted swelling. 0.05 mol% DHPE-Texas Red was added to the lipid mix in both cases to image the membrane (a and d). The GUVs enclose 500 mM sucrose in 10 mM HEPES at pH 7.4. For both lipid compositions, the GUVs were exposed to 500 nM 6H-GFP in 250 mM NaCl and 10 mM HEPES at pH 7.4, to balance the osmotic pressure. (a,b,d,e) The GUVs are exposed to 6H-GFP without any treatment of the membrane. The same vesicles were treated with Co^{3+} coordinated with carbonate for 20 mins. After this treatment, the vesicles again exposed to the 6H-GFP as in (c and f). Scale bars: 5 μm

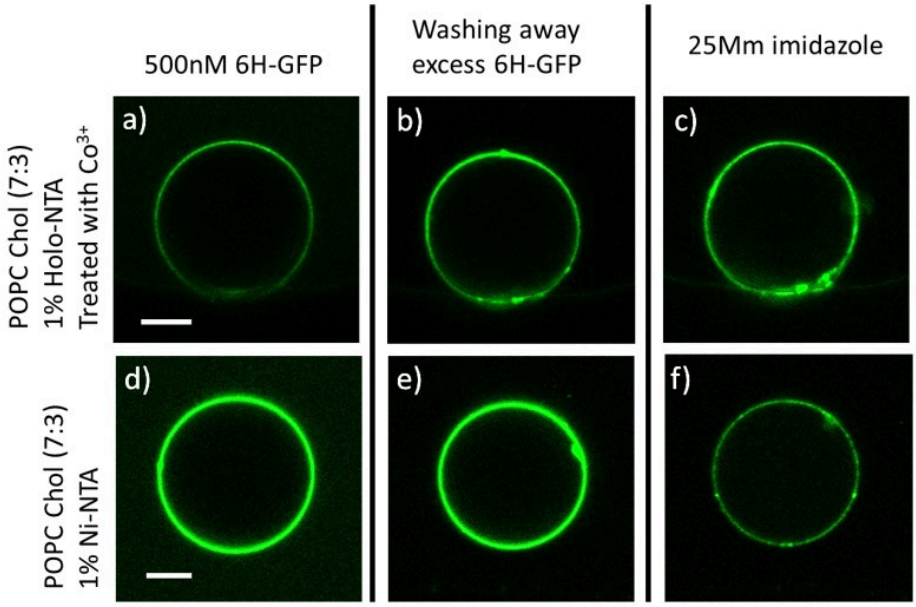

Figure 5.4: Stability of NTA(Co^{3+})-His-tag complex against imidazole. THE GUV membranes composed of POPC and cholesterol in the molar ratio 7:3 doped with 1 mol% Holo-NTA or 1 mol% Ni-NTA. The GUVs were formed using PVA assisted swelling and enclosed 500 mM sucrose in 10 mM HEPES at pH 7.4. The outer solution was exchanged for 250 mM NaCl. The vesicles with Holo-NTA (a-c) were treated with carbonate coordinated with Co^{3+}. (a and d) Vesicles were exposed to 500 nM 6H-GFP. (b and e) Excess 6H-GFP washed away using 250 nM NaCl in 10 mM. (c and f) 25 mM was added to the exterior solution of the GUVs. Scale bars: 5 μm

made with a similar lipid composition, that is, POPC and cholesterol in the molar ratio of 7:3. It was doped with 1 mol% Ni-NTA and 0.05 mol% DHPE-TR for fluorescence imaging. As shown in Figure5.4f, imidazole affects the NTA(Ni^{2+})-6H-GFP more than it affects the NTA(Co^{3+})-6H-GFP complex in Figure5.4c. The lower intensity at the vesicle membrane in 5.4a) compared to that in 5.4d) could be attributed to Co^{3+} not filling all the Holo-NTA sites.

5.2.3 Equilibrium dissociation constant

The dissociation constant for the interaction between NTA(Co^{3+}) and the 6H-GFP can be determined by exposing the GUVs to increasing concentra-

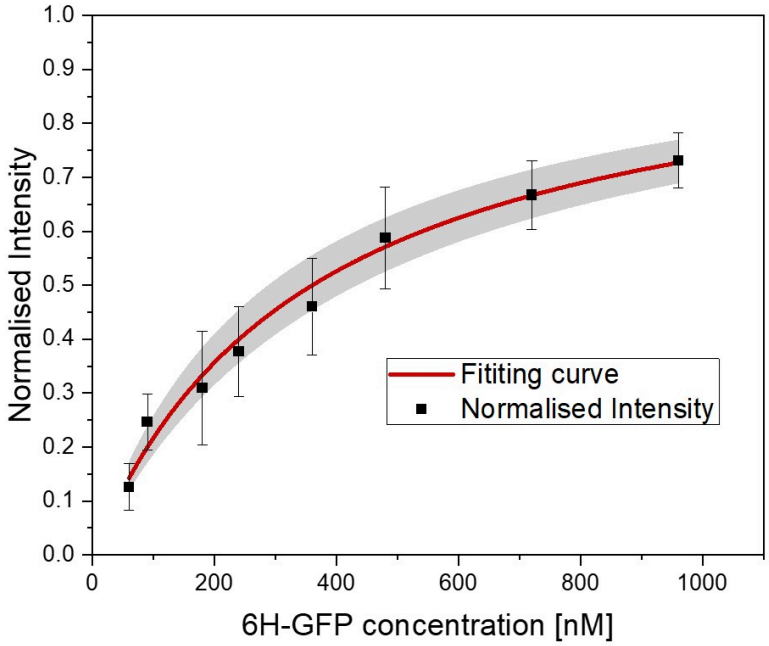

Figure 5.5: Normalized membrane fluorescence versus molar 6H-GFP concentration. The GUVs were made by PVA assisted swelling. The GUVs prepared with 1 mol% of Holo-NTA lipids that were treated with carbonates coordinated by Co^{3+}. The GUVs were exposed to an increasing nanomolar concentration of 6H-GFP at pH 7.4. The fitting curve (red) is provided by equation 4.6 and leads to the equilibrium dissociation constant $K_d = (360.3 \pm 72)$ nM for 6H-GFP. The confidence interval for K_d corresponds to the shaded strip (light grey) around the red fitting curve.

tions of 6H-GFP. The used mole fraction of 1 mole% of Holo-NTA in the membrane implies that the membrane-bound Holo-NTA lipids have an average separation of at least 24 nm[22]. This estimate implies that NTA(Co^{3+}) lipids are also separated by 24 nm. The approximate lateral size of a GFP molecule is 3 nm[132]. Assuming that each 6H-GFP molecule binds only one NTA(Co^{3+}) lipid, the equilibrium dissociation constant can be calculated in the same way as in section 4.2.3. The absolute intensity value was calculated from the radial intensity profile as described previously in section3.4, see Figure3.3. The absolute value of the intensity was fitted to the same

functional form as in equation 4.6 which is given by

$$I_{\text{flu}} = I_{\text{sat}} \frac{X}{K_d + X} \,. \tag{4.6}$$

As shown in Figure5.5, this fitting procedure leads to the dissociation constant $K_d = (360.3 \pm 72)$ nM for the interaction between NTA(Co^{3+}) and 6H-GFP. As 6H-GFP is used as a read-out for whether or not Holo-NTA formed a bond with Co^{3+} the data in Figure5.5 do not provide any estimate of the fraction of Holo-NTA that contain the Co^{3+} ion. Data corresponding to Figure 5.5 is provided in Appendix G.

5.3 Conclusion

The bio-functionalization of membrane systems can be achieved by attaching proteins to the membranes via DGS-NTA anchor lipids and a histidine chain that is attached to the proteins. The formation of this coordinate complex is mediated by transition metal cations. Depending on the choice of the metal cation, the complex may be strong or weak. Commercially the NTA lipid is available with the Ni^{2+} cation. The Ni-NTA - His-tag bond is reversible implying that Ni^{2+} undergoes fast ligand exchange. The Ni^{2+} mediated complex is suitable for experiments that require reversible nature of the complex. On the other hand, when a strong immobilization is required, the Co^{3+} mediated complex proves indispensable. In this chapter, I demonstrated the formation of the NTA(Co^{3+}) complex starting from the Holo-NTA lipid without any metal ion in the GUV membrane. The addition of Co^{3+} is achieved by exposing the vesicles with the Holo-NTA lipid to a solution where Co^{3+} is coordinated with carbonate ions. The 6H-GFP was added as a read-out for the NTA-Co^{3+} complex. The equilibrium dissociation constant for the NTA(Co^{3+})- 6H-GFP was estimated to be (360.3 ± 72) nM. The stability of the complex against imidazole was also tested. The Co^{3+} mediated complex is found to be more stable against imidazole compared to the Ni^{2+} mediated complex.

Chapter 6

Reconstitution of atlastin in giant vesicles

Introduction

The different organelles inside an eukaryotic cell perform various functions for the maintenance of the cell. To avoid content mixing these organelles are mostly bound by lipid membranes. Preparing and integrating these organelles in a synthetic cell is an important goal for the field of bottom-up assembly of a cell. Certain advances have been made in this direction by encapsulating enzyme reaction systems inside GUVs or polymersomes[18,143–145]. However, unlike cell organelles, these synthetic organelles mostly have a spherical shapes. Cellular organelles like the Golgi apparatus, mitochondria and the endoplasmic reticulum (ER) have very complex architectures. Each mitochondrium is enclosed by two lipid bilayers and forms a network inside the cell and undergoes continuous fission and fusion processes depending on the cell environment. The Golgi apparatus involves stacks of flat lipid membrane sheets. The ER spans the whole cells as a single membrane. The peripheral ER is a complex tubular network, whereas close to the nucleus, the ER forms membrane sheets. The ER divides the cytoplasmic region into two separate compartments, the lumen of the ER and the cytosolic region. Molecules can transported withing the cell

by diffusion, directed movement by molecular motors, flowing in the tubular water channels in the ER lumen or via the lipids in the ER membrane.

The ER tubes are connected via three-way junctions and the typical diameter of these tubes is between 50 to 100 nm. For a long time, it was believed that the ER network is formed by molecular motors walking on microtubules pulling the membrane tubes[146,147]. However, several *in-vitro* reconstitution studies have demonstrated that the formation of the ER network does not require the cytoskeletal components[148–151]. The ER is network is formed and maintained by two evolutionary conservative protein families, the reticulons and the receptor expression enhancing proteins (REEPs). These proteins are not only involved in the bending and shaping the ER membrane, but also affect the trafficking of molecules between the ER and the Golgi apparatus and in cell apoptosis[152,153].

Atlastin is a membrane protein that forms dimers coupled to the hydrolysis of GTP. Two proteins which are located on the same membrane, form cis-dimers whereas two atlastin proteins which are located on separate membranes form trans-dimers[154], see Figure6.1a. The homotypic trans-dimerization of two atlastin proteins leads to membrane fusion and to the formation of three-way junctions at which three membrane nanotubes meet. However, the functional significance of cis-dimerization, which is also coupled to GTP hydrolysis, has been elusive so far. In this chapter, we hypothesize that the cis-dimerization of altastin generates an effective membrane tension. Such a tension is also important to understand other aspects of the ER architecture, such as the predominant presence of three-way junctions in the reticulate networks[155].

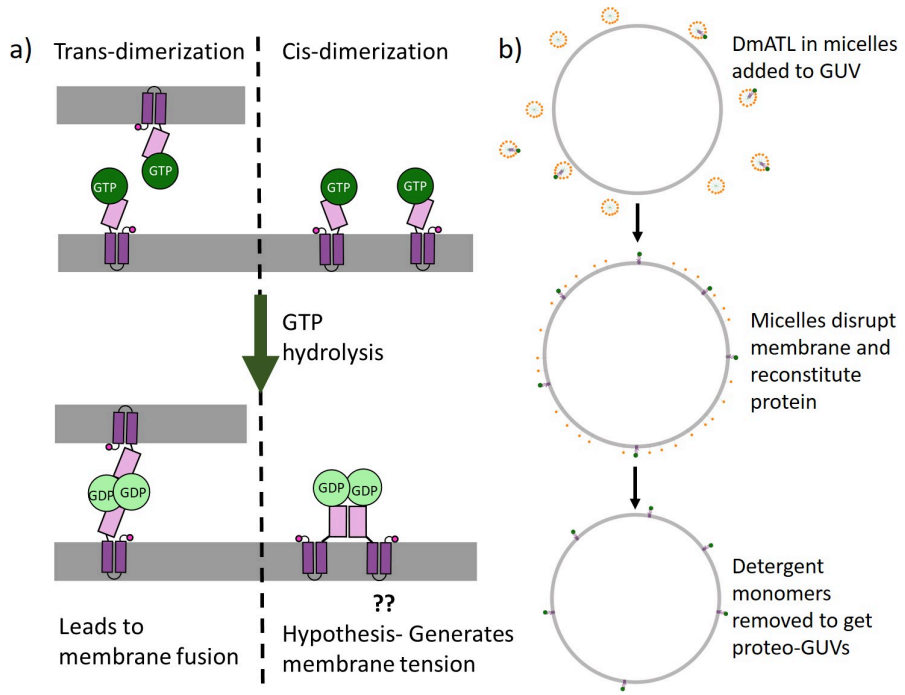

Figure 6.1: **a)** Trans- and cis-dimerization of DmATL. Trans-dimerization occurs when the two atlastin proteins are in separate membrane segments. This trans-dimerization brings the two segments together leading to fusion. Cis-dimerization occurs between two proteins located in the same membrane segment. The reason for the cis-dimerization is unknown. **b)** Protocol for preparing proteo-GUVs with DmATL. The GUVs are incubated with the DmATL present in detergent micelles. The micelles deliver the protein to the membrane. The excess deteregent is adsorbed and removed from the GUV membrane, leaving behind proteo-GUVs.

In this chapter, we describe some preliminary results of detergent assisted reconstitution of *Drosophila Melanogaster* atlastin (DmATL) in GUVs. We used a protocol for detergent-assistant reconstitution[37], as shown in Figure6.1b. Previous studies of DmATL reconstituition in liposomes were based on LUVs that have the diameters between 100 and 200 nm[151,154]. This small size does not allow to perform systematic studies using conventional optical microscopy. The reconstitution of atlastin in GUVs will make it possible to study the effects of atlastin dimerization on the membrane properties using the already established experimental techniques.

6.1 Experimental methods

6.1.1 Protein purification and labeling

The DmATL protein was expressed and purified according to the protocol in Ref[151]. The final buffer of purified atlastin consisted of 25 mM HEPES pH 7.5, 100 mM KCl, 10% (v/v) glycerol, 1% Triton X-100, 2 mM DTE, and 10 mM glutathion reduced. The protein was labeled with Oregon Green 488 succinimidyl ester purchased from Thermo Fischer. The protein and dye was mixed in the molar ratio 1:1 and incubated at 4°C overnight. The free dye was removed using a dialysis membrane with a cutoff of 7kDa.

6.1.2 Making GUVs and incorporating DmATL

The GUVs were made by PVA (polyvinyl alcohol) assisted swelling of lipid bilayers following the optimized protocol in section 3.1. Briefly, 20 μL of 40 mg/mL PVA solution was deposited on a glass slide, spread using a pipette tip, and dried on a hot plate at 60°C for 30 mins. 8 μL of 2 mM lipid mix (POPC:POPG:Chol in the molar ratio of 7:1:2) was spread uniformly on the PVA bed. The chloroform was evaporated by drying under a stream of nitrogen. A small chamber was formed around the dried lipid using a Teflon spacer, another glass slide and fold-back clips. The chamber was filled with the atlastin buffer (25 mM HEPES pH 7.4, 100 mM KCl, 10% glycerol, 1 mM EDTA, 2 mM β-mercaptoethanol). The vesicles were harvested after 30 mins.

Detergent assisted reconstitution of DmATL to GUVs was modified and adapted from the protocol by Dezi et al[37]. The vesicle solution was incubated with the Oregon Green labeled DmATL. The protein buffer already contained the detergent Triton X-100. This detergent destabilized the GUV membrane that could be observed as deformation of the GUV on addition of the detergent, as in Figure 6.2b. This destabilization and the deformation assisted in the incorporation of atlastin. The mixture of GUVs and protein in detergent micelles was incubated for 15 mins at room temperature. The excess detergent was removed by incubating with Bio-Beads SM-2 Resin

(Bio-Rad) for 2 h at 4°C. During this time period of 2 hour, the Bio-Beads were replaced with fresh Bio-Beads every 30 minutes.

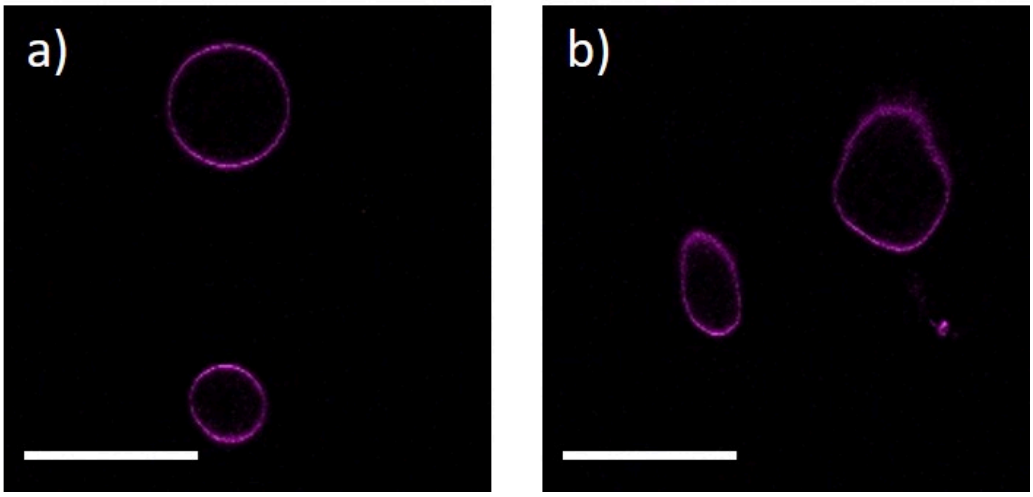

Figure 6.2: **a)** GUV composed of POPC POPG and cholesterol in the molar ration of 7:1:2 doped with 0.05mol% DHPE-TR. **b)** The GUVs are incubated with the DmATL present in detergent micelles. The micelles destabilize the GUV membrane that can be observed as deformation of the GUV membrane. Scale bars: 50 μm.

All samples were imaged using a confocal microscope. The GUVs were settled on the coverslide, using a low-density buffer, the imaging buffer (70 mM HEPES pH 7.4, 340 mM KCl, 8% glycerol, 1 mM EDTA, 2 mM β-mercaptoethanol). The osmolarity of this imaging buffer is the same as that of the atlastin buffer mentioned above. The solution containing the GUVs or the proteo-GUVs was mixed with the imaging buffer in the volume ratio of 2:1 respectively. The imaging buffer was just used to settle the proteo-GUVs and had no other functional role.

6.2 Results

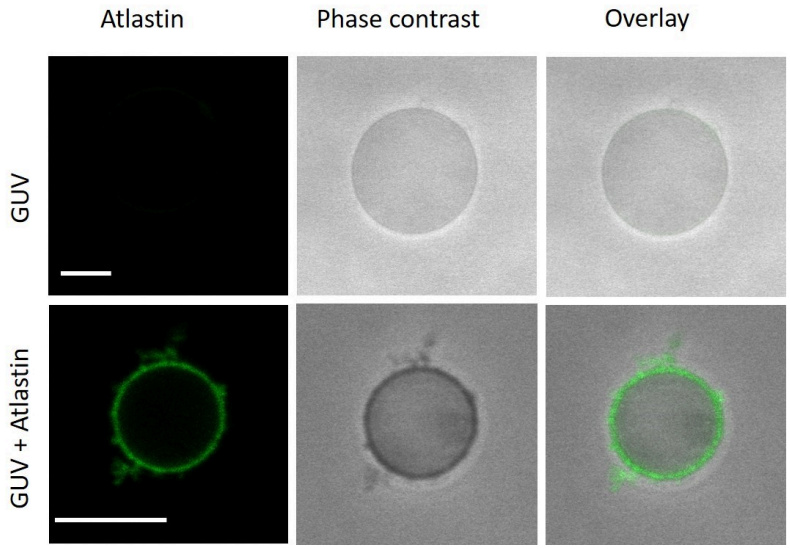

Figure 6.3: Incorporation of atlastin (DmATL) into GUV membranes. GUVs are prepared by PVA assisted swelling with the lipid composition of POPC, POPG, and Chol in the molar ratio 7:1:2. The vesicle solution is incubated with fluorescently labeled atlastin (green), which inserts into the membrane in the presence of the detergent Triton X-100. The detergent is adsorbed and removed using Bio-Beads. The images display some atlastin-containing membrane protrusions. Both scale bars: 10 μm.

Figure 6.3 demonstrates the incorporation of Oregon Green labeled DmATL into a GUV membrane. Being a membrane protein, the purification of DmATL requires the presence of detergent to stabilize it and prevent its aggregation. The DmATL is added to the GUVs with the detergent at a concentration of approixmately 1.6 mM, which is higher than the critical micelle concentration (cmc) of TRITON-X 100 which is 0.2 mM[37]. This ensures that the lipid membrane is disturbed by the protein containing micelles. In order to detect the membrane-bound atlastin, fluorescently labeled DmATL was used for the reconstitution in the membrane. The labeling could affect the GTP hydrolysis function of the protein, hence in further experiments, we will use the unlabeled DmATL.

Complete membrane fusion proceeds via several steps- adhesion, hemi-

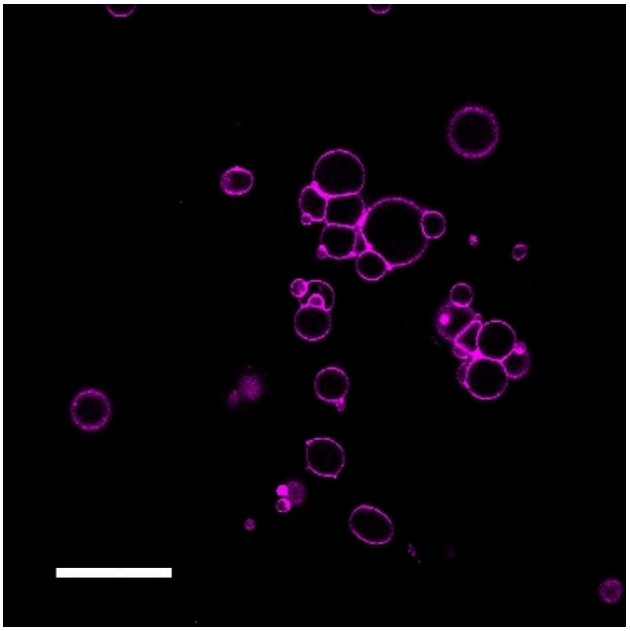

Figure 6.4: DmATL incorporated into the membranes of GUVs made of POPC:POPG:Chol in the molar ratio 7:1:2. The resulting proteo-GUVs were incubated overnight with GTP in the presence of magnesium ions. The vesicles appear to adhere to each other, which is the first step towards membrane fusion. Scale bar 50 μm.

fusion and finally full fusion[156]. In Figure6.4, the proteo-GUVs appear to sdhere to each other, which is necessary in order to achieve membrane fusion.

6.3 Conclusion and outlook

The results presented in this chapter are preliminary and a systematic study remains to be done in order to understand the role of cis-dimerization of the DmATL. We have already achieved to prepare GUVs with DmATL in the membrane, the next step to follow is to show membrane fusion by GTP hydrolysis caused by membrane bound DmATL, Figure6.5. Additional experiments are required to measure the membrane tension of the proteo-GUVs in the presence and absence of GTP.

The ER network consists of irregular polygons connected by three-way junctions of membrane nanotubes with contact angles close to 120°. Main-

tenance of this structure requires continuous supply of GTP and GTP hydrolyzing atlastin. Using micropipette aspiration and other experimental methods to study GUVs. It will become possible to measure the membrane tension and its dependence on GTP hydrolysis[155].

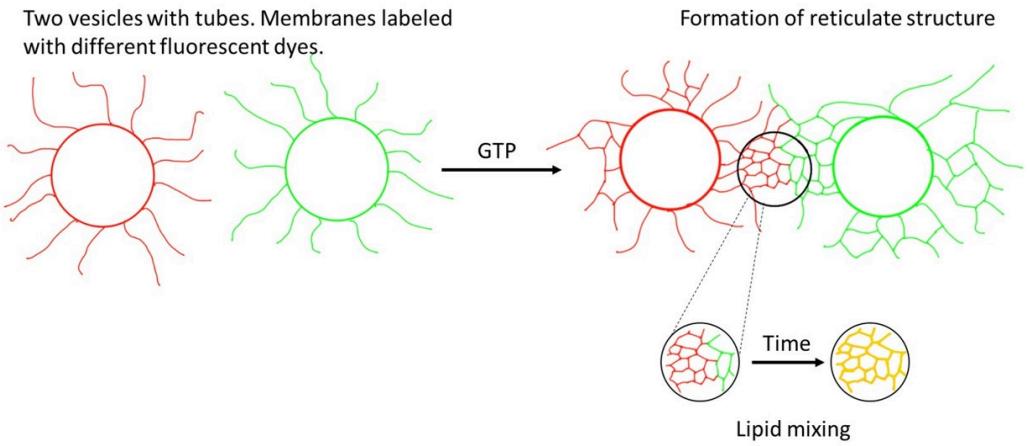

Figure 6.5: Putative experimental approach to demonstrate membrane fusion by atlastin proteins. We start with two populations of GUVs that are labeled with two different dyes that do not interfere with the fluorescence of each other. Nanotubes can be generated on the outside of vesicles by using asymmetric solution conditions (left). These tubulated vesicles will be supplemented by GTP and Mg^{2+} ions, causing them to form three-way junctions by fusing the nanotubes (right). Over time, we should observe lipid mixing and co-localization of the two fluorescent dyes.

Outlook for the thesis

The research field of biomimetic membrane systems has many applications. One of its recent applications is in vaccine technology. mRNA vaccines are based on liposomes that encapsulate RNA and are taken up by human cells. The RNA is transcribed by the cell into parts of pathogenic proteins that are encountered by the immune system, which develops immunity against the actual pathogen. Another application of the biomimetic membrane system is to address questions about the origin of life. Creating a synthetic cell is an ambitious goal and many groups of scientists are working hard to assemble different modules of a cell, such as the ability to form compartments, grow and divide. Proteins play a major role as functional molecules in biomimetic systems.

In this thesis, I explored in detail the different protocols for preparing giant unilamellar vesicles and reconstitution of membrane proteins in them. I also designed a microfluidic device that enabled me to perform various experiments. The results from this work can be applied to further studies such as analysis of changes in the vesicle morphology or the membrane properties due to protein reconstitution via anchor lipids or insertion into the lipid bilayer. The microfluidic device can be employed to study the effect of small molecules such ions or proteins on the membranes of giant vesicles.

Bibliography

[1] Komal Bhattacharyya, David Zwicker, and Karen Alim. Memory capacity of adaptive flow networks. *Physical Review E*, 107(3):034407, 2023.

[2] Richard Dawkins. *The selfish gene*. Oxford university press, 2016.

[3] Erwin Schrodinger. *What is life? The physical aspect of the living cell*. At the University Press, 1951.

[4] Stanley L Miller. A production of amino acids under possible primitive earth conditions. *Science*, 117(3046):528–529, 1953.

[5] Eric T Parker, James H Cleaves, Aaron S Burton, Daniel P Glavin, Jason P Dworkin, Manshui Zhou, Jeffrey L Bada, and Facundo M Fernández. Conducting miller-urey experiments. *JoVE (Journal of Visualized Experiments)*, (83):e51039, 2014.

[6] Joaquín Criado-Reyes, Bruno M Bizzarri, Juan Manuel García-Ruiz, Raffaele Saladino, and Ernesto Di Mauro. The role of borosilicate glass in miller–urey experiment. *Scientific reports*, 11(1):21009, 2021.

[7] Martin Ferus, Fabio Pietrucci, Antonino Marco Saitta, Antonín Knížek, Petr Kubelík, Ondřej Ivanek, Violetta Shestivska, and Svatopluk Civiš. Formation of nucleobases in a miller–urey reducing atmosphere. *Proceedings of the National Academy of Sciences*, 114(17): 4306–4311, 2017.

[8] Michael C Chen, Brian J Cafferty, Irena Mamajanov, Isaac Gallego, Jaheda Khanam, Ramanarayanan Krishnamurthy, and Nicholas V Hud. Spontaneous prebiotic formation of a β-ribofuranoside that self-assembles with a complementary heterocycle. *Journal of the American Chemical Society*, 136(15):5640–5646, 2014.

[9] Shunsuke Tagami and Peiying Li. The origin of life: Rna and protein co-evolution on the ancient earth. *Development, Growth & Differentiation*, 65(3):167–174, 2023.

[10] Elizaveta Guseva, Ronald N Zuckermann, and Ken A Dill. Foldamer hypothesis for the growth and sequence differentiation of prebiotic polymers. *Proceedings of the National Academy of Sciences*, 114(36): E7460–E7468, 2017.

[11] Manfred Eigen. Selforganization of matter and the evolution of biological macromolecules. *Naturwissenschaften*, 58(10):465–523, 1971.

[12] John I Glass, Chuck Merryman, Kim S Wise, Clyde A Hutchison, and Hamilton O Smith. Minimal cells—real and imagined. *Cold Spring Harbor Perspectives in Biology*, 9(12):a023861, 2017.

[13] Clyde A Hutchison III, Scott N Peterson, Steven R Gill, Robin T Cline, Owen White, Claire M Fraser, Hamilton O Smith, and J Craig Venter. Global transposon mutagenesis and a minimal mycoplasma genome. *Science*, 286(5447):2165–2169, 1999.

[14] Clyde A Hutchison III, Ray-Yuan Chuang, Vladimir N Noskov, Nacyra Assad-Garcia, Thomas J Deerinck, Mark H Ellisman, John Gill, Krishna Kannan, Bogumil J Karas, Li Ma, et al. Design and synthesis of a minimal bacterial genome. *Science*, 351(6280):aad6253, 2016.

[15] James Lefley, Christopher Waldron, and C Remzi Becer. Macromolecular design and preparation of polymersomes. *Polymer Chemistry*, 11 (45):7124–7136, 2020.

[16] Manzar Abbas, Wojciech P Lipiński, Jiahua Wang, and Evan Spruijt. Peptide-based coacervates as biomimetic protocells. *Chemical Society Reviews*, 50(6):3690–3705, 2021.

[17] Bastiaan C Buddingh' and Jan CM van Hest. Artificial cells: synthetic compartments with life-like functionality and adaptivity. *Accounts of chemical research*, 50(4):769–777, 2017.

[18] Sunidhi C Shetty, Naresh Yandrapalli, Kerstin Pinkwart, Dorothee Krafft, Tanja Vidakovic-Koch, Ivan Ivanov, and Tom Robinson. Directed signaling cascades in monodisperse artificial eukaryotic cells. *ACS nano*, 15(10):15656–15666, 2021.

[19] Simon Christ, Thomas Litschel, Petra Schwille, and Reinhard Lipowsky. Active shape oscillations of giant vesicles with cyclic closure and opening of membrane necks. *Soft Matter*, 17(2):319–330, 2021.

[20] Agustín Mangiarotti, Nannan Chen, Ziliang Zhao, Reinhard Lipowsky, and Rumiana Dimova. Wetting and complex remodeling of membranes by biomolecular condensates. 2023.

[21] Kristina A Ganzinger, Adrián Merino-Salomón, Daniela A García-Soriano, A Nelson Butterfield, Thomas Litschel, Frank Siedler, and Petra Schwille. Ftsz reorganization facilitates deformation of giant vesicles in microfluidic traps. *Angewandte Chemie International Edition*, 59(48):21372–21376, 2020.

[22] Jan Steinkühler, Roland L Knorr, Ziliang Zhao, Tripta Bhatia, Solveig M Bartelt, Seraphine Wegner, Rumiana Dimova, and Reinhard Lipowsky. Controlled division of cell-sized vesicles by low densities of membrane-bound proteins. *Nature communications*, 11(1): 1–11, 2020.

[23] Yannik Dreher, Kevin Jahnke, Elizaveta Bobkova, Joachim P Spatz, and Kerstin Göpfrich. Division and regrowth of phase-separated gi-

ant unilamellar vesicles. *Angewandte Chemie International Edition*, 60(19):10661–10669, 2021.

[24] Yannik Dreher, Kevin Jahnke, Martin Schröter, and Kerstin Göpfrich. Light-triggered cargo loading and division of dna-containing giant unilamellar lipid vesicles. *Nano Letters*, 21(14):5952–5957, 2021.

[25] Kevin Jahnke, Vanessa Huth, Ulrike Mersdorf, Na Liu, and Kerstin Göpfrich. Bottom-up assembly of synthetic cells with a dna cytoskeleton. *ACS nano*, 16(5):7233–7241, 2022.

[26] Nishkantha Arulkumaran, Mervyn Singer, Stefan Howorka, and Jonathan R Burns. Creating complex protocells and prototissues using simple dna building blocks. *Nature Communications*, 14(1): 1314, 2023.

[27] Rumiana Koynova and Boris Tenchov. Phase transitions and phase behavior of lipids. *Encyclopedia of Biophysics*, pages 1841–1854, 2013.

[28] Charlotte E Conn and John M Seddon. Structures of lipid membranes: Cubic and inverse hexagonal phases. In *Handbook of Lipid Membranes*, pages 49–63. CRC Press, 2021.

[29] Monika Rojewska, Wojciech Smułek, Ewa Kaczorek, and Krystyna Prochaska. Langmuir monolayer techniques for the investigation of model bacterial membranes and antibiotic biodegradation mechanisms. *Membranes*, 11(9):707, 2021.

[30] Joshua A Jackman and Nam-Joon Cho. Supported lipid bilayer formation: beyond vesicle fusion. *Langmuir*, 36(6):1387–1400, 2020.

[31] Sireesha Chemburu, Kyle Fenton, Gabriel P Lopez, and Reema Zeineldin. Biomimetic silica microspheres in biosensing. *Molecules*, 15(3):1932–1957, 2010.

[32] Yohan Lee, Sujin Park, Feng Yuan, Carl C Hayden, Siyoung Q Choi, and Jeanne C Stachowiak. Lateral compression of lipids drives transbilayer coupling of liquid-like protein condensates. *bioRxiv*, pages 2022–12, 2022.

[33] Gonzalo Pérez-Mitta and Roderick MacKinnon. Freestanding lipid bilayer tensiometer for the study of mechanosensitive ion channels. *Proceedings of the National Academy of Sciences*, 120(12): e2221541120, 2023.

[34] Jan Steinkühler, Erdinc Sezgin, Iztok Urbančič, Christian Eggeling, and Rumiana Dimova. Mechanical properties of plasma membrane vesicles correlate with lipid order, viscosity and cell density. *Communications biology*, 2(1):337, 2019.

[35] Ankush Singhal and GJ Agur Sevink. A core-shell approach for systematically coarsening nanoparticle–membrane interactions: application to silver nanoparticles. *Nanomaterials*, 12(21):3859, 2022.

[36] Rikhia Ghosh, Vahid Satarifard, Andrea Grafmueller, and Reinhard Lipowsky. Budding and fission of nanovesicles induced by membrane adsorption of small solutes. *ACS nano*, 15(4):7237–7248, 2021.

[37] Manuela Dezi, Aurelie Di Cicco, Patricia Bassereau, and Daniel Lévy. Detergent-mediated incorporation of transmembrane proteins in giant unilamellar vesicles with controlled physiological contents. *Proceedings of the National Academy of Sciences*, 110(18):7276–7281, 2013.

[38] Ida Louise Jørgensen, Gerdi Christine Kemmer, and Thomas Günther Pomorski. Membrane protein reconstitution into giant unilamellar vesicles: a review on current techniques. *European Biophysics Journal*, 46:103–119, 2017.

[39] Matthias Garten, Sophie Aimon, Patricia Bassereau, and Gilman ES Toombes. Reconstitution of a transmembrane protein, the voltage-gated ion channel, kvap, into giant unilamellar vesicles for microscopy and patch clamp studies. *JoVE (Journal of Visualized Experiments)*, (95):e52281, 2015.

[40] Eva M Schmid, David L Richmond, and Daniel A Fletcher. Reconstitution of proteins on electroformed giant unilamellar vesicles. In *Methods in cell biology*, volume 128, pages 319–338. Elsevier, 2015.

[41] Joshua A Bornhorst and Joseph J Falke. [16] purification of proteins using polyhistidine affinity tags. In *Methods in enzymology*, volume 326, pages 245–254. Elsevier, 2000.

[42] Lutz Schmitt, Christian Dietrich, and Robert Tampe. Synthesis and characterization of chelator-lipids for reversible immobilization of engineered proteins at self-assembled lipid interfaces. *Journal of the American Chemical Society*, 116(19):8485–8491, 1994.

[43] Steven Knecht, Daniel Ricklin, Alex N Eberle, and Beat Ernst. Oligohis-tags: mechanisms of binding to ni2+-nta surfaces. *Journal of Molecular Recognition*, 22(4):270–279, 2009.

[44] Jeanne C Stachowiak, Eva M Schmid, Christopher J Ryan, Hyoung Sook Ann, Darryl Y Sasaki, Michael B Sherman, Phillip L Geissler, Daniel A Fletcher, and Carl C Hayden. Membrane bending by protein–protein crowding. *Nature cell biology*, 14(9):944–949, 2012.

[45] Megan Farell, Ava Self, Christine Guza, Hyewon Song, Luigi Apollon, Esther W Gomez, and Manish Kumar. Lipid-functionalized graphene loaded with hmnsod for selective inhibition of cancer cells. *ACS applied materials & interfaces*, 12(11):12407–12416, 2020.

[46] Shodai Togo, Ken Sato, Ryuzo Kawamura, Naritaka Kobayashi, Makoto Noiri, Seiichiro Nakabayashi, Yuji Teramura, and Hiroshi Y

Yoshikawa. Quantitative evaluation of the impact of artificial cell adhesion via dna hybridization on e-cadherin-mediated cell adhesion. *APL bioengineering*, 4(1):016103, 2020.

[47] Seraphine V Wegner and Joachim P Spatz. Cobalt (iii) as a stable and inert mediator ion between nta and his6-tagged proteins. *Angewandte Chemie International Edition*, 52(29):7593–7596, 2013.

[48] Seraphine V Wegner, Franziska C Schenk, and Joachim P Spatz. Cobalt (iii)-mediated permanent and stable immobilization of histidine-tagged proteins on nta-functionalized surfaces. *Chemistry–A European Journal*, 22(9):3156–3162, 2016.

[49] Jacopo Di Russo, Jennifer L Young, Adithya Balakrishnan, Amelie S Benk, and Joachim P Spatz. Nta-co3+-his6 versus nta-ni2+-his6 mediated e-cadherin surface immobilization enhances cellular traction. *Biomaterials*, 192:171–178, 2019.

[50] Annela M Seddon, Paul Curnow, and Paula J Booth. Membrane proteins, lipids and detergents: not just a soap opera. *Biochimica et Biophysica Acta (BBA)-Biomembranes*, 1666(1-2):105–117, 2004.

[51] Kerry M. Strickland, Kasahun Neselu, Arshay J. Grant, Carolann L. Espy, Nael A. McCarty, and Ingeborg Schmidt-Krey. *Reconstitution of Detergent-Solubilized Membrane Proteins into Proteoliposomes and Nanodiscs for Functional and Structural Studies*, pages 21–35. Springer US, 2021.

[52] Adelina-Gabriela Niculescu, Cristina Chircov, Alexandra Cătălina Bîrcă, and Alexandru Mihai Grumezescu. Fabrication and applications of microfluidic devices: A review. *International Journal of Molecular Sciences*, 22(4):2011, 2021.

[53] S Elizabeth Hulme, Sergey S Shevkoplyas, Javier Apfeld, Walter Fontana, and George M Whitesides. A microfabricated array of

clamps for immobilizing and imaging c. elegans. *Lab on a Chip*, 7(11):1515–1523, 2007.

[54] Marian Weiss, Johannes Patrick Frohnmayer, Lucia Theresa Benk, Barbara Haller, Jan-Willi Janiesch, Thomas Heitkamp, Michael Börsch, Rafael B Lira, Rumiana Dimova, Reinhard Lipowsky, et al. Sequential bottom-up assembly of mechanically stabilized synthetic cells by microfluidics. *Nature materials*, 17(1):89–96, 2018.

[55] Oskar Staufer, Silvia Antona, Dennis Zhang, Júlia Csatári, Martin Schröter, Jan-Willi Janiesch, Sebastian Fabritz, Imre Berger, Ilia Platzman, and Joachim P Spatz. Microfluidic production and characterization of biofunctionalized giant unilamellar vesicles for targeted intracellular cargo delivery. *Biomaterials*, 264:120203, 2021.

[56] Qirui Wu, Jinfeng Liu, Xiaohong Wang, Lingyan Feng, Jinbo Wu, Xiaoli Zhu, Weijia Wen, and Xiuqing Gong. Organ-on-a-chip: Recent breakthroughs and future prospects. *Biomedical engineering online*, 19(1):1–19, 2020.

[57] Lei Wang, Wenming Liu, Yaolei Wang, Jian-chun Wang, Qin Tu, Rui Liu, and Jinyi Wang. Construction of oxygen and chemical concentration gradients in a single microfluidic device for studying tumor cell–drug interactions in a dynamic hypoxia microenvironment. *Lab on a Chip*, 13(4):695–705, 2013.

[58] Peter A Galie, Duc-Huy T Nguyen, Colin K Choi, Daniel M Cohen, Paul A Janmey, and Christopher S Chen. Fluid shear stress threshold regulates angiogenic sprouting. *Proceedings of the National Academy of Sciences*, 111(22):7968–7973, 2014.

[59] Zhiyun Xu, Yanghui Gao, Yuanyuan Hao, Encheng Li, Yan Wang, Jianing Zhang, Wenxin Wang, Zhancheng Gao, and Qi Wang. Application of a microfluidic chip-based 3d co-culture to test drug sensitivity for individualized treatment of lung cancer. *Biomaterials*, 34 (16):4109–4117, 2013.

[60] Chen-Ta Ho, Ruei-Zeng Lin, Rong-Jhe Chen, Chung-Kuang Chin, Song-En Gong, Hwan-You Chang, Hwei-Ling Peng, Long Hsu, Tri-Rung Yew, Shau-Feng Chang, et al. Liver-cell patterning lab chip: mimicking the morphology of liver lobule tissue. *Lab on a Chip*, 13 (18):3578–3587, 2013.

[61] Ross Booth and Hanseup Kim. Characterization of a microfluidic in vitro model of the blood-brain barrier (μbbb). *Lab on a Chip*, 12 (10):1784–1792, 2012.

[62] Samantha Peel, Adam M Corrigan, Beate Ehrhardt, Kyung-Jin Jang, Pedro Caetano-Pinto, Matthew Boeckeler, Jonathan E Rubins, Konstantia Kodella, Debora B Petropolis, Janey Ronxhi, et al. Introducing an automated high content confocal imaging approach for organs-on-chips. *Lab on a Chip*, 19(3):410–421, 2019.

[63] Jie Zhang, Xiaofeng Wei, Rui Zeng, Feng Xu, and XiuJun Li. Stem cell culture and differentiation in microfluidic devices toward organ-on-a-chip. *Future science OA*, 3(2):FSO187, 2017.

[64] Bartholomew J Kane, Michael J Zinner, Martin L Yarmush, and Mehmet Toner. Liver-specific functional studies in a microfluidic array of primary mammalian hepatocytes. *Analytical chemistry*, 78 (13):4291–4298, 2006.

[65] Dongeun Huh, Benjamin D Matthews, Akiko Mammoto, Martín Montoya-Zavala, Hong Yuan Hsin, and Donald E Ingber. Reconstituting organ-level lung functions on a chip. *Science*, 328(5986): 1662–1668, 2010.

[66] Kyung-Jin Jang and Kahp-Yang Suh. A multi-layer microfluidic device for efficient culture and analysis of renal tubular cells. *Lab on a Chip*, 10(1):36–42, 2010.

[67] Anna Grosberg, Alexander P Nesmith, Josue A Goss, Mark D Brigham, Megan L McCain, and Kevin Kit Parker. Muscle on a chip:

in vitro contractility assays for smooth and striated muscle. *Journal of pharmacological and toxicological methods*, 65(3):126–135, 2012.

[68] Yuki Imura, Yasuyuki Asano, Kiichi Sato, and Etsuro Yoshimura. A microfluidic system to evaluate intestinal absorption. *Analytical Sciences*, 25(12):1403–1407, 2009.

[69] Daphne Bazopoulou, Amrita R Chaudhury, Alexandros Pantazis, and Nikos Chronis. An automated compound screening for anti-aging effects on the function of c. elegans sensory neurons. *Scientific reports*, 7(1):1–10, 2017.

[70] Peter J Asiello and Antje J Baeumner. Miniaturized isothermal nucleic acid amplification, a review. *Lab on a Chip*, 11(8):1420–1430, 2011.

[71] Yongjian Ai, Ruoxiao Xie, Jialiang Xiong, and Qionglin Liang. Microfluidics for biosynthesizing: from droplets and vesicles to artificial cells. *Small*, 16(9):1903940, 2020.

[72] Naresh Yandrapalli, Julien Petit, Oliver Bäumchen, and Tom Robinson. Surfactant-free production of biomimetic giant unilamellar vesicles using pdms-based microfluidics. *Communications Chemistry*, 4(1):1–10, 2021.

[73] Jeanne C Stachowiak, David L Richmond, Thomas H Li, Allen P Liu, Sapun H Parekh, and Daniel A Fletcher. Unilamellar vesicle formation and encapsulation by microfluidic jetting. *Proceedings of the national academy of sciences*, 105(12):4697–4702, 2008.

[74] Naresh Yandrapalli and Tom Robinson. Ultra-high capacity microfluidic trapping of giant vesicles for high-throughput membrane studies. *Lab on a Chip*, 19(4):626–633, 2019.

[75] Ziliang Zhao, Debjit Roy, Jan Steinkühler, Tom Robinson, Reinhard Lipowsky, and Rumiana Dimova. Super-resolution imaging of highly

curved membrane structures in giant vesicles encapsulating molecular condensates. *Advanced Materials*, 34(4):2106633, 2022.

[76] Tom Robinson, Phillip Kuhn, Klaus Eyer, and Petra S Dittrich. Microfluidic trapping of giant unilamellar vesicles to study transport through a membrane pore. *Biomicrofluidics*, 7(4):044105, 2013.

[77] Yuki Kazayama, Tetsuhiko Teshima, Toshihisa Osaki, Shoji Takeuchi, and Taro Toyota. Integrated microfluidic system for size-based selection and trapping of giant vesicles. *Analytical chemistry*, 88(2): 1111–1116, 2016.

[78] Sabine A Lauer and John P Nolan. Development and characterization of ni-nta-bearing microspheres. *Cytometry: The Journal of the International Society for Analytical Cytology*, 48(3):136–145, 2002.

[79] Franziska A Thomas, Ilaria Visco, Zdeněk Petrášek, Fabian Heinemann, and Petra Schwille. Diffusion coefficients and dissociation constants of enhanced green fluorescent protein binding to free standing membranes. *Data in Brief*, 5:537–541, 2015.

[80] Franziska A Thomas, Ilaria Visco, Zdeněk Petrášek, Fabian Heinemann, and Petra Schwille. Introducing a fluorescence-based standard to quantify protein partitioning into membranes. *Biochimica et Biophysica Acta (BBA)-Biomembranes*, 1848(11):2932–2941, 2015.

[81] Tripta Bhatia, Simon Christ, Jan Steinkühler, Rumiana Dimova, and Reinhard Lipowsky. Simple sugars shape giant vesicles into multispheres with many membrane necks. *Soft matter*, 16(5):1246–1258, 2020.

[82] Derek Marsh. *Handbook of lipid bilayers*. CRC press, 2013.

[83] Lukas Wettmann and Karsten Kruse. The min-protein oscillations in escherichia coli: an example of self-organized cellular protein waves. *Philosophical Transactions of the Royal Society B: Biological Sciences*, 373(1747):20170111, 2018.

[84] Raffaele Saladino, Claudia Crestini, Fabiana Ciciriello, Samanta Pino, Giovanna Costanzo, and Ernesto Di Mauro. From formamide to rna: the roles of formamide and water in the evolution of chemical information. *Research in Microbiology*, 160(7):441–448, 2009.

[85] Andreas Weinberger, Feng-Ching Tsai, Gijsje H Koenderink, Thais F Schmidt, Rosângela Itri, Wolfgang Meier, Tatiana Schmatko, André Schröder, and Carlos Marques. Gel-assisted formation of giant unilamellar vesicles. *Biophysical journal*, 105(1):154–164, 2013.

[86] Shreya Pramanik, Jan Steinkühler, Rumiana Dimova, Joachim Spatz, and Reinhard Lipowsky. Binding of his-tagged fluorophores to lipid bilayers of giant vesicles. *Soft Matter*, 18(34):6372–6383, 2022.

[87] Mareike S Stephan, Valentin Dunsing, Shreya Pramanik, Salvatore Chiantia, Stefanie Barbirz, Tom Robinson, and Rumiana Dimova. Biomimetic asymmetric bacterial membranes incorporating lipopolysaccharides. *Biophysical Journal*, 2022.

[88] Kerstin Goepfrich, Barbara Haller, Oskar Staufer, Yannik Dreher, Ulrike Mersdorf, Ilia Platzman, and Joachim P Spatz. One-pot assembly of complex giant unilamellar vesicle-based synthetic cells. *ACS synthetic biology*, 8(5):937–947, 2019.

[89] M Angelova and Dimiter S Dimitrov. A mechanism of liposome electroformation. *Trends in colloid and interface science II*, pages 59–67, 1988.

[90] Hammad A Faizi, Annie Tsui, Rumiana Dimova, and Petia M Vlahovska. Bending rigidity, capacitance, and shear viscosity of giant vesicle membranes prepared by spontaneous swelling, electroformation, gel-assisted, and phase transfer methods: a comparative study. *Langmuir*, 38(34):10548–10557, 2022.

[91] John P Reeves and Robert M Dowben. Formation and properties of thin-walled phospholipid vesicles. *Journal of cellular physiology*, 73 (1):49–60, 1969.

[92] Kanta Tsumoto, Hideki Matsuo, Masahiro Tomita, and Tetsuro Yoshimura. Efficient formation of giant liposomes through the gentle hydration of phosphatidylcholine films doped with sugar. *Colloids and Surfaces B: Biointerfaces*, 68(1):98–105, 2009.

[93] Rumiana Dimova and Carlos Marques. *The giant vesicle book*. CRC Press, 2019.

[94] Kim S Horger, Daniel J Estes, Ricardo Capone, and Michael Mayer. Films of agarose enable rapid formation of giant liposomes in solutions of physiologic ionic strength. *Journal of the American chemical society*, 131(5):1810–1819, 2009.

[95] Eric Parigoris, Daniel L Dunkelmann, and Unai Silvan. Generation of giant unilamellar vesicles (guvs) using polyacrylamide gels. *Bioprotocol*, 10(21):e3807–e3807, 2020.

[96] Rafael B Lira, Rumiana Dimova, and Karin A Riske. Giant unilamellar vesicles formed by hybrid films of agarose and lipids display altered mechanical properties. *Biophysical journal*, 107(7):1609–1619, 2014.

[97] DS Dimitrov and MI Angelova. Swelling and electroswelling of lipids—theory and experiment. *Stud. Biophys*, 113:15–20, 1986.

[98] Jan Steinkühler, Philippe De Tillieux, Roland L Knorr, Reinhard Lipowsky, and Rumiana Dimova. Charged giant unilamellar vesicles prepared by electroformation exhibit nanotubes and transbilayer lipid asymmetry. *Scientific reports*, 8(1):1–9, 2018.

[99] Yukihisa Okumura and Yuuichi Iwata. Electroformation of giant vesicles on indium tin oxide (ito)-coated poly (ethylene terephthalate)(pet) electrodes. *Membranes*, 1(2):109–118, 2011.

[100] Valerio Pereno, Dario Carugo, Luca Bau, Erdinc Sezgin, Jorge Bernardino de la Serna, Christian Eggeling, and Eleanor Stride. Electroformation of giant unilamellar vesicles on stainless steel electrodes. *ACS omega*, 2(3):994–1002, 2017.

[101] Himadri Gourav Behuria, Bijesh Kumar Biswal, and Santosh Kumar Sahu. Electroformation of liposomes and phytosomes using copper electrode. *Journal of Liposome Research*, 31(3):255–266, 2021.

[102] Yi Li, Jing Jing, Xuejun Zhang, Jie Cao, Yiwei Li, and Sihui Zhan. Great application prospect in vivo: Efficient electroformation of giant vesicles on novel carbon fiber microelectrode. *Electrochemistry communications*, 25:151–154, 2012.

[103] Peter Walde, Katia Cosentino, Helen Engel, and Pasquale Stano. Giant vesicles: preparations and applications. *ChemBioChem*, 11(7): 848–865, 2010.

[104] Zvonimir Boban, Ivan Mardešić, Witold Karol Subczynski, and Marija Raguz. Giant unilamellar vesicle electroformation: what to use, what to avoid, and how to quantify the results. *Membranes*, 11(11): 860, 2021.

[105] Tanja Pott, Hélène Bouvrais, and Philippe Méléard. Giant unilamellar vesicle formation under physiologically relevant conditions. *Chemistry and physics of lipids*, 154(2):115–119, 2008.

[106] Christoph Herold, Grzegorz Chwastek, Petra Schwille, and Eugene P Petrov. Efficient electroformation of supergiant unilamellar vesicles containing cationic lipids on ito-coated electrodes. *Langmuir*, 28 (13):5518–5521, 2012.

[107] Hongmei Bi, Bin Yang, Lei Wang, Wenwu Cao, and Xiaojun Han. Electroformation of giant unilamellar vesicles using interdigitated ito electrodes. *Journal of materials chemistry A*, 1(24):7125–7130, 2013.

[108] Pauline Lefrançois, Bertrand Goudeau, and Stéphane Arbault. Electroformation of phospholipid giant unilamellar vesicles in physiological phosphate buffer. *Integrative biology*, 10(7):429–434, 2018.

[109] Joanne Crowe, Brigitte Steude Masone, and Joachim Ribbe. One-step purification of recombinant proteins with the 6xhis tag and ni-nta resin. *Molecular biotechnology*, 4:247–258, 1995.

[110] Mikhail A Malyarick, Andrey B Ilyuhin, and Svetlana P Petrosyants. Seven-and eight-coordinate complexes of indium (iii) with nitrilotriacetate. *Main Group Metal Chemistry*, 17(10):707–718, 1994.

[111] Tarita Biver, Rossella Friani, Chiara Gattai, Fernando Secco, Maria Rosaria Tiné, and Marcella Venturini. Mechanism of indium (iii) exchange between nta and transferrin: A kinetic approach. *The Journal of Physical Chemistry B*, 112(38):12168–12173, 2008.

[112] Hélène Bouvrais, Lars Duelund, and John H Ipsen. Buffers affect the bending rigidity of model lipid membranes. *Langmuir*, 30(1):13–16, 2014.

[113] Judith U De Mel, Sudipta Gupta, Rasangi M Perera, Ly Ngo, Piotr Zolnierczuk, Markus Bleuel, Sai Venkatesh Pingali, and Gerald J Schneider. Influence of external nacl salt on membrane rigidity of neutral dopc vesicles. *Langmuir*, 36(32):9356–9367, 2020.

[114] Pabitra Maity, Baishakhi Saha, Gopinatha Suresh Kumar, and Sanat Karmakar. Effect of counterions on the binding affinity of na+ ions with phospholipid membranes. *RSC advances*, 6(87):83916–83925, 2016.

[115] Van A Ngo, Sumantra Sarkar, Chris Neale, and Angel E Garcia. How anionic lipids affect spatiotemporal properties of kras4b on model membranes. *The Journal of Physical Chemistry B*, 124(26):5434–5453, 2020.

[116] Matías A Crosio, Matías A Via, Candelaria I Cámara, Agustin Mangiarotti, Mario G Del Pópolo, and Natalia Wilke. Interaction of a polyarginine peptide with membranes of different mechanical properties. *Biomolecules*, 9(10):625, 2019.

[117] Frederick A Heberle and Gerald W Feigenson. Phase separation in lipid membranes. *Cold Spring Harbor perspectives in biology*, 3(4): a004630, 2011.

[118] Hiroki Himeno, Naofumi Shimokawa, Shigeyuki Komura, David Andelman, Tsutomu Hamada, and Masahiro Takagi. Charge-induced phase separation in lipid membranes. *Soft Matter*, 10(40):7959–7967, 2014.

[119] Roland L Knorr, Jan Steinkühler, and Rumiana Dimova. Micron-sized domains in quasi single-component giant vesicles. *Biochimica et Biophysica Acta (BBA)-Biomembranes*, 1860(10):1957–1964, 2018.

[120] Reinhard Lipowsky. Remodeling of membrane shape and topology by curvature elasticity and membrane tension. *Advanced Biology*, 6 (1):2101020, 2022.

[121] Teresa Peiró-Salvador, Oscar Ces, Richard H Templer, and Annela M Seddon. Buffers may adversely affect model lipid membranes: a cautionary tale. *Biochemistry*, 48(47):11149–11151, 2009.

[122] Li-Qing Chen, Lily S Cheung, Liang Feng, Widmar Tanner, and Wolf B Frommer. Transport of sugars. *Annual Review of Biochemistry*, 84:865–894, 2015.

[123] Heidi D Andersen, Chunhua Wang, Lise Arleth, Günther H Peters, and Peter Westh. Reconciliation of opposing views on membrane–sugar interactions. *Proceedings of the National Academy of Sciences*, 108(5):1874–1878, 2011.

[124] Xiao You, Euihyun Lee, Cong Xu, and Carlos R Baiz. Molecular mechanism of cell membrane protection by sugars: a study of interfacial h-bond networks. *The Journal of Physical Chemistry Letters*, 12(39):9602–9607, 2021.

[125] Yashar Bashirzadeh, Nadab H Wubshet, and Allen P Liu. Confinement geometry tunes fascin-actin bundle structures and consequently the shape of a lipid bilayer vesicle. *Frontiers in molecular biosciences*, 7:610277, 2020.

[126] Lucia Baldauf, Felix Frey, Marcos Arribas Perez, Timon Idema, and Gijsje H Koenderink. Branched actin cortices reconstituted in vesicles sense membrane curvature. *Biophysical journal*, 2023.

[127] Lori Van de Cauter, Federico Fanalista, Lennard Van Buren, Nicola De Franceschi, Elisa Godino, Sharon Bouw, Christophe Danelon, Cees Dekker, Gijsje H Koenderink, and Kristina A Ganzinger. Optimized cdice for efficient reconstitution of biological systems in giant unilamellar vesicles. *ACS Synthetic Biology*, 10(7):1690–1702, 2021.

[128] Marzieh Karimi, Jan Steink$'$uhler, Debjit Roy, Raktim Dasgupta, Reinhard Lipowsky, and Rumiana Dimova. Asymmetric ionic conditions generate large membrane curvatures. *Nano letters*, 18(12): 7816–7821, 2018.

[129] Chanh Thi Minh Le, Aamd Houri, Nimalka Balage, Brian J Smith, and Adam Mechler. Interaction of small ionic species with phospholipid membranes: The role of metal coordination. *Frontiers in Materials*, 5:80, 2019.

[130] Avigdor Leftin, Trivikram R Molugu, Constantin Job, Klaus Beyer, and Michael F Brown. Area per lipid and cholesterol interactions in membranes from separated local-field 13c nmr spectroscopy. *Biophysical journal*, 107(10):2274–2286, 2014.

[131] Ganesh Shahane, Wei Ding, Michail Palaiokostas, and Mario Orsi. Physical properties of model biological lipid bilayers: insights from all-atom molecular dynamics simulations. *Journal of molecular modeling*, 25:1–13, 2019.

[132] James AJ Arpino, Pierre J Rizkallah, and D Dafydd Jones. Crystal structure of enhanced green fluorescent protein to 1.35 å resolution reveals alternative conformations for glu222. *PLoS ONE 7*, 2012.

[133] Gokul Raghunath and R Brian Dyer. Kinetics of histidine-tagged protein association to nickel-decorated liposome surfaces. *Langmuir*, 35(38):12550–12561, 2019.

[134] Suman Lata, Martynas Gavutis, Robert Tampé, and Jacob Piehler. Specific and stable fluorescence labeling of histidine-tagged proteins for dissecting multi-protein complex formation. *Journal of the American Chemical Society*, 128(7):2365–2372, 2006.

[135] Suman Lata, Annett Reichel, Roland Brock, Robert Tampé, and Jacob Piehler. High-affinity adaptors for switchable recognition of histidine-tagged proteins. *Journal of the American Chemical Society*, 127(29):10205–10215, 2005.

[136] Yevgen O Posokhov, Alexander Kyrychenko, and Alexey S Ladokhin. Steady-state and time-resolved fluorescence quenching with transition metal ions as short-distance probes for protein conformation. *Analytical biochemistry*, 407(2):284–286, 2010.

[137] Samuel S Tan, Su Jeong Kim, and Eric T Kool. Differentiating between fluorescence-quenching metal ions with polyfluorophore sensors built on a dna backbone. *Journal of the American Chemical Society*, 133(8):2664–2671, 2011.

[138] Roger Y Tsien. The green fluorescent protein. *Annual review of biochemistry*, 67(1):509–544, 1998.

[139] Rajasekar R Prasanna and Mookambeswaran A Vijayalakshmi. Immobilized metal-ion affinity systems for recovery and structure–function studies of proteins at molecular, supramolecular, and cellular levels. *Pure and Applied Chemistry*, 82(1):39–55, 2010.

[140] Tommy Dam, Victoria Junghans, Jane Humphrey, Manto Chouliara, and Peter Jönsson. Calcium signaling in t cells is induced by binding to nickel-chelating lipids in supported lipid bilayers. *Frontiers in Physiology*, 11:613367, 2021.

[141] Jeremy Mark Berg. *Principles of bioinorganic chemistry*. University Science Books, 1994.

[142] Amelie S Benk, Lucia T Benk, Seraphine Wegner, Peter Comba, and Joachim P Spatz. Site-specific, kinetically inert conjugation of labels and/or carriers to target molecules such as his-tagged proteins via metal complex reagents, October 13 2022. US Patent App. 17/620,087.

[143] Tomaz Einfalt, Dominik Witzigmann, Christoph Edlinger, Sandro Sieber, Roland Goers, Adrian Najer, Mariana Spulber, Ozana Onaca-Fischer, Jörg Huwyler, and Cornelia G Palivan. Biomimetic artificial organelles with in vitro and in vivo activity triggered by reduction in microenvironment. *Nature communications*, 9(1):1–12, 2018.

[144] Keel Yong Lee, Sung-Jin Park, Keon Ah Lee, Se-Hwan Kim, Heeyeon Kim, Yasmine Meroz, L Mahadevan, Kwang-Hwan Jung, Tae Kyu Ahn, Kevin Kit Parker, et al. Photosynthetic artificial organelles sustain and control atp-dependent reactions in a protocellular system. *Nature biotechnology*, 36(6):530–535, 2018.

[145] Lado Otrin, Christin Kleineberg, Lucas Caire da Silva, Katharina Landfester, Ivan Ivanov, Minhui Wang, Claudia Bednarz, Kai Sundmacher, and Tanja Vidaković-Koch. Artificial organelles for energy regeneration. *Advanced Biosystems*, 3(6):1800323, 2019.

[146] Otto Baumann and Bernd Walz. Endoplasmic reticulum of animal cells and its organization into structural and functional domains. 2001.

[147] Christopher Lee and Lan Bo Chen. Dynamic behavior of endoplasmic reticulum in living cells. *Cell*, 54(1):37–46, 1988.

[148] Lars Dreier and Tom A Rapoport. In vitro formation of the endoplasmic reticulum occurs independently of microtubules by a controlled fusion reaction. *The Journal of cell biology*, 148(5):883–898, 2000.

[149] Robert E Powers, Songyu Wang, Tina Y Liu, and Tom A Rapoport. Reconstitution of the tubular endoplasmic reticulum network with purified components. *Nature*, 543(7644):257–260, 2017.

[150] Genny Orso, Diana Pendin, Song Liu, Jessica Tosetto, Tyler J Moss, Joseph E Faust, Massimo Micaroni, Anastasia Egorova, Andrea Martinuzzi, James A McNew, et al. Homotypic fusion of er membranes requires the dynamin-like gtpase atlastin. *Nature*, 460(7258):978–983, 2009.

[151] Miguel A Betancourt-Solis, Tanvi Desai, and James A McNew. The atlastin membrane anchor forms an intramembrane hairpin that does not span the phospholipid bilayer. *Journal of Biological Chemistry*, 293(48):18514–18524, 2018.

[152] Yvonne S Yang and Stephen M Strittmatter. The reticulons: a family of proteins with diverse functions. *Genome biology*, 8(12):1–10, 2007.

[153] Ning Wang, Lindsay D Clark, Yuan Gao, Michael M Kozlov, Tom Shemesh, and Tom A Rapoport. Mechanism of membrane-curvature generation by er-tubule shaping proteins. *Nature Communications*, 12(1):568, 2021.

[154] Tina Y Liu, Xin Bian, Fabian B Romano, Tom Shemesh, Tom A Rapoport, and Junjie Hu. Cis and trans interactions between atlastin molecules during membrane fusion. *Proceedings of the National Academy of Sciences*, 112(15):E1851–E1860, 2015.

[155] Reinhard Lipowsky, Shreya Pramanik, Amelie S. Benk, Miroslaw Tarnawski, Joachim Spatz, and Rumiana Dimova. Elucidating the morphology of the endoplasmic reticulum: Puzzles and perspectives. *ACS Nano (in press)*, 2023.

[156] Rafael B Lira, Tom Robinson, Rumiana Dimova, and Karin A Riske. Highly efficient protein-free membrane fusion: a giant vesicle study. *Biophysical journal*, 116(1):79–91, 2019.

APPENDICES

A Percentage of NTA-Ni lipid affects fluorescence intensity

Statistics for the fluorescence intensity of GUV membranes exposed to 6H-FITC for different electroformation methods and two different mole fractions of NTA lipids, corresponding to the data in Figure 3.7. The membranes were prepared with 3 mol% or 30 mol% NTA lipids and exposed to a 120 nM solution of 6H-FITC at pH 7.45.The number of GUVs used for the statistics is denoted by #GUVs. The numerical values for the mean value and the standard deviation of the coverage are given in arbitrary units.

Preparation method	#GUVs	Intensity, 3 mol%	#GUVs	Intensity, 30 mol%
Pt wire electroformation	17	34.4 ± 4.9	7	42.1 ± 16.1
ITO glass electroformation	12	6.1 ± 7.6	6	17.8 ± 7.3

B Adding Co^{3+} to vesicles made with ITO glasses electroformation

In section 3.4.3, we hypothesized two possibilities for observing the lowest fluorescence at the membrane of GUVs made using ITO glass electroformation. The first hypothesis that the Ni^{2+} is lost during the electroformation is tested in this section. If this is the case, the GUVs would still consist of the NTA-lipids without any metal ions. This would be similar to the GUVs with the Holo-NTA lipids used in chapter 5. The GUVs were trapped in the microfluidic device and exposed to 500 nM 6H-GFP before and after treatment with carbonate of cobalt.

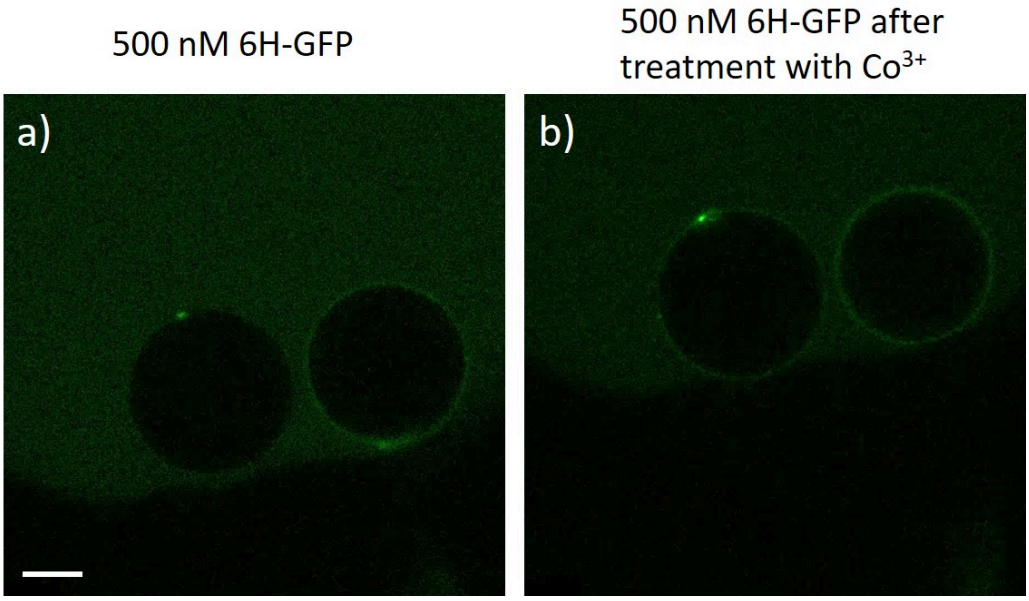

Figure B.1: GUVs with membrane composition POPC:cholesterol in the molar ratio of 8:2 and doped with 3 mol% DGS-NTA(Ni) lipid, electroformed on ITO glasses. The GUVs enclose 500 mM sucrose in 10 mM HEPES buffer at pH 7.4. The GUVs are trapped in the microfluidic device and exposed to 500 nM 6H-GFP **(a)** without any treatment; and **(b)** after treating with carbonate of cobalt, as mentioned in section 5.2.1. Scale bar: 5 μm

C Fluorescence quenching by nickel sulphate

In section 4.2.4, we demonstrated that LUVs consisting of the DGS-NTA(Ni) lipid quench the fluorescence of 6H-FITC. Similar quenching can be observed when 6H-FITC is exposed to Ni^{2+} cations in the form of nickel sulphate salt.

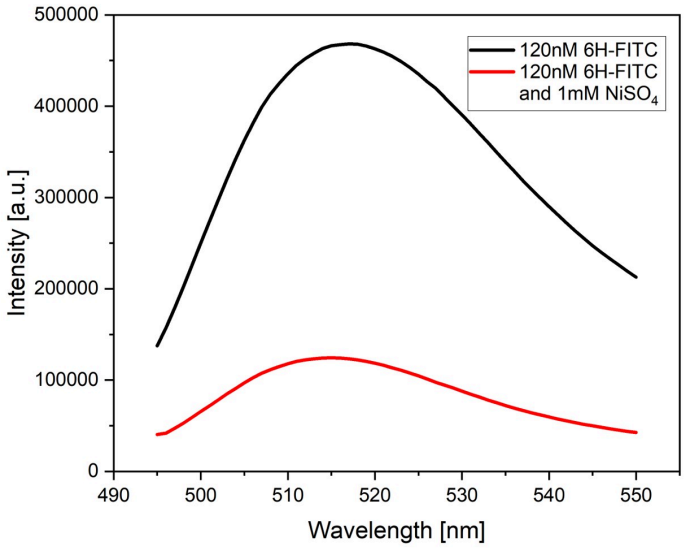

Figure C.1: Nickel sulphate quenches the fluorescence of 6H-FITC. Fluorescence intensity versus wavelength measured for a solution of (a) 120 nM 6H-FITC and (b) 120 nM 6H-FITC in the presence of 1mM nickel sulphate.

D Surface coverage of GUV membranes by 6H-GFP and 6H-FITC

Statistics for the surface coverage of GUV membranes by 6H-GFP as obtained for three different preparation methods, corresponding to the data in Figure3.5. The membranes contained 3 mol% NTA lipids and were exposed to **D.1** 320 nM solution of 6H-GFP at pH 7.45; and **D.2** 240 nM solution of 6H-FITC at pH 7.45. The number of GUVs used for the statistics is denoted by #GUVs and displayed in the 2nd column. The numerical values for the mean value and the standard deviation (SD) of the coverage are given in units of membrane-bound molecules per μm^2.

Table D.1: Vesicles exposed to 320 nM 6H-GFP

Preparation method	#GUVs	Mean coverage	SD
Pt wire electroformation	19	53 703	4 449
PVA hydrogel swelling	18	31 742	9 071
ITO glass electroformation	18	7 261	4 582

Table D.2: Vesicles exposed to 240 nM 6H-GFP

Preparation method	#GUVs	Mean coverage	SD
Pt wire electroformation	29	55 718	8 751
PVA hydrogel swelling	20	12 411	4 376
ITO glass electroformation	29	13 904	8 230

E Membrane composition affects fluorescence intensity

Statistics for fluorescence intensity of GUV membranes arising from membrane bound 120 nM 6H-FITC for different two compositions of the membrane, POPC doped with 3 mol% DGS-NTA(Ni) and POPC: cholesterol in the molar ratio 8:2 doped with 3 mol% DGS-NTA(Ni). The number of GUVs used for the statistics is denoted by #GUVs. The numerical values for the mean value and the standard deviation (SD) of the coverage are given in arbitrary units.

Lipid composition	#GUVs	Intensity	SD
POPC, 3 mol% DGS-NTA(Ni)	8	13.06	4.01
POPC: Chol (8:2), 3 mol% DGS-NTA(Ni)	17	34.36	4.94

F pH affects fluorescence intensity

Statistics for the fluorescence intensity of GUV membranes arising from membrane-bound **F.1** 20 nM 6H-GFP; and **F.2** 120 nM 6H-FITC for different pH values in the exterior solution, corresponding to the data in Figure 4.3. The membranes were prepared by platinum wire electroformation with 3 mol% NTA lipids and were exposed to a 20 nM solution of 6H-GFP or 120 nM solution of 6H-FITC. The pH was varied by the addition of HCl or NaOH solution. The number of GUVs used for the statistics is denoted by #GUVs. The numerical values for the mean value and the standard deviation (SD) of the coverage are given in arbitrary units.

Table F.1: GUVs exposed to 20 nM 6H-GFP at different pH

pH	#GUVs	Intensity	SD
6.38	5	14.8	5.9
6.98	5	36.8	18.0
7.25	5	70.1	16.9
7.43	5	72.4	21.5
8.02	5	80.2	24.8
8.54	5	110.6	27.0
9.06	5	108.3	29.7
9.36	5	114.3	29.2

Table F.2: GUVs exposed to 120 nM 6H-FITC at different pH

pH	#GUVs	Intensity	SD
6.38	5	10.3	2.0
6.98	5	14.0	4.0
7.25	5	21.4	2.9
7.43	5	33.7	4.1
8.02	5	56.8	6.7
8.54	5	76.9	7.3
9.06	5	67.4	7.5
9.36	5	20.7	3.0

G Data for determining the dissociation constant

Statistics for the normalised fluorescence intensity of GUV membranes exposed to different molar concentrations X of 6H-FITC and 6H-GFP, corresponding to the data in Figures 4.4, 4.5 and 5.5. TThe number of GUVs used for the statistics is denoted by #GUVs and displayed in the 2nd column. The numerical values for the mean value and the standard deviation (SD) of the normalised intensity are dimentionless.

Table G.1: GUVs composed of POPC:Chol (8:2) doped with 3 mol% DGS-NTA(Ni), electroformed using Pt wires, exposed to different molar concentrations X of 6H-GFP at pH 7.45, corresponding to the data in Figure 4.4a

X [nM]	#GUVs	Mean intensity	SD
0	4	0.002	0.001
20	4	0.296	0.047
40	4	0.567	0.048
80	4	0.674	0.055
120	4	0.771	0.061
160	4	0.813	0.056
240	4	0.851	0.064
320	4	0.894	0.062

Table G.2: GUVs composed of POPC:Chol (8:2) doped with 3 mol% DGS-NTA(Ni), electroformed using Pt wires, exposed to different molar concentrations X of 6H-FITC at pH 7.45, corresponding to the data in Figure 4.4b

X [nM]	#GUVs	Mean coverage	SD
0	3	0.014	0.004
15	4	0.347	0.088
30	4	0.585	0.050
60	4	0.707	0.184
120	4	0.748	0.085
180	4	0.822	0.127
240	4	0.818	0.075
480	4	0.834	0.027

Table G.3: GUVs composed of POPC:Chol (8:2) doped with 3 mol% DGS-NTA(Ni), electroformed using Pt wires, exposed to different molar concentrations X of 6H-FITC at pH 8.3, corresponding to the data in Figure 4.5

X [nM]	#GUVs	Mean coverage	SD
0	3	0.005	0.001
15	4	0.207	0.038
30	4	0.397	0.097
45	4	0.512	0.101
60	4	0.585	0.111
120	4	0.662	0.173
240	4	0.807	0.143
480	4	0.948	0.165

Table G.4: GUVs composed of POPC:Chol (8:3) doped with 1 mol% Holo-NTA lipids are prepared by swelling on PVA.The GUVs are treated using carbonate of cobalt and then exposed to different molar concentrations X of 6H-GFP at pH 7.5, corresponding to the data in Figure 5.5

X [nM]	#GUVs	Mean coverage	SD
60	8	0.126	0.042
90	9	0.246	0.051
180	8	0.310	0.105
240	9	0.377	0.083
360	10	0.460	0.090
480	9	0.588	0.094
720	9	0.0.667	0.624
960	9	0.7311	0.051